Cellular Mechanisms and Immunological Contexts of Lysosomal Damage Protection in Macrophages

by

Amanda Oi-Yun Wong

A dissertation submitted in partial fulfillment
of the requirements for the degree of
Doctor of Philosophy
(Immunology)
in the University of Michigan
2017

Doctoral Committee:

Professor Joel A. Swanson, Co-Chair
Professor Michele S. Swanson, Co-Chair
Professor Andrew P. Lieberman
Professor Bethany Moore
Associate Professor Mary O'Riordan

Amanda O. Wong

aowong@umich.edu

ORCID iD: 0000-0002-9662-324X

DEDICATION

To my family: Mom, Dad, Jessica, Jacqueline, and Grandma

ACKNOWLEDGMENTS

First and foremost, I would like to thank my mentor, Joel Swanson, for guiding my development into a scientist and a scholar. From him I have learned most of what I know about the logic, methods, and art of experimental science. His consistently cheerful demeanor and eagerness to discuss all data, whether good or "bad," have made it a joy to come into lab every day.

Thanks also to all of the members of the Swanson lab. I would like to give particular thanks to Matangi Marthi, who for the past few years has been a fellow traveler in the quest to crack the puzzle of renitence. Her diligent efforts were instrumental to the completion of the studies described here. She probably now sees renitence vacuoles in everyday objects, as well as in her sleep, an unfortunate occupational hazard of the life of a microscopist.

A former member of the lab, Brian Gregorka, has taught me almost all I know about the principles and practice of microscopy. Our many conversations at the white board during my early days in the lab are among some of my fondest memories. Thanks also to Zachary Mendel, Sei Yoshida, and David Friedman, current members of the lab, as well as past members Isabella Gaeta, Olivia Alge, Regina Pacitto, Lad Dombrowski, and many others for making the lab a stimulating and cooperative environment to work in.

I am extremely grateful for the mentorship of my co-advisor, Michele Swanson. In addition to supporting my progress through my thesis, she has offered invaluable advice that has helped me to hone my skills of critical thinking and written and oral communication.

I would like to thank the other members of my thesis committee – Andrew Lieberman, Beth Moore, and Mary O'Riordan – for their thoughtful advice and encouragement throughout all of the stages of my thesis.

I would also like to thank the members of the three communities I have been a part of during my research training at Michigan: the Medical Scientist Training Program (MSTP), the Immunology Graduate Program, and the Molecular Mechanisms of Microbial Pathogenesis (MMMP) training program. In particular, I would like to thank Ron Koenig, Ellen Elkin, Justine Hein, Hilkka Ketola, and Laurie Koivupalo of the MSTP; Beth Moore and Zarinah Aquil of the Immunology Graduate Program; and Vernon Carruthers, Victor DiRita, and Margaret Allen of the MMMP training program. Each program has provided extraordinary academic and administrative support and fostered a training environment that has promoted my scientific, professional, and personal development. My interactions with the members within these programs have greatly enriched my experiences both academically and socially.

Finally, I would like to thank my family – my mom and dad; my sisters, Jessica and Jacqueline; and my grandma – who are a constant source of love and encouragement. The whole of my upbringing has instilled in me the values and attitudes that have been most important in getting through the most trying parts of my thesis. It is thus an understatement that this thesis is dedicated to them.

TABLE OF CONTENTS

LIST OF FIGURES

LIST OF SUPPLEMENTAL VIDEOS

ABSTRACT

As professional phagocytes, macrophages are susceptible to endolysosomal membrane damage inflicted by the pathogens and noxious particles they ingest. Whether macrophages have mechanisms for limiting such damage is a fundamental question of macrophage biology that is poorly understood. Previously we reported a phenomenon, termed "inducible renitence," in which LPS activation of macrophages protected their endolysosomes from membrane damage initiated by the phagocytosis of silica beads. In this thesis, I uncover mechanistic details of the underlying process and more broadly define the immune contexts in which renitence can be induced.

Applying a quantitative, fluorescence microscopy assay for measuring lysosomal damage, I determined that mechanistically renitence limits the release of small but not large molecules from lysosomes by restricting the time window of release. Morphological analysis of a large imaging data set derived from these studies led to the discovery of a novel, structural correlate of renitence: large, damage-resistant vacuoles that form adjacent to bead-containing phagosomes in LPS-activated but not resting macrophages. These structures, which we term "renitence vacuoles" (RVs), formed coincident with silica bead uptake in a process associated with macropinocytosis, and persisted around bead-containing phagosomes. RVs fused with lysosomes, whereas phagosomes associated with RVs did not, consistent with a model in which RVs act as structural barriers to prevent fusion between damaged phagosomes and intact lysosomes.

Complementing these studies of cellular mechanism, several molecular candidates – namely, cholesterol, synaptotagmin-7, and the autophagy component Atg7 - were evaluated for their contribution to renitence based on their established roles in resistance against or repair of organellar damage in other contexts. However, none of these factors were found to definitively underlie renitence.

A growing body of literature finds evidence for the existence of several functionally distinct macrophage populations *in vivo*. To expand our understanding of the inflammatory contexts in which renitence acts, I examined whether macrophages of these well-defined subtypes exhibit renitence. These studies revealed that classically activated and regulatory macrophages, but not alternatively activated macrophages, exhibit renitence. Furthermore, stimulation of a subset of Toll-like receptors was sufficient to induce renitence. Of the macrophage subtypes examined, those harboring the greatest capacity for renitence shared similarities in their cytokine secretion profile. Likewise, macrophages subtypes less capable of inducing renitence possessed a common profile of cytokine secretion distinct from that associated with renitent macrophages. Thus, the polarization state of macrophages influences their susceptibility to lysosomal damage.

Taken together, this work establishes renitence as an activity of macrophages specialized in host defense or immune regulation and identifies a novel mechanism by which endocytic processes contribute to the reinforcement of lysosomal integrity.

CHAPTER 1

Introduction

1.1 Statement of research problem

Situated at the front line of immune defense, macrophages serve essential roles in pathogen detection and destruction, tasks they accomplish through the cellular equivalent of eating and digestion. Through a process called phagocytosis, macrophages internalize extracellular particles, including microbes, into membrane-bounded compartments called phagosomes. These phagosomes undergo a series of maturation events involving the exchange of membranes and content with vesicles of increasing acidity, collectively termed "endosomes." This process terminates with the fusion of late-stage endosomes with the lysosome, an acidic organelle that houses digestive enzymes for breaking down ingested material. The high phagocytic capacity of macrophages necessitates the maintenance of an intact endolysosomal compartment capable of efficiently receiving and degrading phagocytic targets. However, as many of the pathogens and particles macrophages ingest have the potential to perforate host membranes, this same phagocytic burden carries with it a continual threat to the macrophage's phagolysosomal integrity. How, then, do macrophages preserve the integrity of their phagolysosomal membranes against damage by the pathogens and particles they ingest?

Previous work in our lab described a novel macrophage activity for reinforcing the integrity of lysosomes against membrane damage. Macrophages stimulated with lipopolysaccharide (LPS), a component of the cell wall of gram-negative bacteria, were better

able to resist damage to their lysosomes compared to unstimulated, resting macrophages, a phenomenon we termed "inducible renitence" (Davis *et al.*, 2012). As the conditions found to induce renitence – stimulation with LPS, as well as with interferon-gamma (IFN-γ), tumor necrosis factor-alpha (TNF-α), and heat-killed *Listeria monocytogenes* – were ones conventionally associated with macrophage activation, we reasoned that renitence likely represents a macrophage effector function that promotes host defense. The work contained in this thesis both expands upon and questions this assumption. This chapter considers the role of the macrophage in host defense and presents a synthesis of our current understanding of innate immune mechanisms for recognizing and responding to phagolysosomal injury.

1.2 Basics of macrophage biology

Macrophages are derived from circulating monocytes, which themselves develop from myeloid precursor cells in the bone marrow. Under steady state and inflammatory conditions, monocytes are released from the bone marrow into the bloodstream and circulate to various tissue sites, into which they migrate and differentiate into tissue-resident macrophages (Geissmann *et al.*, 2010). Adding a layer of complexity to this conventional view of macrophage development are recent findings that the majority of resident macrophages at several tissue sites are in fact directly derived from the yolk sac or fetal liver rather than from hematopoietic stem cells in the bone marrow (Ginhoux *et al.*, 2010; Hoeffel *et al.*, 2012; Schulz *et al.*, 2012).

Regardless of their precise developmental origin, macrophages are found in nearly every tissue of the body. Macrophages residing in different anatomical locations are functionally heterogeneous and historically were given different names. These include the alveolar macrophages of the lungs, Kupffer cells of the liver, and microglia within nervous tissue (Gordon and Taylor, 2005). Positioned in the submucosa of many tissue interfaces, tissue

macrophages are typically the first immune cell that encounters a pathogen that has breached an epithelial surface. Host defense is initiated once the infectious pathogen becomes engulfed by the macrophage through phagocytosis. Phagocytosis not only sets an internalized microbe down the path of phagosome maturation towards the degradative (and microbicidal) lysosome, but also brings the microbial surface of the pathogen in close proximity to a large number of cell surface receptors whose detection of microbial molecules alerts the cell to infection. This second process initiates intracellular signaling cascades leading to the induction of a number of transcriptional and post-translational activities that contribute to microbial killing, a phenomenon generally referred to as "macrophage activation." These activities either directly promote the killing of microbes or activate the next stage of the immune response, indirectly leading to the containment of infection.

Activities belonging to the former category include activation of the oxidative burst, which involves the generation of reactive oxygen species (ROS) within the phagosome by the enzyme NADPH oxidase (Nauseef, 2008). Accompanying ROS production is the production of reactive nitrogen species (RNS) by nitric oxide synthase (iNOS2) (MacMicking *et al.*, 1997). ROS and RNS are toxic to pathogens (and if released outside of phagolysosomes, to the host), and together create an inhospitable phagosomal environment for pathogens. Their production, along with the trafficking of pathogen-containing phagosomes to the lysosome, represent major mechanisms utilized by macrophages to kill microbes directly.

Macrophages also participate in the immune response by secreting large numbers of cytokines and chemokines, which function to recruit additional innate and adaptive immune cells to the site of infection. In doing so, macrophages initiate a state of inflammation that can effectively limit the spread of an infection, but if unchecked, can also lead to pronounced

damage to the host (Nathan and Ding, 2010). Thus, built into the immune response are immunoregulatory mechanisms for dampening inflammation once an infection has been cleared (Serhan and Savill, 2005). Some of these immunoregulatory functions, as will be seen later, are performed by macrophages (Cohen and Mosser, 2013; Hamidzadeh *et al.*, 2017).

A final major immune function of macrophages is antigen presentation, although this task is predominantly performed by their close relative, the dendritic cell (DC). The phagocytosis of microbes and their digestion in the lysosome generates microbial antigens that can be processed by macrophages and DCs and presented to T lymphocytes, a process that bridges the innate and adaptive immune responses (Blum *et al.*, 2013).

Thus, recognition of microbial infection induces changes in the macrophage that render it "activated," and more equipped to fight infection. Presented so far has been the classical view of macrophage activation, a concept that over the past several years has evolved to reflect an updated understanding of the diversity and plasticity of macrophages. The next section presents this broader view of macrophage activation.

1.3 Concept of macrophage activation

Macrophage activation as a concept originated with the discovery by Mackaness that mice infected with a sub-lethal dose of *Listeria monocytogenes* were resistant to subsequent challenge with the pathogen (Mackaness, 1962). Later studies by Mackaness and others demonstrated that macrophages isolated from these mice exhibited anti-microbial properties *in vitro*, stimulation of macrophages with the cytokines interferon-gamma (IFN-γ) and tumor necrosis factor-alpha (TNF-α) recapitulated this phenotype, and macrophages possessing these properties formed the cellular basis for the protective immunity originally observed in animals

(Mackaness, 1970; Adams and Hamilton, 1984). Since then, activated macrophages with roles other than the promotion of host defense have been discovered, leading to the realization that macrophages exhibit enormous functional diversity (Mosser, 2003; Mosser and Edwards, 2008). The concept of macrophage activation has been expanded to encompass this large range of macrophage functional states.

The particular state a macrophage assumes is dictated by the balance of external cues sensed in the tissue environment (Mosser and Edwards, 2008). Enabling their role as sentinels of infection and of other perturbations to tissue homeostasis, macrophages express a large number of receptors capable of sensing microbial factors, host cytokines, growth factors, and other types of ligands. Upon the detection of environmental cues, macrophages initiate intracellular signaling cascades that lead ultimately to the activation of cellular processes and pathways that effect an appropriate response to the situation sensed. This diverse set of cues allows for a vast number of macrophage activation states, each defined by the factors that stimulate their generation as well as by their functional properties. While several organizational schemes for classifying macrophages exist, three major classes with functional roles *in vivo* have been defined. These include the classically-activated macrophages (CA-Mφ), alternatively-activated macrophages (AA-Mφ), and regulatory macrophages (Reg-Mφ), which will be considered in turn below.

CA-Mφ are specialized for microbial killing and pro-inflammatory cytokine secretion, activities essential for host defense. They include macrophages of the type originally described by Mackaness, and are generated following exposure to TNF-α, produced by macrophages following Toll-like receptor (TLR) stimulation by microbial ligands, and IFN-γ, released by natural killer (NK) cells and T helper 1 (Th1) cells recruited to the site of infection. AA-Mφ

participate in the wound healing response following tissue injury and become activated upon exposure to IL-4 and/or IL-13, cytokines produced by T helper 2 (Th2) cells (Loke *et al.*, 2007). Mast cells and basophils also provide an early source of IL-4 in response to tissue injury (Reese *et al.*, 2007). Reg-Mφ, like CA-Mφ, are generated in response to TLR stimulation, but in combination with a second signal that reprograms the macrophage such that it assumes an immunosuppressive, rather than inflammatory, state (Mosser and Edwards, 2008). The first reprogramming signal discovered was the IgG immune complex, whose presence coupled with TLR stimulation inhibited the production of the pro-inflammatory cytokine IL-12 (Sutterwala *et al.*, 1997) and induced the formation of high levels of the anti-inflammatory cytokine IL-10 (Sutterwala *et al.*, 1998). Since then, other molecules have been identified for their ability to serve as a reprogramming signal that promotes differentiation to Reg-Mφ. These include prostaglandins, adenosine, apoptotic cells, and IL-10 itself (Mosser and Edwards, 2008). The working model is that these molecules signal the resolution of an immune response and polarize macrophages such that they can aid in the dampening of immune responses. As evidence of their immunoregulatory functions, transfer of Reg-Mφ into WT mice receiving a normally lethal dose of endotoxin protected mice from lethality (Fleming *et al.*, 2015).

A systematic side-by-side comparison of the biochemical and functional properties of these three macrophage classes *in vitro* helped to define markers of each of these classes (Edwards *et al.*, 2006). This study found that Reg-Mφ in fact resemble CA-Mφ much more than they do AA-Mφ, even though Reg-Mφ and AA-Mφ were historically classified under the category of "alternatively-activated" macrophages. Both CA-Mφ and Reg-Mφ showed high levels of nitric oxide (NO) production, low arginase activity (a defining feature of AA-Mφ), high CD86 costimulatory molecule expression, and the ability to effectively present antigen to T cells.

These two classes were mainly distinguished by their reciprocal levels of production of IL-12 and IL-10. CA-Mφ produced high levels of IL-12 and low levels of IL-10, whereas Reg-Mφ produced high levels of IL-10 and low levels of IL-12. Interestingly, production of TNF-α, IL-1, and IL-6, key pro-inflammatory cytokines produced by CA-Mφ, was also elevated in Reg-Mφ (Gerber and Mosser, 2001). Microarray analysis also showed few transcriptional differences between the two classes, with fewer than 0.5% of transcripts found to be upregulated more than two-fold in Reg-Mφ than in CA-Mφ. Yet the subtle transcriptional and biochemical differences between the two classes confer large functional differences, as transfer of Reg-Mφ into WT mice can protect from lethal endotoxemia, whereas the transfer of macrophages with properties of CA-Mφ in fact induces lethality in mice treated with a sub-lethal dose of endotoxin (Cohen and Mosser, 2013; Fleming *et al.*, 2015). This immunoregulatory activity of Reg-Mφ can likely be attributed to their secretion of high levels of IL-10, which can inhibit the production and activity of pro-inflammatory cytokines (Mosser and Edwards, 2008). AA-Mφ, in striking contrast to Reg-Mφ and CA-Mφ, do not secrete detectable levels of IL-10 or IL-12, and instead express high levels of the gene *Relm-α*, determined in this study to be a reliable marker of AA-Mφ activation (Edwards *et al.*, 2006).

1.4 Macrophages in innate immunity

While acknowledging the multitude of activation states a given macrophage can take, the work in this thesis is primarily concerned with the host defense functions of the LPS-activated macrophage. The next section of this chapter focuses on macrophage biology in the context of innate immunity.

1.4.1 Immune recognition of infectious non-self versus non-infectious self

Pathogen recognition by macrophages occurs through a set of germline-encoded receptors capable of recognizing molecules conserved in microbes but not found in the healthy host. The set of host receptors are collectively referred to as "pattern recognition receptors," and the microbial ligands they recognize we refer to as "pathogen-associated molecular patterns" (PAMPs). This concept of pattern recognition was originally introduced by Charles Janeway as a model for how the innate immune system discriminates infectious non-self from non-infectious self, the fundamental challenge the immune system faces (Janeway, 1989).

Pattern recognition receptors can be divided into those that recognize microbes or their products at the cell surface or within endosomes (topologically-equivalent compartments) and those that recognize microbial ligands that have accessed the cytosol. The most well-characterized of the extracellular pattern recognition receptors are the Toll-like receptors (TLRs), which will be considered first.

1.4.2 Toll-like receptors

To date, 10 functional TLRs have been discovered in humans and 13 in mice (Murphy, 2011). These receptors recognize a variety of PAMPs. Those PAMPs and their cognate TLRs relevant to our discussion in later chapters include the following: lipopolysaccharide (LPS), a component of the gram-negative bacterial cell wall, which is recognized by TLR4; bacterial lipoproteins from gram-negative and gram-positive bacteria, which are recognized by TLR2; flagellin, a structural component of the bacterial flagellum, which is recognized by TLR5; double-stranded RNA (dsRNA), a replicative intermediate of many viruses, which is recognized by TLR3; single-stranded RNA (ssRNA), found in viral genomes, but confined within the nucleus of the healthy host, which is recognized by TLR7; and DNA containing unmethylated CpG dinucleotides, a common feature of bacterial but not mammalian genomes, which are

recognized by TLR 9 (Akira *et al.*, 2006). The latter three of these receptors – TLR3, TLR7, and TLR9 – comprise the set of TLRs that recognize nucleic acids, and are localized within endosomal membranes. Their endosomal localization enables their function: nucleic acids from microbes are typically only released after the microbe has been degraded in the acidified endosome, and thus would first be accessible to the host within this compartment (Murphy, 2011). All other known TLRs in macrophages localize to the cell surface. TLR4 is unique for its ability to recognize its ligands both at the cell surface and within endosomes (Kawai and Akira, 2010).

Structurally, TLRs are single-pass transmembrane proteins composed of an extracellular region containing multiple leucine-rich repeats (LRRs) and an intracellular Toll-IL-1 receptor (TIR) domain (Akira *et al.*, 2006). Recognition of their cognate PAMPs induces TLRs to dimerize and the TIR domains of the two receptors to cluster, a process that activates the receptor pair and initiates downstream signaling. Most TLRs form homodimers, except for TLR2, which forms heterodimers with either TLR1 or TLR6 depending on the PAMP detected (Akira *et al.*, 2006). The outcome of TLR signaling is the activation of a number of transcription factors that induce the expression of pro-inflammatory cytokines and chemokines that initiate the next stage of the immune response. The major transcription factors activated include nuclear factor-κB (NF-κB), as well as those in the mitogen-activated protein kinase (MAPK), and interferon-regulatory factor (IRF) families. NF-κB and MAPK activation upregulates the expression of pro-inflammatory cytokines such as TNF-α, IL-12, IL-6, and pro-IL-1β, whereas IRF activation induces the expression of the type I interferons IFN-α and IFN-β, which have roles in anti-viral immunity (Akira *et al.*, 2006).

The intracellular signaling cascades leading from TLR ligation to transcription factor activation are extremely complex and will not be reviewed here, except to note the significance of the adaptor molecules that activated TLRs recruit. The TIR domains brought together by TLR dimerization act as signaling hubs that recruit and interact with the TIR domains of cytoplasmic adaptor molecules (Akira *et al.*, 2006). In mammals, four such adaptor molecules exist: MyD88 (myeloid differentiation factor 88), MAL (MyD88 adaptor-like), TRIF (TIR domain-containing adaptor-inducing IFN-β), and TRAM (TRIF-related adaptor molecule) (Kawai and Akira, 2010). Each TLR when activated recruits a specific combination of adaptor molecules. TLRs 5, 7 and 9 recruit MyD88 only; TLR 3 recruits TRIF only; TLR 2/1 and TLR 2/6 heterodimers signal through MyD88 paired with MAL; TLR4 signals through MyD88/MAL when activated at the cell surface, but through TRIF/TRAM when activated endosomally (Kawai and Akira, 2010). The combination of receptor(s) activated and adaptors recruited influences the specific signaling events triggered. Experimentally, the effect of eliminating TLR signaling on a cellular process can be investigated using animals with genetic deficiencies in both MyD88 and TRIF.

1.4.3 Cytosolic sensors of infection

Several classes of intracellular sensors exist for detecting the "violation of the sanctity of the cytosol," which indicates the presence of microbes or their secreted factors in a cellular compartment that under normal circumstances should be sterile (Lamkanfi and Dixit, 2009). These sensors also respond to signs of cell injury that are indicative of a breach of the cell's defenses. The cell perceives this breach as a serious threat, and responds accordingly through initiating a form of programmed cell death called "pyroptosis," to be described in more detail below (Bergsbaken *et al.*, 2009).

While several classes of intracellular sensors exist, here we focus on those that upon detection of PAMPs or signs of cellular damage assemble into high molecular weight complexes called "inflammasomes." These sensors include those of the nucleotide-binding oligomerization domain (NOD), leucine-rich repeat-containing protein (NLR) family, of which the most well characterized is NLRP3, whose activity will be described in more detail in the next section. As a general pattern, recognition of a microbial or stress signal by an NLR inflammasome sensor triggers its activation and the recruitment of an adaptor protein named ASC, whose pyrin domain (PYD) interacts with the PYD of the sensor and whose caspase recruitment domain (CARD) allows its interaction with the protease caspase 1 (Broz and Dixit, 2016). The oligomerization of the sensor component, ASC adaptor, and caspase 1 completes the assembly of the inflammasome complex. Auto-activation of caspase 1 renders it catalytically active and able to cleave the inactive forms of the pro-inflammatory cytokines IL-1β and IL-18 into their active forms, which are then secreted from the cell (Broz and Dixit, 2016).

IL-1β and IL-18 serve to potentiate the inflammatory response against infection. Their processing and release accompanies several other programmed cellular responses induced during pyroptosis, a cell death pathway triggered by the activation of caspase 1. These responses include plasma membrane rupture leading to cell lysis and the release of pro-inflammatory mediators (Bergsbaken *et al.*, 2009). The presumed effect of this inflammatory form of cell death is the rapid removal of infected cells and the perpetuation of inflammation geared toward the elimination of infection (Jorgensen and Miao, 2015).

Of note, the expression of pro-IL-1β and pro-IL-18, inactive precursors of the mature cytokines, is triggered downstream of TLR signaling. Thus, inflammasome activation requires two signals: (1) priming by TLR stimulation and (2) activation of a cytosolic inflammasome

sensor, whose expression is also stimulated by TLR activation (Latz *et al.*, 2013). This two-signal requirement allows the TLR and NLR pathways to cooperate to eliminate pathogenic threats in the appropriate spatiotemporal context. In addition, such a system would prevent inappropriate activation of inflammasomes, and the potent inflammatory response they incite, in the absence of microbial recognition (Vance *et al.*, 2009).

1.4.4 Updates to the Pattern Recognition Receptor-PAMP model: Patterns of pathogenesis

The paradigm introduced so far, of pattern recognition receptor recognition of PAMPs, holds enormous explanatory power and provides a useful framework for understanding the cellular basis of innate immune recognition (Medzhitov, 2009). However, additional mechanisms need to be invoked to explain how the host distinguishes between pathogenic and non-pathogenic microbes, such as the vast number of commensal bacteria that reside in the mammalian gut. Both groups of microbes present PAMPs – or, more accurately, microbe-associated molecular patterns (MAMPs) – and yet immune responses are mounted against the former and not the latter. Further complicating the PAMP model, several pathogens are able to modify their PAMPs such that they are less immunogenic, suggesting that PAMP recognition may not serve as the only means for host recognition of an infection (Matsuura, 2013; Reddick and Alto, 2014). A model proposed by Vance, Isberg, and Portnoy attempts to reconcile these ideas (Vance *et al.*, 2009). The model starts with the assumption that pathogens utilize a limited number of strategies to cause disease, a well-accepted principle of microbial pathogenesis (Finlay and Falkow, 1997; Vance *et al.*, 2009). Just as the host can detect a limited set of PAMPs using a restricted number of receptors, it is possible that the host also has the capacity to detect a limited number of signatures associated with host damage caused by pathogens. These

signatures they term “patterns of pathogenesis,” in keeping with the existing pattern recognition receptor/PAMP nomenclature. One pattern of pathogenesis proposed was cytosolic access of microbial molecules through phagolysosome perforation, an outcome we propose inducible renitence serves to prevent. However, in cases where pathogen cytosolic access occurs, two major host mechanisms exist to detect and clear pathogens: inflammasome activation and autophagy. These mechanisms are discussed in the next section, which begins with an overview of the pathogen and particles whose uptake by macrophages can induce phagolysosomal damage.

1.5 Host responses to pathogen-induced and particle-induced phagolysosomal damage

The focus in this section will be on examples of pathogen-induced - and in particular, bacteria-induced - phagolysosomal injury. In addition, several host and environmentally-derived particulate agents, which have been determined to induce lysosomal injury and to be associated with the development of human disease, will be discussed.

1.5.1 Examples of pathogen-induced phagolysosomal damage

To survive within host cells, intracellular bacteria have evolved several strategies to avoid delivery to the degradative lysosome. These strategies can be grouped into three general categories: (1) phagolysosomal escape into the cytosol, (2) inhibition of phagosome-lysosome fusion and prolonged residence in a vacuolar compartment, and (3) modification of the bacteria-containing vacuole (another term for a bacteria-containing phagosome; BCV) with various host membranes that render the vacuole incapable of participating in endosomal trafficking (Scott *et al.*, 2003). Pathogens utilizing the first strategy clearly must possess mechanisms for perforating and even rupturing phagolysosomes. One such pathogen is *Listeria monocytogenes*, a Gram-positive bacterium that mediates its escape from macrophage phagosomes through the expression

of a pore-forming toxin called Listeriolysin O (LLO). LLO causes phagosomal perforation through a multi-step process. Its insertion into the phagosomal membrane first creates small pores that permit the exchange of protons and calcium ions before expanding into larger pores that enable the escape of the bacterium into the cytosol (Shaughnessy *et al.*, 2006).

Bacteria utilizing the second two pathogenic strategies introduced above also express virulence factors for accessing the cytosol. Through coordinating the expression and assembly of needle-like secretion apparatuses that penetrate the phagosomal membrane or plasma membrane, these bacteria can deliver effector proteins from the BCV to the host cytosol (Deng *et al.*, 2017). It is through these effectors that bacteria can manipulate host proteins (eg. cytoskeletal proteins and membranous organelles) in such a way as to halt phagosome maturation or modify the BCV (Bhavsar *et al.*, 2007).

Some pathogens use a combination of the three pathogenic strategies. With improved methods available for detecting phagolysosomal leakage, phagosome escape has been observed for many intracellular pathogens whose pathogenesis was conventionally thought not to involve direct cytosolic access (Fredlund and Enninga, 2014). For example, *Mycobacterium tuberculosis*, a bacterium whose intracellular lifecycle has been well-established to involve the arrest of phagosome maturation and replication and residence in a non-acidified phagosome, has recently been discovered to harbor mechanisms for translocating from the vacuole to the cytosol (Simeone *et al.*, 2016). Phagosomal escape by *M. tuberculosis* depends on its expression of the type VII secretion system, ESX-1 (van der Wel *et al.*, 2007). Interestingly, the attenuated BCG vaccine strain, which lacks ESX-1, is unable to mediate phagosome escape (van der Wel *et al.*, 2007). Complementation of the strain with functional ESX-1 conferred the ability to escape

phagosomes and restored virulence, reinforcing the concept that the ability to induce phagolysosomal injury is a key bacterial virulence trait (Simeone *et al.*, 2012).

1.5.2 Host recognition of phagolysosomal damage by inflammasomes

The same mechanisms that allow pathogens to escape phagolysosomes or to modify their intracellular niche also potentially alert the host of their presence. Thus, the outcome of any host-pathogen interaction depends on the balance of virulence traits expressed by the pathogen and immune strategies against such virulence mechanisms evolved by the host. A major host strategy evolved for detecting cytosolic access of pathogens – inflammasome sensing and activation – has been described in general terms in an earlier section. Here we focus on a specific member of the NLR family of inflammasome sensors, NLRP3, to illustrate concepts of how inflammasome sensors detect the presence of intracellular infection.

Two non-mutually exclusive models have been proposed for how such pathogen sensing occurs (Vance *et al.*, 2009). According to the first model, receptors in the cytosol directly sense translocated PAMPs released by bacteria from outside the cell or within phagosomes. As these PAMPs cannot diffuse across cellular membranes, their presence in the cytosol implies the presence of a breach to plasma membrane or phagolysosomal integrity, such as that mediated by bacterial secretion systems and pore-forming toxins. A second model proposes that the host can sense physical damage associated with pathogen perforation or rupture of cellular membranes. Examples of both types of detection have been demonstrated for the NLRP3 inflammasome sensor.

Unlike most TLRs, NLRP3 as a single sensor is capable of recognizing infection by a broad range of pathogens. For example, infection with several fungi (*Candida albicans*,

Saccharomyces cerevisiae), bacteria (*Listeria monocytogenes*, *Staphylococcus aureus*), and viruses (Sendai virus, adenovirus, and influenza virus) have been shown to activate the NLRP3 inflamamsome (Schroder and Tschopp, 2010). In the case of *S. aureus* infection, the specific microbial molecule responsible for NLRP3 activation (the *S. aureus* alpha-toxin) has been identified (Craven *et al.*, 2009).

In addition to recognizing microbial PAMPs, NLRP3 also recognizes a large number of host-derived molecules. These include substances released by cells undergoing necrosis, a form of cell death that, unlike the immunologically silent apoptosis, involves rupture of the plasma membrane and release of cellular contents into the extracellular space (Kono and Rock, 2008). These contents include DNA, ATP, heat shock proteins, and nuclear proteins such as HMGB1 (high-mobility group box 1 protein), and are collectively referred to as endogenous danger signals or "DAMPs" (damage-associated molecular patterns) (Kono and Rock, 2008). As these molecules are typically contained within cellular organelles, and not found extracellularly, a model has been proposed in which these danger signals can be recognized by innate immune sensors (Kono and Rock, 2008). Two such molecules released from injured cells that activate the NLRP3 inflammasome are ATP and hyaluronan (Mariathasan *et al.*, 2006; Yamasaki *et al.*, 2009).

A number of exogenously-derived particles also activate the NLRP3 inflammasome. These include the monosodium urate (MSU) crystals deposited in the joints of patients with gout and the amyloid-β peptide found in plaques associated with Alzheimer's disease; several environmental irritants, including silica and asbestos; and aluminum salts, a common adjuvant (Schroder and Tschopp, 2010). A commonality of these crystalline particulate agents is their ability to cause lysosomal damage. As such, one model proposes that lysosomal damage may

serve as a common signal recognized by NLRP3, for example through the release of lysosomal contents that can be detected by the sensor. Cathepsin B, a lysosomal protease released into the cytoplasm from damaged lysosomes, was proposed to serve as a ligand that directly activates NLRP3 (Halle *et al.*, 2008; Hornung *et al.*, 2008). In support of this model, inhibition of cathepsin B activity impaired NLRP3 activation, as judged by reduced IL-1β release following lysosomal injury induced by ingested silica particles (Hornung *et al.*, 2008). However, as genetic deficiency of cathepsin B in macrophages did not affect caspase 1 activation or IL-1β release following stimulation with a number of NLRP3 activators, the precise role of cathepsin B in NLRP3 activation is unclear (Dostert *et al.*, 2009). However, regardless of the specific signal detected, sterile rupture of lysosomes (i.e. in the absence of pathogen or silica-induced damage) was sufficient to activate NLRP3, suggesting that lysosomal damage or its consequences can indeed be sensed by the host cytosolic sensor (Hornung *et al.*, 2008).

Thus, phagolysosomal damage, whether triggered by pathogen or particulate uptake, induces inflammasome activation. The main effector function of activated inflammasomes, as described earlier, is pyroptosis. Not surprisingly, many of the particulate agents (eg. silica, asbestos, MSU) capable of activating the inflammasome also lead to pathologies associated with the development of a chronic inflammatory state (silicosis, asbestosis, and gout, respectively) (Schroder and Tschopp, 2010).

1.5.3 Host clearance of damaged phagolysosomes by autophagy

Another form of host defense used to recognize cytosolic pathogen access is autophagy. Autophagy is a cellular pathway that sequesters cytosolic contents, such as soluble macromolecules, damaged organelles, and aggregated proteins, into double-membrane vesicles termed “autophagosomes,” for delivery to and degradation in the lysosome (Levine *et al.*, 2011).

The pathway likely evolved as a mechanism for bulk degradation of cytoplasmic material to supply the cell with nutrients during conditions of low extracellular nutrient availability. However, the same base machinery for bulk autophagy has been adapted to allow the cell to selectively degrade cargo such as damaged mitochondria (through "mitophagy") or pathogens (through "xenophagy") (Randow and Youle, 2014). Here we focus on mechanisms by which host cells, including macrophages, perform two forms of selective autophagy: xenophagy of intracellular bacteria and "lysophagy," a recently discovered form of autophagy for the sequestration and clearance of damaged lysosomes.

The mechanism of autophagosome formation in both bulk and selective autophagy involves the same key steps: initiation of the process through the formation of a double membrane segment termed the "phagophore," elongation of the phagophore around eventual autophagic cargo, and closure of the autophagosomal membrane, achieved by fusion of the two phagophore ends, to yield a mature autophagosome (Mizushima *et al.*, 2011). These steps are carefully orchestrated by a set of autophagy-related (Atg) proteins, first discovered in yeast (Mizushima *et al.*, 2011). Through assembly into ubiquitin-like protein complexes, several of these proteins contribute to the task of conjugating the protein LC3 (microtubule-associated protein 1A/1B-light chain 3), a mammalian homolog of Atg8, to phosphatidylethanolamine (PE) in the autophagosomal membrane (Mizushima *et al.*, 2011). The lipidated form of LC3 (LC3-II) is commonly used as an autophagic marker (Mizushima *et al.*, 2010).

Additional mechanisms for cargo recognition during the elongation stage of autophagosome formation distinguishes selective from bulk autophagy. The selectivity for specific cargo in xenophagy is achieved by analogous mechanisms as those first described for the clearance of damaged mitochondria in mitophagy (Youle and Narendra, 2011). Both

mechanisms depend on the recognition by a set of cytosolic cargo receptors of "eat-me" signals presented by their respective substrates (Randow and Youle, 2014). Upon recognition of these substrate-associated signals, the receptors recruit components of the autophagy machinery to the damaged organelle or cytosolic pathogen, leading to sequestration and eventual clearance of the target cargo (Randow and Youle, 2014).

Two major "eat-me" signals recognized during xenophagy have been described. The first is the accumulation of carbohydrate-binding proteins, called galectins, on membranes of damaged pathogen-containing vacuoles. Galectins have been established as markers of endosomal membrane damage through their ability to bind β(1-4)-linked galactosides, glycans normally only present at the cell surface and on the lumenal side of endosomes, but that following membrane damage are made accessible to galectins residing in the cytosol (Paz *et al.*, 2010). Cargo receptors that recognize galectins and recruit the autophagy machinery include NDP52, whose recruitment to galectin 8-associated vacuoles damaged by *S. Typhimurium* targets the bacteria for autophagy and restricts its exit into the cytoplasm (Thurston *et al.*, 2012).

Also recognized as "eat-me" signals are bacteria or host-membranes coated with ubiquitin. Ubiquitination has been observed to mediate recognition of damaged mitochondria and cytosolic bacteria by the autophagy machinery (Randow and Youle, 2014). For example, vacuoles damaged by *S. Typhimurium*, as well as *S. Typhimurium* that have escaped phagosomes, become rapidly decorated with ubiquitin (Perrin *et al.*, 2004; Birmingham *et al.*, 2006). Several receptors, including p62 (Zheng *et al.*, 2009), NDP52 (Thurston *et al.*, 2009), and optineurin (Wild *et al.*, 2011), are capable of detecting the ubiquinated bacteria and delivering them to autophagosomes.

The studies reviewed here indicate that autophagy can target bacteria within damaged vacuoles as well as free bacteria in the cytoplasm after their escape from vacuoles. In addition, autophagy proteins can facilitate the maturation of intact bacteria-containing phagosomes through a form of non-canonical autophagy called LC3-associated phagocytosis (LAP). Phagocytosis of targets (eg. bacteria, IgG-opsonized beads) that trigger either TLR stimulation or Fcγ receptor (FcγR) ligation induces the recruitment and conjugation of LC3 to the phagosomal membrane (Sanjuan *et al.*, 2007; Huang *et al.*, 2009). As activation of LAP enhances the rate of phagosome maturation, and thus the rate of delivery of pathogens for degradation in the lysosome, it has been proposed to function as an anti-microbial defense mechanism (Sanjuan *et al.*, 2007). LAP requires several Atg members associated with canonical autophagy (eg. Atg5, Atg7), but not those acting at the step of *de novo* phagophore formation, which is not relevant for LAP (Martinez *et al.*, 2011). Therefore, dissecting the contribution of LAP versus autophagy to a cellular process requires the use of knockout animals deficient in one pathway but not the other. Mechanistically, LAP depends on ROS generation by the NADPH oxidase (NOX2), suggesting that activation of NOX2 not only promotes the direct killing of microbes, but also activates a separate anti-microbial pathway that promotes the delivery of any pathogens not successfully killed by ROS to the degradative lysosome (Huang *et al.*, 2009).

1.5.4 Host clearance of damaged phagolysosomes by autophagy: Focus on lysophagy

The lysosome thus serves as the endpoint for several endocytic and autophagic pathways. The large number of membrane-damaging pathogens and particulate agents that can be delivered to the lysosome through these pathways renders this cellular compartment particularly susceptible to injury. Given their acidic nature and large complement of hydrolytic enzymes, the consequences of lysosomal damage are severe. These include not only pathogen escape in

settings of infection, but also the release of acid and hydrolytic enzymes from the lysosome to the cytosol, a situation associated with cell death (Boya and Kroemer, 2008). Even in the absence of cell death, compromise of lysosomal integrity would lead to the compromise of lysosomal function, thereby limiting the cell's degradative and catabolic capacity. Furthermore, the lysosome's newly described roles in coordinating nutrient sensing with signaling related to cellular metabolism and lysosomal biogenesis suggests that lysosomal damage would have profound consequences that extend beyond the individual lysosome or cell affected (Settembre *et al.*, 2013). Thus, mechanisms for preventing lysosomal injury or rapidly repairing or clearing damaged lysosomes likely are essential for maintaining cellular homeostasis.

The recently-described process of lysophagy is thought to represent one such mechanism. The term describes the process by which damaged lysosomes are sequestered by autophagy and cleared through delivery to intact lysosomes. The studies in which lysophagy was discovered were performed using non-pathogen-mediated methods for damaging lysosomes. In one study, cells were subjected to lysosomal damage through treatment with either L-leucyl-L-leucine methyl ester (LLOMe), a lysosomotropic agent that upon accumulation in lysosomes is converted into a membranolytic species (Thiele and Lipsky, 1990), or ground silica, whose ingestion and trafficking to lysosomes has been well-established to cause lysosomal damage (Thibodeau *et al.*, 2004). Lysosomes in these cells were found to co-localize with markers of both galectin 3 and ubiquitin (Maejima *et al.*, 2013). Only those lysosomes marked with galectin 3 (representing damaged lysosomes) recruited p62 and LC3, suggesting that the autophagy machinery selectively recognized damaged lysosomes. These galectin 3-positive lysosomes were successfully delivered to intact, acidic lysosomes.

A separate study followed the autophagic response to lysosomal damage induced through photochemical means. Cells whose lysosomes were labeled with the photosensitizer disulfonated aluminum phthalocyanine (AlPcS2a) were then exposed to light that activates the photosensitizer and leads to the generation of ROS, which disrupt lysosomal membrane integrity (Hung *et al.*, 2013). Furthermore, using this method, individual lysosomes could be targeted, allowing for precise spatiotemporal control of lysosomal damage. The damage induced by this method led to lysosomal permeabilization (indicated by a rise in the pH of the compartment) without inducing lysosomal rupture (indicated by the ability of lysosomes to retain a 10 kDa fluorescein dextran dye pre-loaded into lysosomes). Thus, compared to the extent of damage induced by LLOMe, which is known to result in the massive rupture of lysosomes and to trigger cell death (Uchimoto *et al.*, 1999; Boya and Kroemer, 2008), the extent of damage induced using this light-activated method was much more limited (Hung *et al.*, 2013). Still, lysosomes damaged through this method were shown to be ubiquitinated, to recruit p62 and LC3, and to be delivered to acidic lysosomes. The ubiquitination was specific to damaged lysosomes and occurred approximately 30 to 50 min after the onset of damage.

Together, these two studies establish that autophagic mechanisms for sensing and clearing damaged lysosomes are activated in response to multiple forms of lysosomal injury.

1.6 Inducible renitence in the context of innate immunity and organization of thesis

In this overview, we have attempted to present a model, supported by a large body of literature, of how the innate immune system responds to phagolysosomal injury. Inflammasome sensors and autophagy receptors detect cytosolic pathogen access or vacuolar damage and activate the effector mechanisms of pyroptosis and autophagic delivery to lysosomes, respectively. We propose that renitence, an inducible activity within macrophages to reinforce

their lysosomes against damage, may serve as a complementary mechanism to inflammasome activation and autophagy by preventing or limiting the extent of phagolysosomal injury following pathogen or particle-mediated damage.

In fact, the discovery of renitence supports a corollary of the patterns of pathogenesis model introduced earlier. According to that model, an infection is recognized as pathogenic when microbial ligands are recognized in the context of host damage. With the discovery of renitence, our lab demonstrated that macrophages pre-exposed to microbial ligands respond to phagolysosomal damage differently than macrophages in the absence of microbial stimulation. That is, the host response to phagolysosomal damage depends on the immunological context in which it is sensed.

This advance in macrophage biology was enabled by the development of a novel, quantitative fluorescence microscopy method for inducing and measuring lysosomal damage in macrophages (Davis and Swanson, 2010; Davis *et al.*, 2012). In this method, damage is measured by monitoring the release of a pH-sensitive dye (fluorescein dextran; Fdx) from acidic lysosomes, into which the dye has been pre-loaded, into the pH-neutral cytoplasm following the induction of lysosomal damage. Damage is induced by administering macrophages silica beads. Like crystalline silica, these beads cause phagolysosomal damage upon their uptake into the cell (Davis and Swanson, 2010; Joshi *et al.*, 2015), but their use carries two advantages over the use of ground silica: greater uniformity in the extent of lysosomal damage caused between different batches of beads, and ready visualization of beads within discrete phagolysosomes by phase contrast microscopy. In resting macrophages, silica bead uptake leads to pronounced leakage of Fdx from lysosomes. The extent of Fdx release is significantly reduced in macrophages pre-

treated with LPS, IFN-γ, TNF-α, and heat-killed *L. monocytogenes*, the principal finding in the original characterization of renitence (Davis *et al.*, 2012).

This thesis seeks to build on these previous observations by determining (1) the cellular mechanisms that protect against phagolysosomal damage in macrophages stimulated with LPS and (2) the functional relevance of renitence through identifying the immunological contexts in which it acts. Initial studies of mechanism focused on identifying key cell biological differences between resting and LPS-activated macrophages that could explain the susceptibility to lysosomal damage in the former and propensity for protection in the latter. This approach is described in Chapter 2, which examines the kinetics and size-range of dye release following silica-mediated mediated lysosomal damage in resting versus LPS-treated macrophages. Morphological comparison of features of resting versus LPS-treated macrophages following bead-mediated injury led to the discovery of novel cellular structures, which we term "renitence vacuoles," that form adjacent to phagolysosomes in the setting of damage and protect against the fusion of damaged phagosomes with intact lysosomes. The discovery and characterization of renitence vacuoles are also described in Chapter 2. Thematically, this work is continued in Chapter 4, in which several candidate molecular factors – namely, cholesterol, synaptotagmin-7, and autophagy - are considered for their contribution to renitence. Chapter 3 takes a broader view of the "activated" macrophage and examines the range of well-defined macrophage states that exhibit renitence. Together, this work advances our understanding of both cellular mechanisms and immunological contexts of renitence.

CHAPTER 2

Renitence Vacuoles Facilitate Protection against Phagolysosomal Damage in Activated Macrophages

This work was performed in collaboration with Matangi Marthi, Brian Gregorka, Michele S. Swanson, and Joel A. Swanson. A.O.W, M.M., and J.A.S. designed the project and performed experiments. B.G. and M.S.S participated in data analysis. A.O.W. and J.A.S wrote the manuscript, which was submitted to *Molecular Biology of the Cell*. At the time of this writing, reviewer comments have been received and revisions are in progress.

2.1 Abstract

Macrophages, as professional phagocytes, incur damage to their endolysosomes upon phagocytosis of pathogens and noxious particles. Whether macrophages have mechanisms for limiting such damage is not well understood. Previously we reported a phenomenon, termed "inducible renitence," in which LPS activation of macrophages protected their endolysosomes against damage initiated by phagocytosis of silica beads. To gain mechanistic insight into the process, we analyzed the kinetics of renitence and morphological features of LPS-activated versus resting macrophages following silica bead-mediated injury. We discovered novel vacuolar structures that form in LPS-activated but not resting macrophages following silica bead phagocytosis. Because of their correlation with renitence and damage-resistant nature, we termed these structures "renitence vacuoles." Renitence vacuoles formed coincident with silica bead uptake in a process associated with membrane ruffling and macropinocytosis. However,

unlike normal macropinosomes, which shrink within 20 minutes of formation, renitence vacuoles persisted around bead-containing phagosomes. Renitence vacuoles fused with lysosomes, while associated phagosomes did not. Together, these findings support a model in which renitence vacuoles act as persistent macropinosomes that prevent the fusion of damaged phagosomes with intact lysosomes and thereby preserve endolysosomal integrity.

2.2 Introduction

In multicellular organisms, phagocytosis is principally performed by specialized cells, such as macrophages, which serve homeostatic and immune roles through the clearance of apoptotic bodies, particulate matter, and pathogenic microbes. As much of the material that macrophages ingest has the potential to perforate phagolysosomes, mechanisms to mitigate such damage likely exist. Innate immune responses to pathogen-mediated phagolysosomal injury include the sequestration of escaped pathogens or damaged phagolysosomes by autophagy (Levine *et al.*, 2011) and the triggering of pro-inflammatory responses after the cytosolic sensing of pathogens or their products by inflammasomes (Schroder and Tschopp, 2010). However, whether cells have mechanisms to prevent phagolysosomal injury from occurring in the first place is not known.

Earlier work demonstrated that macrophages primed against infection can reinforce their lysosomal integrity. Using a ratiometric fluorescence microscopic assay for measuring lysosomal damage in macrophages, we discovered that macrophages exposed to LPS, IFN-γ, heat-killed *Listeria monocytogenes,* or other host and microbial factors associated with macrophage activation were better protected from lysosomal damage initiated by phagocytosis of acid-washed (AW) silica beads than were unstimulated, resting macrophages (Davis *et al.*, 2012). The protection against lysosomal damage conferred by macrophage activation we termed

"renitence." As LPS activation of macrophages upregulates a number of anti-microbial activities, including reactive oxygen species production, autophagy, inflammasome priming, and cytokine secretion, we propose that renitence represents another measure within LPS-activated macrophages that increases resistance to infection by pathogens capable of perforating phagolysosomes. How cells might strengthen the integrity of their endolysosomal compartments in anticipation of potentially injurious threats is not well understood, and to date has primarily been addressed using pathogens as agents of damage

Recent studies of host factors that affect the integrity of bacteria-containing phagosomes in macrophages implicate endocytic processes in the maintenance of vacuolar integrity. IFN-γ-activation of macrophages preserves the integrity of phagosomes containing *Mycobacterium tuberculosis* (Mtb) through regulating the spaciousness of Mtb-containing phagosomes (Schnettger *et al.*, 2017). That is, Mtb, as well as other microbes, can enter macrophages either in tight-fitting phagosomes, in which the incoming bacterium is tightly enclosed by the phagosomal membrane, or spacious phagosomes, enlarged compartments in which the bacterium and phagosomal membrane are separated by aqueous space (Case *et al.*, 2016), easily observed in micrographs of infected macrophages. While resting macrophages internalize Mtb into tight phagosomes, which Mtb can penetrate through its expression of a type VII secretion system, IFN-γ treatment increases the frequency with which Mtb is internalized into spacious phagosomes, which are less permissive to disruption (Schnettger *et al.*, 2017). An influx of endocytic vesicles following infection converts tight phagosomes into spacious ones. Earlier work showed that spacious phagosomes likewise interfere with the ability of other Mycobacterium species to inhibit phagosome-lysosome fusion, a common strategy used by pathogens to avoid degradation in lysosomes. Whereas *Mycobacterium avium* residing within

tight phagosomes could inhibit phagosome maturation and resist delivery to lysosomes, *M. avium* artificially made to enter spacious phagosomes through the covalent attachment of latex beads to the bacterial surface were delivered to lysosomes with much higher frequency (de Chastellier *et al.*, 2009).

How the spaciousness of phagosomes might preserve their integrity is unknown, but Schnettger and colleagues proposed that the increased physical separation between the bacterium and the phagosomal membrane might prevent penetration of the membrane by bacterial virulence factors (Schnettger *et al.*, 2017). Overall, this study demonstrated a link between increased endocytic activity, spacious phagosome formation, and protection against membrane injury.

Other examples of increased endocytic activity and spacious phagosome formation affecting phagolysosomal integrity or bacterial survival have been described, but usually in terms of the benefit for the pathogen. Infection of macrophages with *Salmonella typhimurium* (*S. Tm*), another intracellular pathogen capable of perforating phagosomes, induces generalized membrane ruffling and macropinocytosis, an endocytic process for the non-selective uptake of extracellular fluid (Alpuche-Aranda *et al.*, 1994; Swanson and Watts, 1995). Depending on its opsonization status, *S.Tm* is internalized by macrophages into spacious phagosomes, which are morphologically identical to and likely represent macropinosomes (MPs), or into tight-fitting phagosomes that upon fusion with MPs become spacious. Spacious phagosome formation induced by *S. Tm* depends on its expression of a specific virulence factor, as bacteria lacking the factor fail to induce spacious phagosomes. Moreover, these mutants are defective for survival, suggesting that spacious phagosome formation promotes *Salmonella* survival within macrophages. Thus, whereas spacious phagosomes harboring Mtb are host-protective through promoting maintenance of phagosome integrity and promoting fusion with lysosomes (de

Chastellier *et al.*, 2009; Schnettger *et al.*, 2017), those containing *S. Tm* appear to be necessary for survival of the pathogen (Alpuche-Aranda *et al.*, 1994). Bacterial virulence factor expression also induces macropinocytosis that promotes the uptake of *Legionella pneumophila* into mouse macrophages (Watarai *et al.*, 2001) or phagosome rupture by *Shigella flexneri* in epithelial cells (Weiner *et al.*, 2016).

Taken together, these studies on the host and microbial factors governing the integrity of pathogen-containing phagolysosomes provides evidence for a link between endocytic vesicle formation and phagolysosomal injury. Whether the connection is protective or deleterious to the host likely depends on the interplay between host and microbial factors. Not known is whether the host response to phagolysosomal damage caused by pathogens represents a general mechanism that reinforces endolysosomes against multiple forms of membrane injury. To examine host responses to membrane damage in the absence of confounding effects of virulence factor expression by pathogens, we used silica beads as an agent for inducing phagolysosomal injury. Phagocytosis of silica beads by macrophages induces membrane damage leading to the leakage of fluorescent probes pre-loaded into endolysosomes (Davis *et al.*, 2012; Joshi *et al.*, 2015).

Using this experimental system, we investigated the cellular mechanism of renitence, focusing specifically on how LPS stimulation of macrophages confers protection against lysosomal damage. We first identified key differences in the response of LPS-activated versus resting macrophages to silica bead-mediated injury. Through this approach, we defined the kinetics of renitence and the size range of molecules released after bead challenge. Morphological comparison of resting versus LPS-treated macrophages in these studies led us to discover a structural correlate of renitence: large, damage-resistant vacuoles positioned adjacent

to bead-containing phagosomes. These structures, which, for reasons outlined later, we term "renitence vacuoles," resembled spacious phagosomes. Here we report the dynamics of renitence vacuole formation and their contribution to lysosomal damage protection by renitence. Overall, this work characterizes the responses of resting and LPS-activated macrophages to lysosomal injury and provides evidence for a model in which endocytic processes aid in the protection against lysosomal damage in activated macrophages.

2.3 Materials and Methods

2.3.1 Materials

DMEM, RPMI 1640, fetal bovine serum (certified), HBSS, fluorescein dextran (Fdx; average molecular weight 3, 10, 40, and 70 kDa), Texas Red dextran (70 kDa), nigericin, valinomycin, and 12 mm circular coverslips were purchased from ThermoFisher (Waltham, MA). Recombinant mouse macrophage colony-stimulating factor (M-CSF) for macrophage differentiation was purchased from Peprotech (Rocky Hill, NJ), and that used for assays of macropinocytosis was purchased from R&D Systems (Minneapolis, MN). LPS from *Salmonella typhimuirum* (no. 225) was purchased from List Biological Laboratories (Campbell, CA). EIPA was purchased from Tocris (Minneapolis, MN). 35 mm dishes with attached 14 mm coverglass were purchased from MatTek Corporation (Ashland, MA). 0.01% poly-L-lysine solution and BSA were purchased from Sigma (St. Louis, MO).

2.3.2 Particle preparation

3 μm silica dioxide microspheres were purchased from Microspheres-Nanospheres, a subsidiary of Corpuscular Inc (Cold Spring, NY). Before use, the microspheres were acid-washed (AW) overnight in 1N HCl, then rinsed several times with Milli-Q water. To generate non-damaging beads, AW beads were first coated with 0.1 M poly-L-lysine (PLL) for 30 min,

washed several times in water, then coated for 30 min with 5 mg/ml bovine serum albumin (BSA).

2.3.3 Bone marrow macrophage isolation and culture

C57BL6/J mice were purchased from The Jackson Laboratory (Bar Harbor, ME). Bone marrow-derived macrophages (BMM) were obtained as previously described (Davis *et al.*, 2012), with slight modification. Briefly, marrow cells extruded from the femurs and tiba of mice were differentiated into macrophages through culture for 6-8 days in DMEM containing 10% FCS and 50 ng/ml recombinant M-CSF. All animal-related procedures were approved by the University of Michigan Committee on Use and Care of Animals.

2.3.4 Cell culture and stimulation

BMM were plated onto glass-bottom microwell dishes (MatTek) in RPMI 1640 containing 10% FCS. To label lysosomes, BMM were incubated overnight with 150 μg/ml fluorescein dextran (Fdx) of various molecular weights (3, 10, 40, or 70 kDa), and the next day rinsed in Ringer's buffer and returned to unlabeled media for at least 3 hours before the start of imaging. LPS (100 ng/ml) was added to cells during both the overnight pulse and chase period. Lysosomal damage was induced by feeding BMM 3 μm AW beads in RPMI lacking serum for 60 min. AW beads were added at a concentration empirically determined to result in uptake of on average 3 to 4 beads per cell by both resting and LPS-activated BMM. All analyses of damage were performed on cells that had internalized 3 to 7 beads per cell.

In studies assessing the effect of macropinocytosis on renitence, macropinocytosis was stimulated and inhibited with the following treatments. To stimulate macropinocytosis, M-CSF (200 ng/ml) was included in the media during the time of AW bead incubation. To inhibit

macropinocytosis, BMM were pre-treated with EIPA (25 μM) for 30 min before the start of bead incubation, then fed beads in RPMI containing 25 μM EIPA.

2.3.5 Measurement of lysosomal damage by ratiometric imaging

Damage to lysosomes was measured as previously described, using an assay for ratiometric measurement of pH (Davis and Swanson, 2010; Davis *et al.*, 2012). BMM containing Fdx-labelled lysosomes were imaged by fluorescence microscopy after 60 min incubation in the presence or absence of AW or BSA-coated beads. Images were acquired on a Nikon TE300 inverted microscope equipped with a mercury arc lamp, 60× Plan-Apochromat 1.4-numerical aperture objective, cooled digital CCD camera (Quantix Photometrics, Tucson, AZ), temperature-controlled stage, and a FITC ratiometric dichroic mirror (Chroma Technology Corporation, Bellows Falls, VT). For each field of cells imaged, three images were acquired: one phase-contrast image, which allowed enumeration of bead number per cell, and two fluorescent images, from which pH information was obtained. Fluorescence images of Fdx were captured using a single emission filter centered at 535 nm and two different excitation filters, centered at 440 nm or 490 nm. Image acquisition and analysis were performed using Metamorph software (Molecular Devices, Sunnyvale, CA).

When excited at 440 nm, the fluorescent signal emitted by Fdx is relatively insensitive to pH; when excited at 490 nm, Fdx signal varies with pH. Taking the ratio of fluorescence intensities captured in the 490 and 440 channels respectively (i.e. Fdx ex. 490/Fdx ex. 440) yields volume-corrected pH information for each pixel in the image. To convert 490 nm/440 nm fluorescence intensities into pH values, a calibration curve was generated by measuring 490 nm/440 nm excitation ratios of Fdx in BMMs exposed to the ionophores nigericin (10 uM) and valinomycin (10 uM) in clamping buffers (130 mM KCl, 1 mM $MgCl_2$, 15 mM HEPES, 15 mM

MES) held at a fixed pH (pH 9, 7.5, 7.0, 6.5, 6.0, 5.5, 5.0, 4.5, or 4.0). Average 490 nm/440 nm ratio values were determined for Fdx within cells bathed in each pH buffer, and a four-variable sigmoidal standard curve was generated using GraphPad PRISM software (GraphPad Software Inc; La Jolla, CA).

Cellular pH maps were generated by using a color look-up table to assign to each pixel in the image a color that corresponds to the pH value associated with the pixel. Acidic regions were assigned warm colors, whereas pH-neutral regions were assigned cool colors.

Release of dye from lysosomes was indicated by the presence of dye in cellular regions whose pH was greater than 5.5. Masks representing pixels whose pH > 5.5 in Fdx 490 nm/440 nm ratio images were created and transferred to 440 nm excitation images. Due to the insensitivity of Fdx to pH at this wavelength, fluorescence intensity values in 440 nm excitation images are taken to be proportional to the amount of Fdx in each pixel. To determine the fraction of Fdx released from lysosomes within individual cells, the 440 nm fluorescence intensities of pixels whose pH > 5.5 were summed, and this value was divided by the total 440 nm fluorescence intensity for a given cell.

2.3.6 Analysis of vacuole frequency

Renitence vacuole (RV) frequency was determined in acquired images of resting or LPS-treated BMM from which measurements of lysosomal damage were made. Images from experiments in which BMM were fed AW or BSA-coated beads for 60 min were scored for the presence or absence of RVs. Vacuolar structures observed within cells were scored as RVs by the following criteria: (1) appearance on the phase contrast image as a circumscribed phase-dense region adjacent to an internalized bead, and (2) presence of Fdx within the structure. RV frequency

was quantified as the percent of cells containing one or more vacuoles within a given condition. All cells containing at least one bead were included in the analysis.

2.3.7 Macropinosome counting assay

To measure macropinocytosis, resting or LPS-treated BMM plated on 12 mm circular coverslips were pulsed for 10 min with 70 kDa Fdx (0.5 mg/ml). In control conditions, macropinocytosis was stimulated by inclusion of M-CSF (200 ng/ml) during the time of the Fdx pulse or inhibited by 30 min pre-treatment with EIPA (25 μM) before the start of the pulse. Cells were gently washed with HBSS to remove uningested probe, fixed for 30 min at 37°C with fixation buffer (75 mM lysine-HCl, 37.5 mM Na_2HPO_4, 4.5% sucrose, 2% paraformaldehyde, 10 mM sodium periodate), and imaged by fluorescence microscopy. MetaMorph software was used to merge phase contrast and background-subtracted Fdx images. The number of MPs per cell was determined by scoring the number of Fdx-positive phase bright vesicles in the merged images. At least 25 cells were scored for each experiment.

2.3.8 Time-lapse video microscopy

BMM plated onto glass-bottom microwell dishes were incubated overnight with either Lucifer yellow (LY; 1 mg/ml) or 70 kDa Texas Red dextran (TRDx; 50 μg/ml), and then chased in unlabeled media for at least 3 h the next day. Cells containing LY-labelled lysosomes were fed AW beads and immediately mounted for imaging. Cells containing TRDx-labelled lysosomes were fed AW beads and 0.5 mg/ml 70 kDa Fdx for 5 min, washed, and mounted for imaging. Excitation and emission wavelengths used were as follows: LY (ex. 430-em. 535), TRDx (ex. 572-em. 632), Fdx (ex. 490-em. 535). Images were collected on a Nikon TE inverted microscope equipped with ECFP-EYFP-mCherry and DAPI-FITC-Texas Red dichroic mirrors (Chroma Technology Corporation). LY fluorescence images were collected using the former,

and Fdx and TRDx were collected using the latter. Images for each condition were collected in two (Figure 2.7 and Supplemental Video S3) or three (Figures 2.4 and Supplemental Videos S1-S2 and S4-S7) independent experiments.

2.3.9 Statistical methods

Statistical analysis for all experiments was performed using GraphPad Prism software (GraphPad Software Inc; La Jolla, CA). Lysosomal damage levels between groups were compared using two-way ANOVA with multiple comparisons. Comparison of vacuole frequency between groups was performed using a two-tailed, unpaired t-test (Figure 2.3.B) or two-way ANOVA with multiple comparisons (Figure 2.3.D). MP formation between groups was compared using a two-tailed, unpaired t-test with Welch's correction.

2.4 Results

2.4.1 LPS stimulation alters the time course of phagocytosis-mediated lysosomal damage

To characterize the kinetics of lysosomal damage and LPS-mediated protection following silica bead-mediated injury, we performed a time course of bead-mediated damage in resting versus LPS-activated macrophages. Damage to lysosomes within live murine bone marrow-derived macrophages (BMM) was measured using a ratiometric fluorescence microscopy assay developed previously (Davis and Swanson, 2010). Briefly, BMM whose lysosomes were pulse-chase labelled with the pH-sensitive dye, fluorescein dextran (Fdx), were fed 3 μm AW silica beads (AW beads) for various time points to induce phagolysosomal damage. Damage was quantified on a per-cell basis as the percent of Fdx released from pre-labelled lysosomes into the cytoplasm, and reported as the average percent of Fdx release per cell for each condition. Whereas resting macrophages experienced increasing levels of damage over time, proceeding to near-complete dye release, LPS-activated macrophages restricted damage to the first 15 min of

challenge (Figure 2.1.A). After incurring an initial damaging insult, LPS-activated macrophages either limited further progression of damage or quickly repaired the original breach. Thus, the basis of protection in LPS-activated macrophages lies in activities that preserve lysosomal integrity after the first 15 min of damage initiation.

2.4.2 LPS stimulation protects against damage that is all-or-none

As our damage measurements are made on a per-cell basis, we could achieve a more granular analysis by plotting in histogram form the distribution of damage levels measured from the individual cells contributing to the average Fdx release data. The histograms depict the proportion of cells in each condition experiencing a given range of damage after exposure to beads for 15 or 60 min (Figure 2.1.B). By this analysis, we made the surprising observation that damage caused by AW beads in both resting and LPS-treated BMM resulted mostly in either complete (90-100%) or negligible (0-10%) dye release. Only a small proportion of cells (<30%) experienced levels of dye release between these two extremes.

The progression of damage between 15 and 60 min of bead incubation seen at the population level in resting macrophages was accounted for by a reduction in the proportion of cells experiencing low levels of damage and an increase in the proportion of cells experiencing high levels of damage. This shift was resisted in LPS-treated macrophages, for which the proportion of cells experiencing a given range of damage stayed consistent over time. These analyses uncovered two insights about renitence: (1) lysosomal damage caused by AW beads was largely all-or none; and (2) LPS-stimulated macrophages experienced damage heterogeneously; one population had near-complete damage within 15 min of receiving beads, whereas another resisted damage throughout the course of bead incubation. Together, these

kinetic studies indicated that LPS-stimulated macrophages restrict damage to a narrow time window by preventing a protected population of cells from undergoing damage.

2.4.3 Silica bead uptake initiates small membrane breaches

We next determined the size of the membrane breaches formed by ingested AW beads and the size-dependence of LPS-induced renitence. We hypothesized that LPS-treated macrophages prevent the expansion of pores formed by AW beads whereas resting macrophages do not. To test this hypothesis, we measured the upper size limit of Fdx molecules released from lysosomes after bead-mediated injury. Macrophage lysosomes were first loaded with fluorescein dyes conjugated to dextran molecules of various molecular weights, ranging from 3 kDa (the size of dye used in the standard damage assays) to 70 kDa Fdx, and then subjected to 60 min AW bead incubation. Whereas leakage of 3 kDa Fdx from lysosomes occurred readily, the release of larger dyes was more limited (Figure 2.2). The release of the two largest dyes tested (40 and 70 kDa) was almost completely restricted in both resting and LPS-treated BMM, suggesting preferential release of small versus large dyes. The extent of 10 kDa Fdx release showed significant variation between experimental replicates. Release was either comparable to that of 3 kDa (n=2) or almost completely restricted (n=2). To represent this unusually large variation, the individual replicate data was plotted along with the average percent Fdx release values measured across all replicates for a given condition. The variation may be explained by the presence of a mixture of dye sizes in commercially available preparations of Fdx. Regardless of the source of variation, these data suggest that damage induced by AW beads permits the release of small but not large molecules. Renitence likewise preferentially protects against the release of small molecules, as no statistically significant differences were noted in the extent of release of dyes $\geq$ 10 kDa in resting versus LPS-treated BMM. Finally, as the upper limits of the size of membrane

breach caused by AW beads in resting and LPS-treated macrophages were similar, it seems unlikely that differences in the ability to limit pore expansion underlie renitence.

2.4.4 Damage-resistant vacuoles are formed in response to phagolysosomal injury in LPS-activated macrophages

To uncover mechanistic details of renitence, we compared morphological features of resting versus LPS-treated macrophages following AW bead uptake. Using phase contrast and ratiometric fluorescence images, we correlated states of damage or protection with cell morphology. By analyzing profiles of hundreds of cells, we noticed a distinct morphological feature common to LPS-treated macrophages, but rarely seen in resting macrophages. After 60 min bead incubation with AW beads, LPS-treated macrophages often contained large, vacuolar structures adjacent to bead-containing phagosomes (Figure 2.3.A). These vacuoles were visible on phase contrast images as circumscribed phase-dense regions adjacent to internalized beads. They often contained Fdx, suggesting their origin as, or fusion with, lysosomes. Most strikingly, in pseudocolor pH images these vacuoles were the most acidic Fdx-labeled regions within cells (Figure 2.3.A). Even in cells in which most of the lysosomal network was damaged, as judged by the localization of Fdx in pH-neutral regions, the vacuoles persisted as intact, acidic structures.

The acidic content of vacuoles despite their proximity to membrane-damaging beads suggested a possible protective function. To interrogate the role of vacuoles in mediating protection, we first enumerated vacuole frequency in resting and LPS-treated BMM after 60 min incubation with AW beads. Vacuoles were scored as phase-dense structures that contained Fdx and that appeared adjacent to an internalized bead. Analyzing over 2500 cells per condition, we found that AW bead incubation induced vacuole formation in about 25% of LPS-treated BMM,

but in less than 10% of resting BMM (Figure 2.3.B). To determine whether vacuole formation required membrane damage, we assessed vacuole frequency in cells fed damaging versus non-damaging beads. Non-damaging beads were generated by conjugating bovine serum albumin (BSA) to AW silica beads, which attenuates damage presumably by neutralizing the negative charge of the silica beads. Indeed, administration of BSA-coated beads induced very low levels of injury (Figure 2.3.C). Correspondingly, few vacuoles were observed (Figure 2.3.D), suggesting that vacuole formation occurred specifically in response to membrane damage.

2.4.5 Damaging bead uptake induces renitence vacuole and MP formation in LPS-activated but not resting macrophages

To capture the dynamics of vacuole formation, we performed time-lapse imaging of resting vs LPS-treated BMM. Before imaging, lysosomes were pulse-chase labeled with the fluid-phase probe Lucifer Yellow (LY). Upon bead addition, phase contrast and LY fluorescence images were captured every 20 sec for one hour. The resulting movies revealed that phagocytosis of AW beads in LPS-treated, but not resting, BMM was accompanied by the formation of phase-bright vacuoles associated with phagosomes. In a representative LPS-activated macrophage, the appearance of multiple vacuoles surrounding a bead-containing phagosome became visible 7 min after bead incubation (Figure 2.4.B). In multiple cells analyzed, the vacuoles appeared shortly after exposure to beads (Supplemental Video S1). Some vacuoles received LY from lysosomes, indicating their ability to fuse with lysosomes. Notably, the vacuoles did not shrink but instead persisted around the bead throughout its course of trafficking in the cell.

Coincident with bead phagocytosis and vacuole formation, LPS-treated macrophages underwent vigorous membrane ruffling leading to the formation of numerous phase-bright

structures in the cell. Morphologically these structures resembled macropinosomes (MPs), vesicles formed through a form of fluid-phase endocytosis called macropinocytosis (Swanson and Watts, 1995). The large size of vacuoles, their coincident appearance with MPs, and their persistence near a bead even 60 min after administration suggested that they form as MPs that enlarge and persist near phagolysosomes in the context of membrane injury. Neither vacuoles nor MPs were observed within resting macrophages, which did however undergo continuous membrane ruffling upon bead incubation. As the vacuoles observed by time-lapse microscopy share many characteristics with those quantified in fixed time point analyses in Figure 3, they both likely are of the same origin. We refer to these MP-like, periphagosomal organelles as "renitence vacuoles" (RVs).

RVs resembled spacious phagosomes (SPs) previously observed within macrophages infected with the intracellular bacterial pathogen *Salmonella typhimurium* (Alpuche-Aranda *et al.*, 1994). SP formation was thought to be induced by the bacteria to promote their survival within the host environment. Our observation of a compartment of strikingly similar morphology in the setting of non-infectious membrane injury suggests that the structures may be formed instead as a part of a generalized host protective response in activated macrophages. In fact, evidence from time-lapse imaging of LPS-activated BMM fed non-damaging phagocytic targets suggests macropinocytosis and vacuole formation accompany phagocytosis generally. BMM fed either BSA-coated beads (Figure 2.5.A and Supplemental Videos S4-S5), or IgG-opsonized sheep red blood cells (sRBCs) (Figure 2.5.B and Supplemental Video S6), shown previously to be non-damaging to resting or LPS-treated BMM (Davis and Swanson, 2010), also induced the formation of vacuoles adjacent to the internalized bead or sRBC. In contrast,

vacuoles were not observed in resting BMM fed non-damaging BSA-coated beads (Figure 2.5.C and Supplemental Video S7).

How do these results reconcile with those in Figure 2.3.D, in which few vacuoles were detected after 60 min incubation with BSA-coated beads? The presence of vacuoles in dynamic analyses but their absence in static analyses suggested that vacuoles associated with non-damaging bead phagocytosis typically form and shrink before the 60 min time point for analysis. Consistent with this model, the vacuoles in videos capturing the phagocytosis of BSA-coated beads differed in two ways from RVs formed upon AW bead uptake. First, while characteristic RVs formed coincident with bead phagocytosis, the vacuoles accompanying BSA-coated bead phagocytosis formed more slowly, with a delay of several minutes between bead internalization and vacuole formation. Second, once formed, the vacuoles generally shrank quickly, like typical MPs (Supplemental Video S5). Only in one of three independent experiments did we capture a large, bead-adjoining, persistent vacuole in an LPS-treated BMM fed BSA-coated beads (Figure 2.5.A and Supplemental Video S4). These studies suggest that (1) MP and vacuole formation are induced by phagocytosis of damaging and non-damaging particles in LPS-activated macrophages, and (2) phagocytosis of damaging particles induces additional activities that cause RVs to persist.

2.4.6 Macropinocytosis is necessary but not sufficient for renitence

Based on our morphological findings, we hypothesized that RVs, as persistent MPs, contribute to renitence in LPS-activated macrophages. To interrogate the role of macropinocytosis in renitence, we first assessed the extent to which LPS activation of macrophages induces macropinocytosis. Using a microscopic assay for counting MPs, we observed that overnight LPS stimulation of BMM induced MP formation to a similar degree as

that induced by acute stimulation with macrophage colony-stimulating factor (M-CSF) (Figure 2.6.A), long known to induce macropinocytosis in macrophages (Racoosin and Swanson, 1989). Confirming our detection of bona fide MPs, treatment of LPS-activated BMM with the inhibitor 5-(*N*-ethyl-*N*-isopropyl) amiloride (EIPA) reduced MP formation (Figure 2.6.A).

The extent of macropinocytosis increased with the duration of LPS incubation (Figure 2.6.B). The time course of LPS-induced macropinocytosis strikingly paralleled the time course of LPS-induced renitence, in which protection was first seen in BMM after 6 h LPS stimulation and peaked in BMM stimulated with LPS overnight (Davis *et al.*, 2012). Similarly, macropinocytosis was readily detectable in BMM treated for 6 h or 18 h with LPS, but not at earlier time points (Figure 2.6.B). Thus, macropinocytosis is upregulated following LPS stimulation with the same kinetics as renitence.

To investigate whether MP and renitence are directly related, we next assessed the effect of MP induction and inhibition on renitence. Induction of MP through inclusion of M-CSF in the media at the time of AW bead incubation led to a modest reduction in damage, suggesting induction of macropinocytosis is not sufficient to induce renitence in resting BMM (Figure 2.6.C). However, inhibition of MP by EIPA exacerbated damage in LPS-activated macrophages and eliminated renitence (Figure 2.6.D). These results suggested that macropinocytosis contributes to renitence in LPS-activated macrophages.

2.4.7 Renitence vacuoles originate as macropinosomes and fuse with lysosomes

To investigate how MPs contribute to renitence, we visualized the dynamic interactions of MPs, RVs, bead-containing phagosomes, and lysosomes following silica bead uptake. Time-lapse video microscopy of AW bead phagocytosis and RV formation was performed in LPS-treated BMM whose lysosomal and endocytic compartments were labelled with different

fluorescent probes. TRDx (average molecular weight 70 kDa) labelling of lysosomes was followed by co-administration of AW beads and Fdx (average molecular weight 70 kDa), which allowed for the labeling of macropinosomes formed during bead phagocytosis. After 5 min incubation with beads and Fdx, cells were washed to remove extracellular probe, and mounted for time-lapse imaging by phase contrast, Fdx, and TRDx fluorescence microscopy.

At the start of imaging, RVs had already formed and were labelled with Fdx (Figure 2.7.A and Supplemental Video S3), confirming their origin as macropinosomes. RVs persisted next to bead-containing phagosomes through all time points imaged, long after normal MPs would have already shrunk (Racoosin and Swanson, 1993), supporting the conclusion that RVs represent persistent MPs.

MP-derived RVs eventually fused with lysosomes, as evidenced by the localization of TRDx within RVs at later time points (Figure 2.7.A and Supplemental Video S3). Fusion events for two separate RVs were noted 13 min and 21 min after bead incubation (Figure 6A), with similar events observed in multiple cells. These observations corroborate findings from earlier time-lapse movies (Figure 2.4) and images of LPS-treated BMM after 60 min AW bead incubation (Figure 2.3), at which point almost all RVs had received Fdx from pre-labelled lysosomes.

Interestingly, while RVs fused with lysosomes, their associated bead-containing phagosomes did not. Phagosome fusion with lysosomes was judged as TRDx localization around internalized beads. Phagosomes not associated with RVs were able to fuse with lysosomes, whereas phagosomes that associated with RVs were not. Both types of phagosomes could occur within the same cell. In the representative cell shown in Figure 2.7.B, two bead-containing phagosomes, seen at the top of the image, were associated with RVs. While the RVs

themselves clearly received TRDx from lysosomes (TRDx and Merge), the bead-containing phagosomes, denoted by asterisks, did not. In contrast, phagosomes in another region of the same cell did not associate with RVs, but did fuse with lysosomes, as a ring of TRDx fluorescence appears around most beads in the region. The patterns of interactions suggest a mechanism by which RVs may protect against lysosomal damage. Positioned as structural intermediates between potentially damaged bead-containing phagosomes and lysosomes whose integrity is critical to maintain. RVs may act as structural barriers that prevent phagosome-lysosome fusion (Figure 2.8). In doing so, RVs would contain damage to early endocytic compartments and prevent the propagation of damage throughout the entire endolysosomal network.

2.5 Discussion

This work reports the discovery of renitence vacuoles, damage-resistant structures formed in LPS-activated macrophages that protect against phagocytosis-mediated lysosomal injury. The persistence of RVs in the setting of damaging bead uptake, their maintenance of low pH despite their proximity to a damaging particle, and their correlation with renitence provide evidence of a protective function. Characterization of vacuole dynamics by time-lapse microscopy led us to develop a model for how RVs confer protection against lysosomal damage (Figure 2.8): LPS-activated macrophages in the presence or absence of phagocytic challenge undergo membrane ruffling and macropinocytosis. In cells undergoing phagocytosis, macropinocytosis occurs at multiple regions throughout the cell, but is particularly robust in the area surrounding the incoming phagosome. In association with this process, some MPs enlarge and persist around the bead-containing phagosomes as vacuoles. The persistence of RVs likely

relates to their protective function, as conventional MPs and vacuoles formed during uptake of non-damaging beads eventually shrink.

How might these persistent macropinocytic vacuoles confer protection against lysosomal damage? Observations of the dynamic interactions of RVs, bead-containing phagosomes, and lysosomes by time-lapse video microscopy suggested a mechanism. While phagosomes not associated with RVs fused with lysosomes, as did RVs themselves, the phagosomes associated with RVs did not. Based on this pattern of interactions, we propose that RVs act as a physical buffer between bead-containing phagosomes and lysosomes to prevent their fusion. The effect would be to contain damage to compartments upstream of the lysosome by preventing the trafficking of damaged organelles or damaging agents contained within the organelles to lysosomes (Boya and Kroemer, 2008; Hornung *et al.*, 2008). As compromise of lysosome integrity even in the absence of infection would lead to the release of acid and hydrolytic enzymes into the cytoplasm of the cell, it is not surprising that the cell would have measures to avoid this deleterious fate. In addition to acting as decoy vesicles that fuse with lysosomes in the place of damaged phagosomes, RVs could also promote the repair of damaged phagolysosomes, although the topology of membrane interactions that could facilitate such a repair process is difficult to envision.

The striking morphological similarity of RVs to spacious phagosomes (SPs) and their similar context for formation suggests that the two structures are formed through related mechanisms. A notable feature of both RVs and SPs is their persistence. While SPs were first described several years ago (Alpuche-Aranda *et al.*, 1994), little is known about the factors that promote their persistence. Models can be proposed based on our knowledge of the factors that govern how MPs and other endocytic vesicles shrink. MPs formed in macrophages stimulated

with M-CSF shrink via fusion with lysosomes within 15 min after their formation (Racoosin and Swanson, 1993). RVs thus might persist due to defects in their trafficking to lysosomes. However, as RVs are able to receive dye from pre-labelled lysosomes, and in fact nearly all do after 60 min incubation with AW beads, a defect in fusion with lysosomes seems unlikely.

Alternatively, the persistence of RVs may be due to an increase of fluid influx into the compartment. Such increased influx could result from a change in the expression or activity of aquaporins, membrane channels which permit the transport of water. Precise regulation of the level of Aquaporin-1 (AQP1) in mammalian cells is necessary for maintaining the integrity of phagosomes against rupture by Gram-positive group A streptococcus, *Salmonella typhimurium*, or *Listeria monocytogenes* (Radtke *et al.*, 2007; Radtke and O'Riordan, 2008; Radtke *et al.*, 2011), as either an excess or deficiency of AQP1 leads to destabilization of the phagosome and enhanced bacterial escape. Maintenance of homeostatic levels of AQP1 is controlled by the host protein TANK-binding-kinase-1 (TBK1) (Radtke and O'Riordan, 2008). As TBK1 expression is upregulated by LPS activation (Hemmi *et al.*, 2004), it is possible that osmotic effects resulting from perturbations in aquaporin levels or activity by LPS may contribute to renitence vacuole persistence and renitence generally.

MPs themselves could be a source of extracellular fluid that maintains vacuole persistence. Additionally, as membrane-bound vesicles, MPs could contribute membrane necessary for the expansion of the compartment. This work introduces several concepts connecting LPS activation, macropinocytosis, and renitence that are consistent with such a model. We showed that LPS activation induces macropinocytosis in macrophages to a similar degree as that induced by acute stimulation with M-CSF. Additionally, LPS induction of macropinocytosis follows a time course that parallels LPS induction of renitence. The

continuous membrane ruffling and macropinocytosis observed in macrophages stimulated overnight with LPS could potentially supply a constant source of fluid to support the maintenance of a persistent RV. Consistent with this model, we found that macropinocytosis was necessary for renitence, as pre-treatment of macrophages with the macropinocytic inhibitor EIPA abrogated protection in LPS-activated macrophages.

At the molecular level, normal MP shrinkage requires the activity of the phosphatidylinositol-3-phosphate 5-kinase PIKfyve (Shisheva, 2008; Krishna *et al.*, 2016). RV persistence thus could be due to a decrease in PIKfyve activity near damaged phagolysosomes in LPS-activated macrophages. Further investigation of the mechanism of RV persistence will require tools for inhibiting and inducing RV formation. Preliminary studies using pharmacological inhibitors suggest that renitence and RV formation depend on the activation of Akt but not mTOR. As Akt has been found to be recruited to membrane ruffles of forming MPs in macrophages stimulated with LPS (Wall *et al.*, 2017), it is conceivable that Akt activation in the context of phagocytosis-mediated damage could recruit other factors to the MP to initiate the formation and eventual persistence of RVs. Furthermore, TBK1 and PIKfvye, two candidate molecules for regulating RV persistence, are both known to interact with Akt (Berwick *et al.*, 2004; Joung *et al.*, 2011; Er *et al.*, 2013). Further dissection of the molecular mechanism of renitence and RV formation is the focus of ongoing studies.

Our work clarifies the kinetics of lysosomal damage and the sizes of molecules released from lysosomes following silica bead phagocytosis in macrophages. AW beads induced lysosomal damage as early as 15 min after incubation in both resting and LPS-treated BMM, and permitted the release of small (3 kDa and, in some cases, 10 kDa) but not large (40 kDa and 70 kDa) molecules. Our observations are consistent with those of other studies, in which incubation

of macrophages with opsonized or unopsonized silica particles led to the release of 4 kDa fluorescent dextrans from endolysosomes for a limited period following phagocytosis (Joshi *et al.*, 2015). The extent and timing of lysosomal damage we observed using AW beads also resembles that observed in macrophages infected with *Listeria monocytogenes*, an intracellular bacterial pathogen that initiates its escape from phagolysosomes through the expression of a pore-forming toxin, listeriolysin O (LLO). Beginning about 15 min after *L.m.* infection, small perforations of the phagosomal membrane are formed that allow the release of small molecular weight (522 Da) probes and expand over time to permit the release of larger (10 kDa) probes (Shaughnessy *et al.*, 2006). Interestingly, membrane perforations induced by LLO resulted in the inhibition of fusion of *L.m.*-containing phagosomes with lysosomes (Shaughnessy *et al.*, 2006). The block on maturation was thought to be timed to allow *L.m.* to prevent its delivery to the microbicidal environment of the lysosome before its escape into the cytosol, a common strategy employed by intracellular pathogens. However, our observation of a block on fusion of RV-associated AW bead-containing phagosomes in the absence of infection suggests the host may likewise have mechanisms to prevent the maturation of potentially-damaged phagosomes as a means of preserving the integrity of lysosomes. Together, these observations suggest that AW beads induce physiologically relevant levels of phagolysosomal injury, and that RVs form in response to small membrane perforations. Furthermore, renitence, which protects against the release of small but not large dyes, may have evolved as a mechanism of defense against small membrane perforations inflicted by pathogens.

Our assay for lysosomal damage allowed for sensitive detection of damage across a large sample of cells. Analyzing the distribution of damage measured within individual cells revealed that damage induced by AW beads in both resting and LPS-treated BMM was all-or-none. LPS

activation conferred protection by limiting damage to the first 15 min of bead exposure and preventing the progression of damage in a protected subset of cells. Why certain subsets of LPS-treated BMM are susceptible to damage whereas others are resistant, however, is unknown. We considered whether the population of cells that resisted damage were more likely to contain RVs. However, based on preliminary analyses, no correlation exists between vacuole status after 60 min incubation with AW beads and the propensity of cells for protection. While this result was surprising, it is possible that the vacuoles observed at 60 min are remnants of an earlier protective process and may not serve as a marker of damage for a given individual cell. Future studies will continue to dissect the timing and mechanism by which RVs confer protection.

The morphological resemblance of RVs with SPs has been noted. However, the two structures likely represent different compartments topologically. That is, while SPs are phagosomes that have enlarged, likely due to macropinocytic influx into a bacteria-containing phagosome, RVs are formed adjacent to bead-containing phagosomes, and thus likely represent a distinct compartment. Whether RVs and adjoining bead-containing phagosomes can fuse, or whether they exist as separate organelles that do not exchange membrane is not known. The exact ultrastructural details of the topologic relationship of RVs and bead-containing phagosomes could theoretically be gained by electron microscopy, but the use of silica beads as a damaging agent poses technical challenges for sample preparation. However, our light microscopic studies provide evidence that RVs and bead-containing phagosomes likely do not fuse. First, whereas RVs internalize fluid-phase dye by endocytosis and receive dye from pre-labelled lysosomes, their neighboring bead-containing phagosomes do not. Second, the membranes of RVs are intact, as determined by their persistent acidity; adjacent phagosomes, because they contain a damaging particle, likely are damaged. If the two compartments were to

fuse, damage likely would be transferred to RVs, which would no longer be able to maintain their low pH.

The relationship noted here between silica bead-containing phagosomes and their associated RVs resembles the relationship between *Shigella flexneri*-containing vacuoles and nearby MPs described in epithelial cells (Weiner *et al.*, 2016). *Shigella flexneri* induces its entry into non-phagocytic host cells by stimulating macropinocytosis. The process of invasion into host cells was long thought to involve macropinocytic uptake of the bacteria into a compartment called the bacteria-containing vacuole (BCV). While BCVs and MPs were thought to represent various stages of the same compartment, the work by Weiner *et al.* demonstrates that the two structures are distinct. Much as we saw during silica bead uptake in macrophages, *Shigella flexneri* infection of epithelial cells induced extensive membrane ruffling and MP formation near the BCV. As fluid-phase dye that labelled incoming MPs never labelled the BCV, the compartments were established as separate. Interestingly, in the setting of *Shigella flexneri* infection, macropinocytosis was found to be necessary for the destabilization of and *Shigella flexneri* escape from the BCV, suggesting a role for macropinocytosis in facilitating membrane damage. Our work, in contrast, finds a membrane protective role for macropinocytosis, as evidenced by its necessity for renitence. The two findings, however, are not necessarily conflicting. Instead, they support a larger model in which macropinocytosis represents a host protective response that is (1) induced by LPS activation or infection, (2) accompanies phagocytosis of particles or pathogens, (3) promotes membrane protection in the setting of injury, and (4) may be hijacked by some pathogens through the expression of virulence factors. As endocytic processes seem to limit the escape of some pathogens (Schnettger *et al.*, 2017) but promote the pathogenesis of others (Alpuche-Aranda *et al.*, 1994; Watarai *et al.*, 2001; Weiner *et*

al., 2016), phagolysosomal integrity in the context of infection is likely determined by the outcome of the interactions between host and microbial factors.

Our work examined responses of macrophages to phagocytosis-mediated membrane damage. Our model of silica bead-mediated lysosomal damage mimicked injury produced by pathogens and allowed for the interrogation of host responses to membrane damage in the absence of confounding effects of virulence factor expression by pathogens. Using this reductionist approach, we discovered macropinocytosis and renitence vacuole formation as activities accompanying particle phagocytosis in LPS-activated macrophages, activities whose significance during conventional phagocytosis is unclear, but that in the setting of membrane injury confer protection. As analogous processes occur in the context of infection, we believe we have identified a general mechanism upregulated by macrophage activation or infection that preserves endolysosomal integrity following phagocytic encounter with membrane-damaging threats.

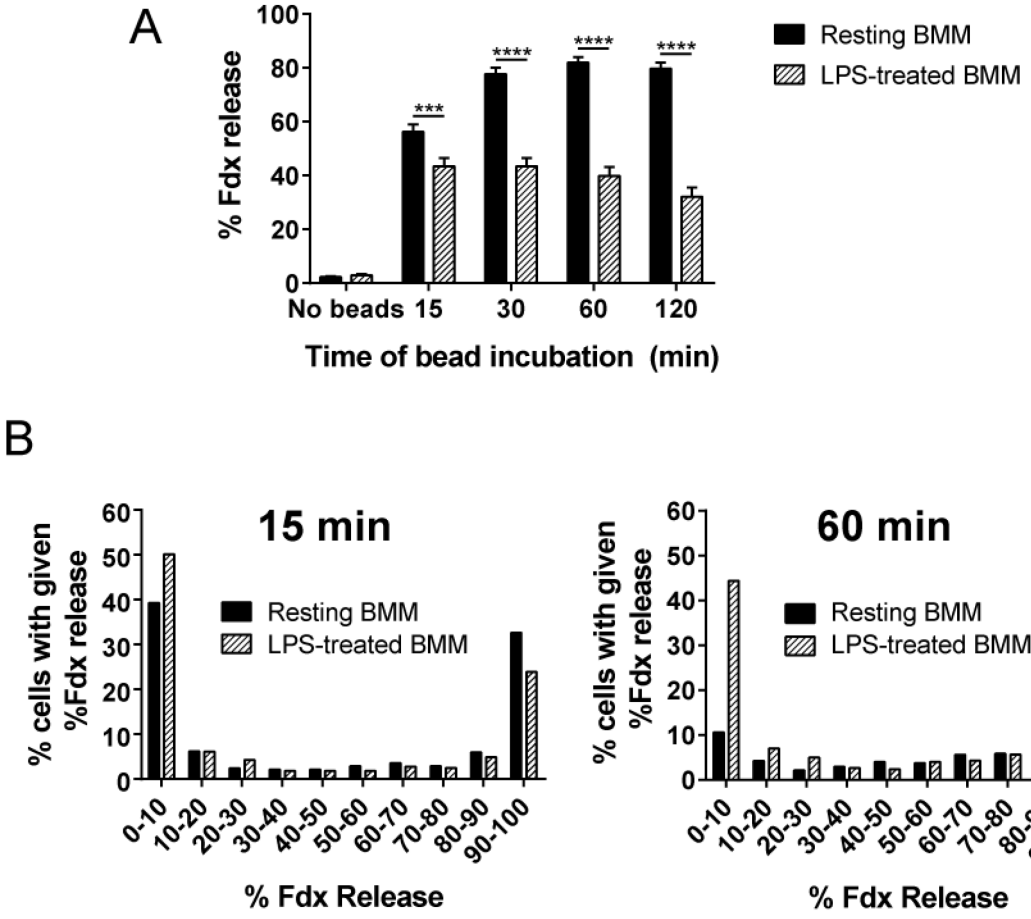

Figure 2.1. LPS stimulation limits the time window of phagocytosis-mediated damage to macrophage lysosomes.

(A) Time course of acid-washed (AW) bead-mediated lysosomal damage in resting or LPS-treated mouse bone marrow-derived macrophages (BMM). Release of fluorescein dextran (Fdx) from pre-labelled lysosomes was measured on a per-cell basis after incubating BMM with AW beads for the indicated times. Bars show average percent Fdx release per cell ± SEM from 4 independent experiments, in which cells containing 3-7 beads were analyzed (n > 120 cells). ***$p \leq 0.001$, ****$p \leq 0.0001$.

(B) Individual cell data from (1A) plotted in histogram form to show the percent of cells within each condition experiencing a given range of lysosomal damage (represented in 10% increments on x-axis) after 15 (left) or 60 min (right) of exposure to AW beads.

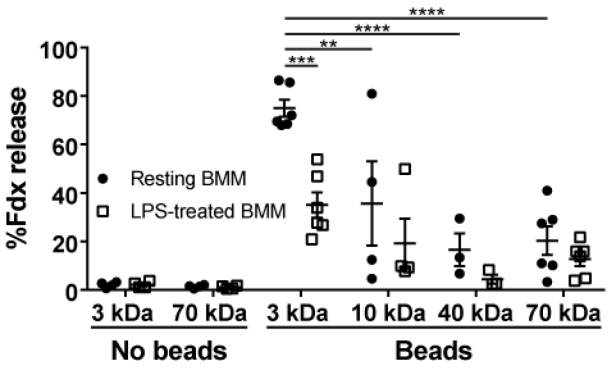

Figure 2.2. Silica bead uptake induces membrane injury that permits the release of small but not large molecules.

Lysosomes within resting or LPS-treated BMM were pulse-chase labelled with Fdx molecules of different sizes: 3, 10, 40, or 70 kDa. The extent of Fdx release after 60 min AW bead incubation was measured for each group of cells in at least 3 independent experiments. As significant variation in damage levels was seen between experiments for BMM pre-loaded with 10 kDa Fdx, Fdx release values from individual experiments are plotted along with the average percent Fdx release ± SEM across all replicates. In all bead-positive conditions, cells containing 3-7 beads were analyzed (n > 35 cells within each individual experiment). $^{**}p \leq 0.01$, $^{***}p \leq 0.001$, $^{****}p \leq 0.0001$.

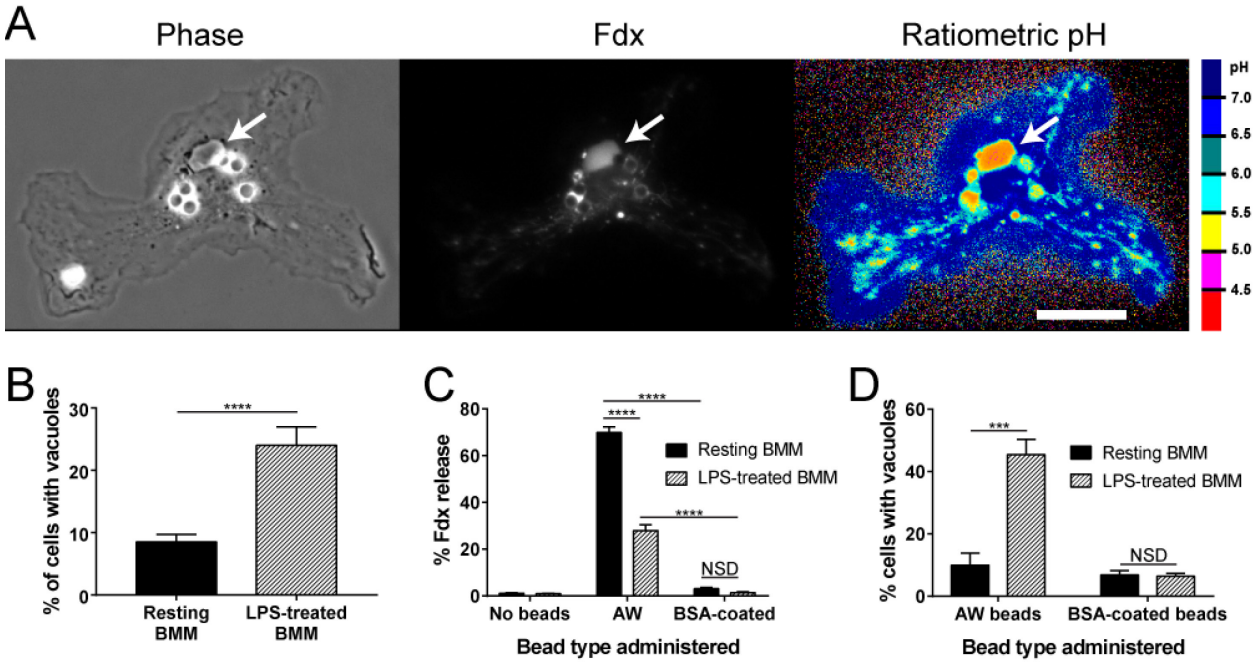

Figure 2.3. LPS-activated macrophages form damage-resistant vacuoles in response to phagolysosomal injury.

(A) Phase contrast, Fdx fluorescence (ex440-em535), and pseudocolor pH images of a representative LPS-treated macrophage harboring a damage-resistant vacuole, indicated with arrow. In the pseudocolor pH map of the cell, each Fdx pixel has been assigned a color representing the pH of the region in which the dye is localized. Blue represents dye that has entered pH neutral regions of the cell (i.e. has been released from lysosomes). Scale bar, 10 μm.

(B) Vacuole frequency in resting or LPS-treated BMM after 60 min AW bead incubation. Vacuoles were defined by the following criteria: (1) appearance on phase contrast image as a circumscribed phase-dense region adjacent to an internalized bead, and (2) presence of Fdx within the structure. Each bar displays the average ± SEM of the percent of cells within each condition harboring one or more vacuoles. All cells containing at least one bead were analyzed. (n = 27 expts, with over 2500 cells analyzed.) ****$p \leq 0.0001$.

(C) Average percent Fdx release ± SEM from pre-labelled lysosomes in resting or LPS-treated BMM after 60 min incubation with damaging (AW) or non-damaging (BSA-coated) beads. Bars represent data from 3 experiments, in which cells containing 3-7 beads per cell were analyzed (n > 170 cells). ****$p \leq 0.0001$.

(D) Vacuole frequency in resting or LPS-treated BMM after 60 min incubation with damaging (AW) or non-damaging (BSA-coated beads). Analysis was performed on the set of images used to determine Fdx release values in (3C). Bars represent the mean percent ± SEM of cells containing one or more vacuoles. ***$p \leq 0.001$.

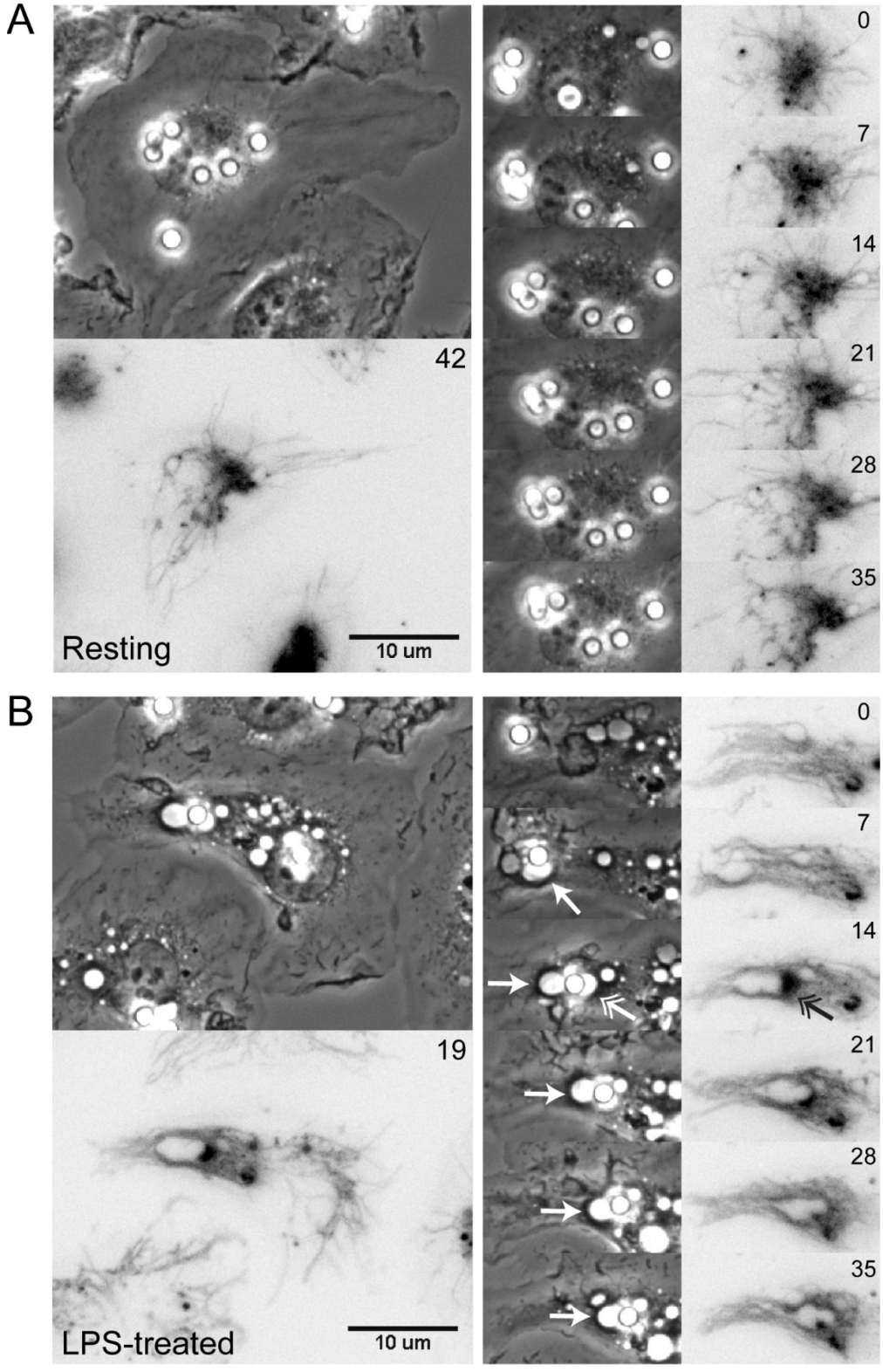
A
0
7
14
21
28
35
42
Resting
10 um
B
0
7
14
21
28
35
19
LPS-treated
10 um

Figure 2.4. Damaging bead uptake induces renitence vacuole and macropinosome formation in LPS-treated but not resting macrophages.

Resting (A) or LPS-treated BMM (B) whose lysosomes were labelled with Lucifer yellow (LY) were fed AW beads and imaged by time-lapse microscopy. Phase contrast and LY fluorescence images were captured every 20 seconds for one hour. Panels show selected frames of phase contrast and inverted contrast LY fluorescence images from corresponding time points in the time series. Elapsed time in minutes after the addition of AW beads (t=0 min) is shown in the top right of each subpanel. Single arrows in (B) mark regions in which numerous macropinosomes and vacuoles surround an incoming phagosome, a characteristic event accompanying phagocytosis in LPS-treated BMM. Double arrow (B, 14 min) indicates a vacuole that has merged with and received LY from lysosomes. Scale bar, 10 μm.

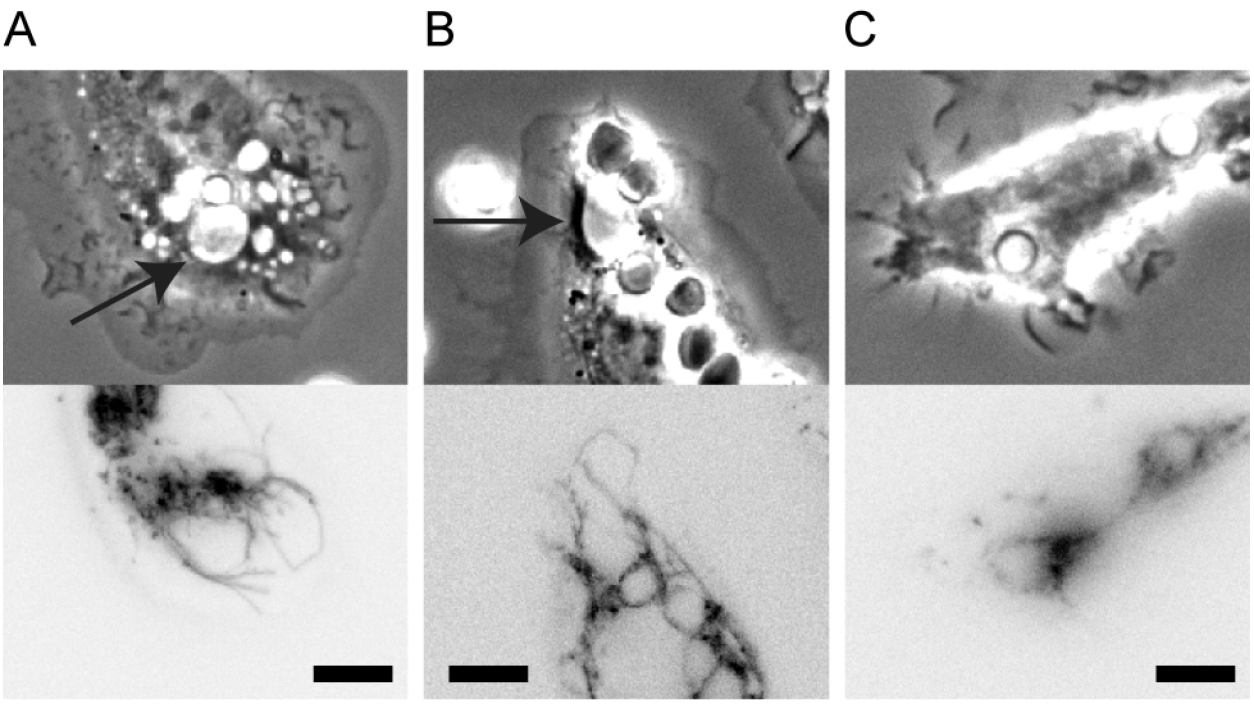

Figure 2.5. Vacuole and macropinosome formation accompanies phagocytosis of non-damaging particles in LPS-activated macrophages.

Single frames of phase contrast and Lucifer yellow (inverted contrast) fluorescence images captured during time-lapse imaging of (A) LPS-treated macrophages fed BSA-coated beads, (B) LPS-treated macrophages fed IgG-opsonized sheep red blood cells, or (C) resting macrophages fed BSA-coated beads, all non-damaging phagocytic targets. Arrows indicate vacuoles appearing in LPS-treated macrophages in (A) and (B). Scale bars, 5 μm.

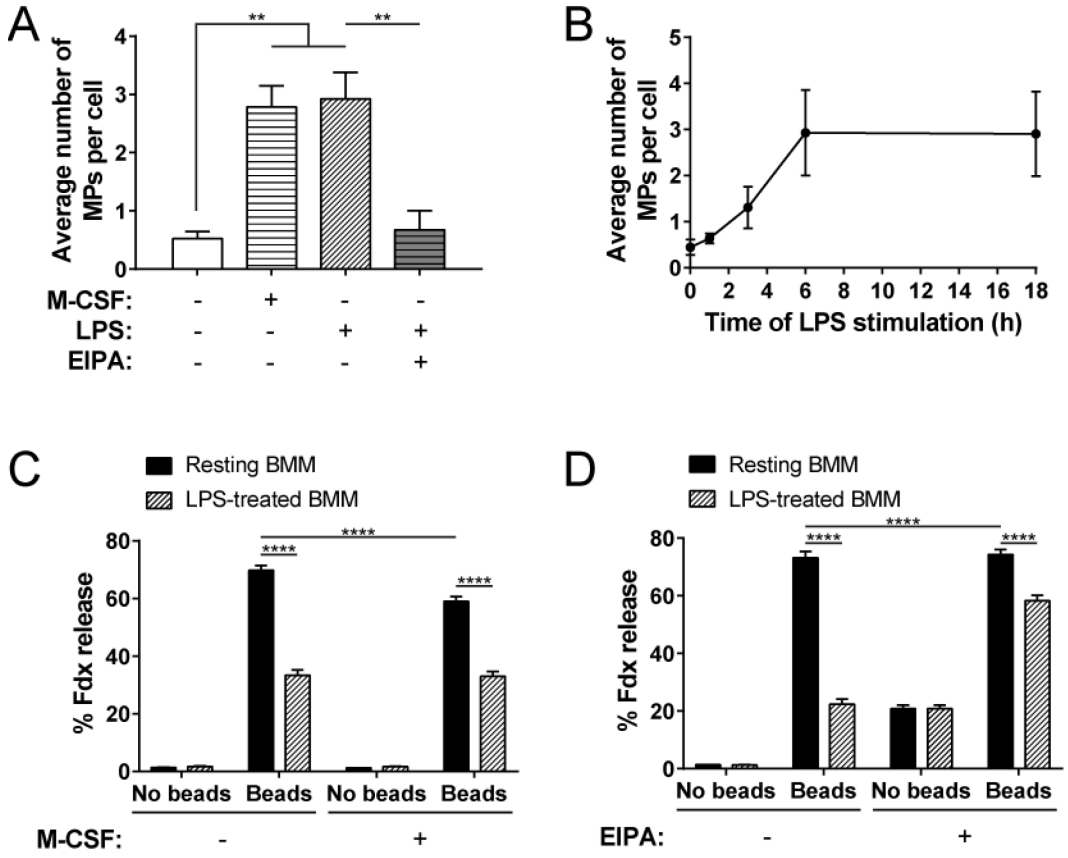
A
Average number of MPs per cell
**
**
M-CSF:
LPS:
EIPA:
B
Average number of MPs per cell
Time of LPS stimulation (h)
C
Resting BMM
LPS-treated BMM
% Fdx release
****
No beads
Beads
M-CSF:
D
EIPA:

Figure 2.6. Macropinocytosis contributes to renitence.

(A) Average macropinosome (MP) number per cell ± SEM was measured in resting and LPS-treated BMM in the presence or absence of macropinocytosis stimulation by M-CSF or inhibition by EIPA. BMM treated with the indicated stimuli were pulsed with 70 kDa Fdx for 10 min, then washed, fixed, and imaged by fluorescence microscopy. Macropinosomes were scored as phase-bright structures within cells that co-localized with 70 kDa Fdx. In control conditions, BMM were either stimulated for 10 min with M-CSF (200 ng/ml) during the Fdx pulse to induce macropinocytosis or pre-treated for 30 min with EIPA (25 μM) before the start of the Fdx pulse to inhibit macropinocytosis. Data from 2 or more independent experiments are shown. $^{**}p \leq 0.01$.

(B) Time course of LPS-induced macropinocytosis induction in macrophages. The average number of macropinosomes per cell ± SEM was measured in BMM treated with LPS for 1, 3, 6, or 18 h or in unstimulated BMM (0 h), after exposure of cells to Fdx for 10 min. Data from at least 2 independent experiments are shown.

(C) Average percent Fdx release ± SEM in resting or LPS-treated BMM fed AW beads for 60 min in the presence or absence of M-CSF to stimulate macropinocytosis. Bars represent data from 3 or more independent experiments. $^{****}p \leq 0.0001$.

(D) Average percent Fdx release ± SEM in resting or LPS-treated BMM pre-treated or not for 30 min with EIPA, an inhibitor of macropinocytosis, before undergoing 60 min incubation with AW beads. Bars represent data from 3 or more independent experiments $^{****}p \leq 0.0001$.

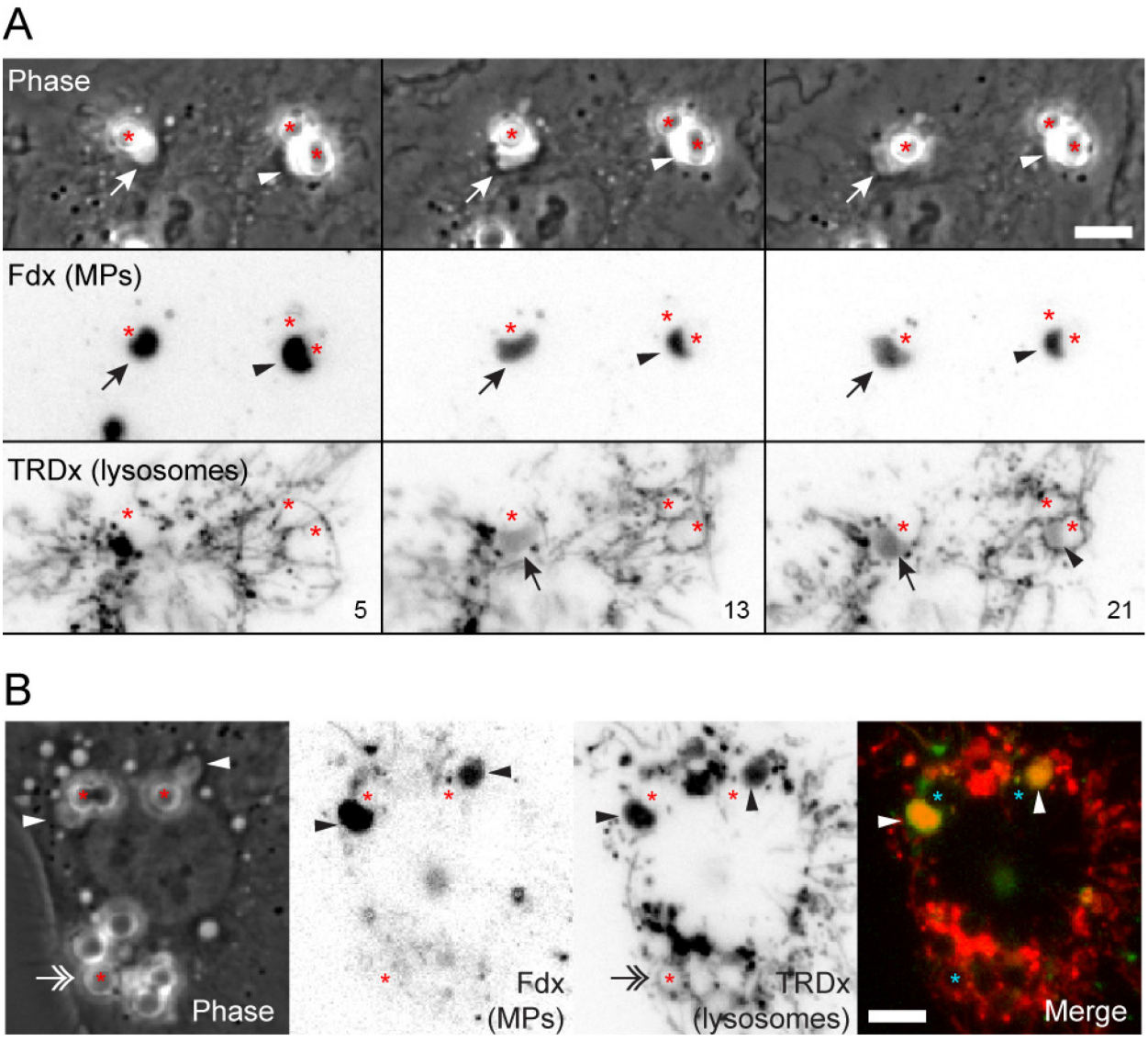
A
Phase
Fdx (MPs)
TRDx (lysosomes)
5
13
21
B
Phase
Fdx
(MPs)
TRDx
(lysosomes)
Merge

Figure 2.7. Renitence vacuoles are persistent macropinosomes that fuse with lysosomes.

LPS-treated BMM whose lysosomes were pre-labelled with 70 kDa TRDx were fed AW beads in media containing 0.5 mg/ml 70 kDa Fdx. After 5 min incubation with beads and Fdx, samples were washed to remove extracellular probe and mounted for time-lapse video microscopy. Phase contrast and fluorescence images of endocytic (Fdx) and lysosomal (TRDx) compartments were taken every 20 sec for 20 min.

(A) Selected frames of phase contrast and inverted contrast Fdx and TRDx images capturing renitence vacuoles before and after their mixing with lysosomes. Elapsed time in minutes after the addition of beads is indicated in the bottom right of each subpanel. Each arrow or arrowhead indicates a specific renitence vacuole tracked between multiple frames. Asterisks denote the position of internalized beads.

(B) Still frames of Phase contrast, Fdx, TRDx, and merged fluorescence images of an LPS-treated BMM captured 29 min after the initial 5 min incubation with AW beads and 70 kDa Fdx. Asterisks are positioned over bead-containing phagosomes. Arrowheads mark two representative renitence vacuoles. Double arrow indicates region of internalized beads that are not associated with renitence vacuoles. Scale bars, 10 μm.

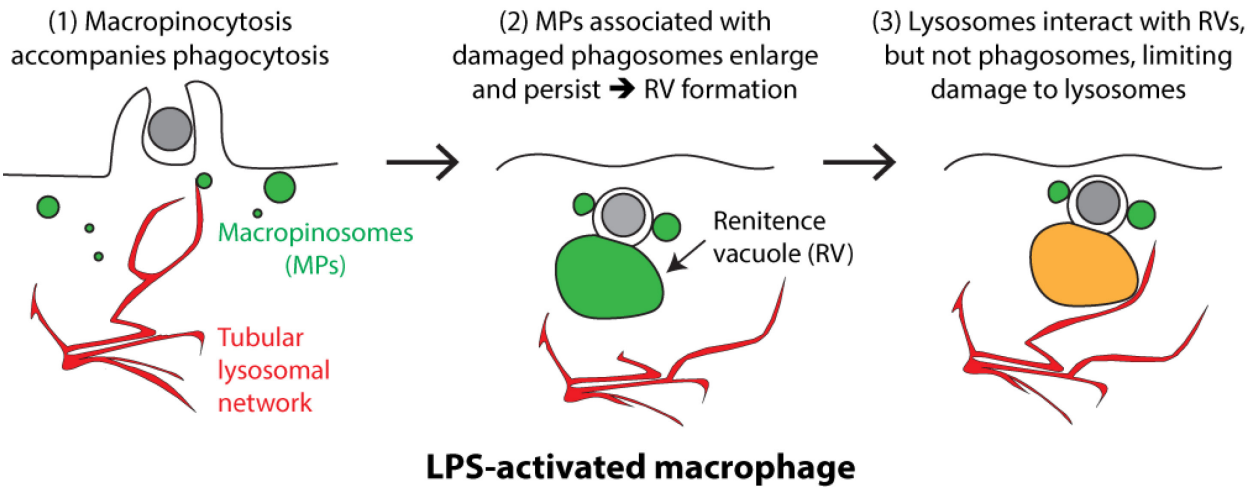

Figure 2.8. Model of cellular events involved in renitence vacuole formation and protection against lysosomal injury.

Sequence of events leading to renitence vacuole formation and lysosomal damage protection in a representative LPS-activated macrophage in which the tubular lysosomal network is represented in red and macropinosomes are represented in green. Phagocytosis is accompanied by membrane ruffling and macropinocytosis. Upon internalization of a damaging particle, multiple macropinosomes accumulate around bead-containing phagosomes, enlarge, and persist. These renitence vacuoles fuse with pre-labelled lysosomes, whereas their associated bead-containing phagosomes do not. Positioned as structural intermediates between intact lysosomes and potentially damaged phagosomes, renitence vacuoles prevent fusion between the two compartments and thereby limit damage to lysosomes.

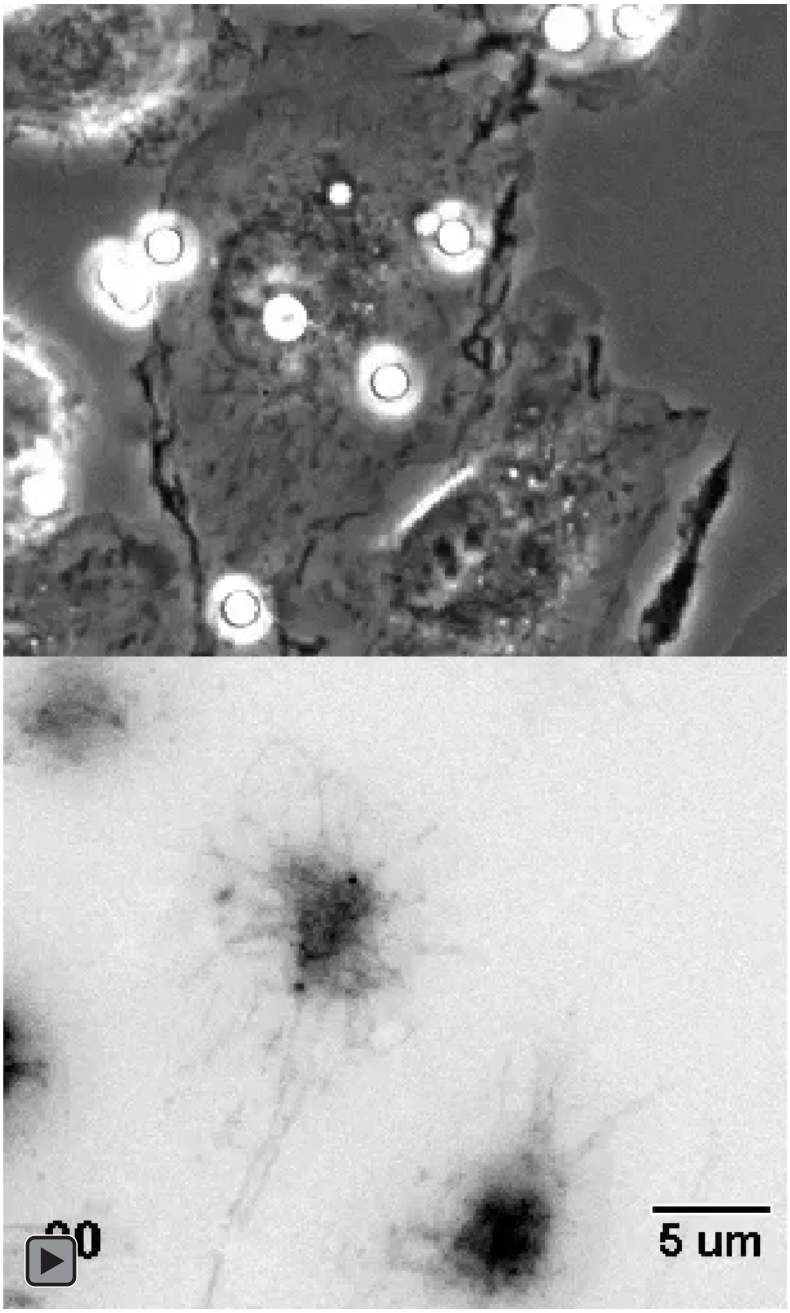

Supplementary Video 1 (Related to Figure 2.4.A). Absence of renitence vacuole formation following silica bead uptake in resting macrophages.

Time-lapse video of AW bead phagocytosis in a resting BMM containing Lucifer yellow (LY)-labelled lysosomes. Beads were added at the start of imaging. Phase contrast (top) and LY fluorescence (bottom; inverted contrast) images were taken every 20 seconds over the course of one hour. Elapsed time in minutes shown in bottom left. AW bead uptake was accompanied by membrane ruffling, but not macropinosome or renitence vacuole formation. Scale bar, 5 μm.

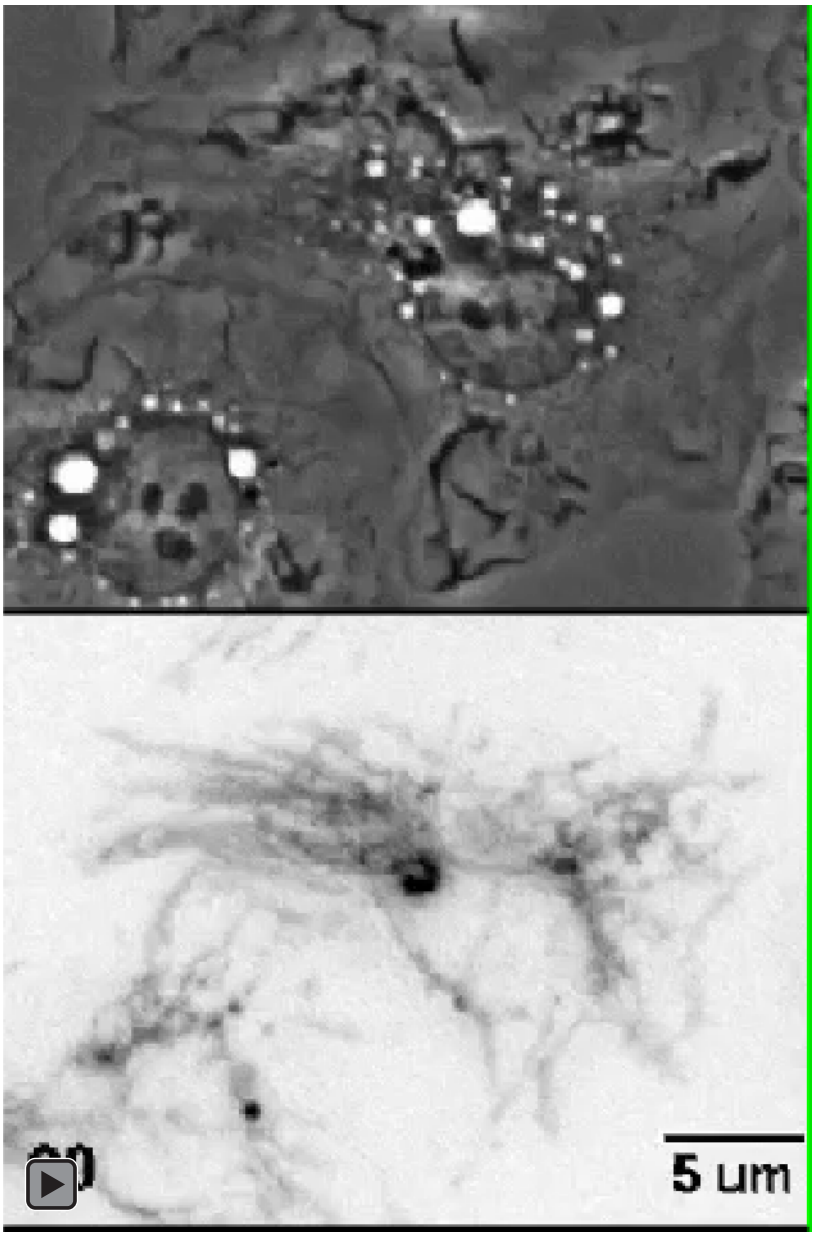

Supplementary Video 2 (Related to Figure 2.4.B). Renitence vacuole and macropinosome formation accompanies silica bead phagocytosis in LPS-activated macrophages.

Time-lapse video of an LPS-treated BMM with LY-labelled lysosomes fed AW beads at the start of imaging. Phase contrast (top) and LY fluorescence (bottom; inverted contrast) images were taken every 20 seconds for one hour. Bead uptake was associated with the formation of numerous phase-bright vesicles that surrounded incoming phagosomes. Some vacuoles received LY from lysosomes, as seen after 14 min. Scale bar, 5 μm.

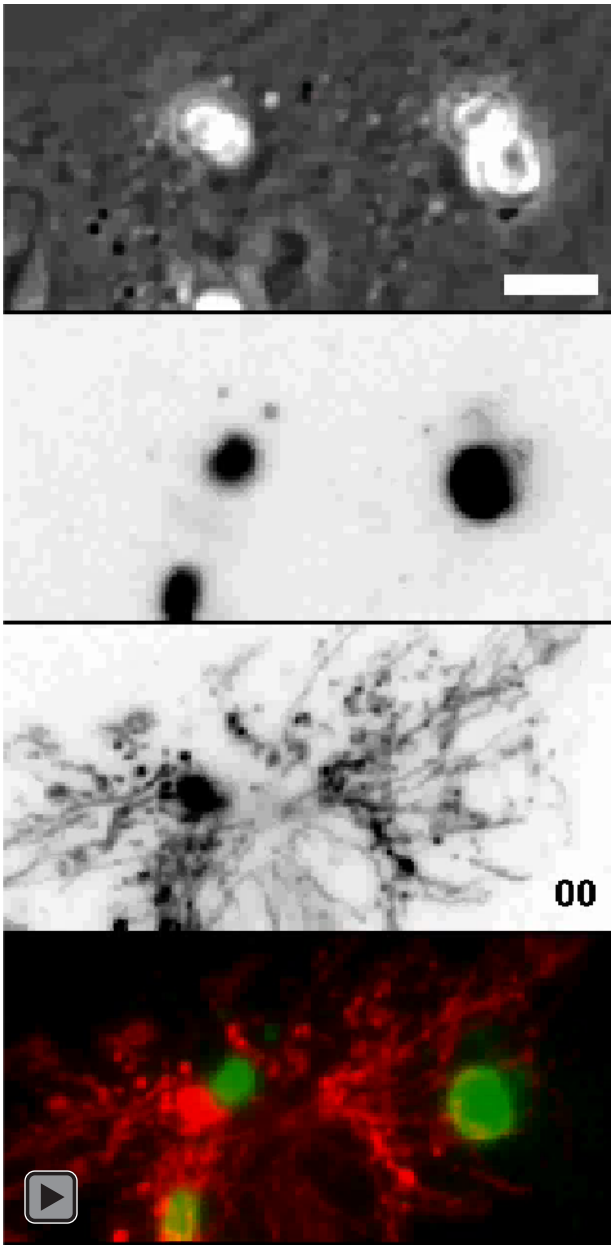

Supplementary Video 3 (Related to Figure 2.7.A). Renitence vacuoles originate from macropinosomes and fuse with lysosomes.

Time-lapse video showing interactions between silica-bead containing phagosomes, macropinosomes, and lysosomes in an LPS-treated BMM. LPS-treated BMM containing 70 kDa TRDx-labelled lysosomes were fed AW beads in the presence of 0.5 mg/ml 70 kDa Fdx for 5 min to label endocytic compartments. Samples were then washed and mounted for imaging. Phase contrast (top), Fdx (second from top; inverted contrast), and TRDx (lysosomes; third from top; inverted contrast) images were taken every 20 seconds for 20 min. Bottom panel shows merged fluorescence images, with Fdx-labelled endosomes in green and TRDx-labelled lysosomes in red. Elapsed time in minutes from the start of imaging (following an initial 5 min pulse with beads and Fdx) is shown in the bottom right of the third panel from the top. Scale bar, 10 μm.

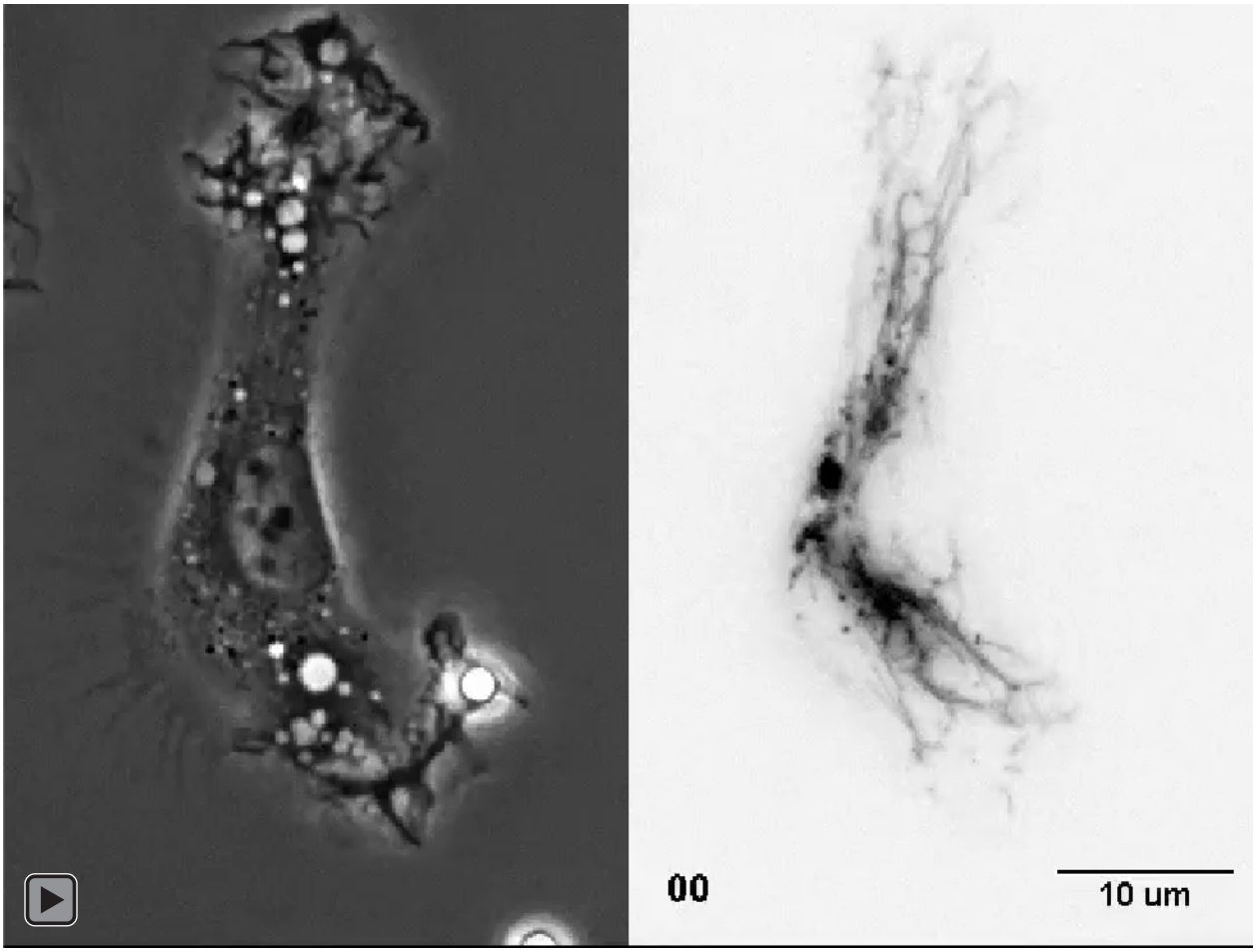

Supplementary Video 4 (Related to Figure 2.5.A). Vacuole formation accompanies the phagocytosis of BSA-coated beads in LPS-activated macrophages.

Time-lapse video of an LPS-treated BMM with LY-labelled lysosomes fed BSA-coated beads at the start of imaging. Phase contrast (top) and LY fluorescence (bottom; inverted contrast) images were taken every 20 seconds for one hour. A large vacuole adjacent to the BSA bead-containing phagosome began to form approximately 27 min after the start of imaging and persisted through the remaining time points observed. The vacuole persistence was an atypical event, as most vacuoles formed following non-damaging bead uptake quickly shrank, as seen in the cells captured in Supplementary Video 5. Scale bar, 10 μm.

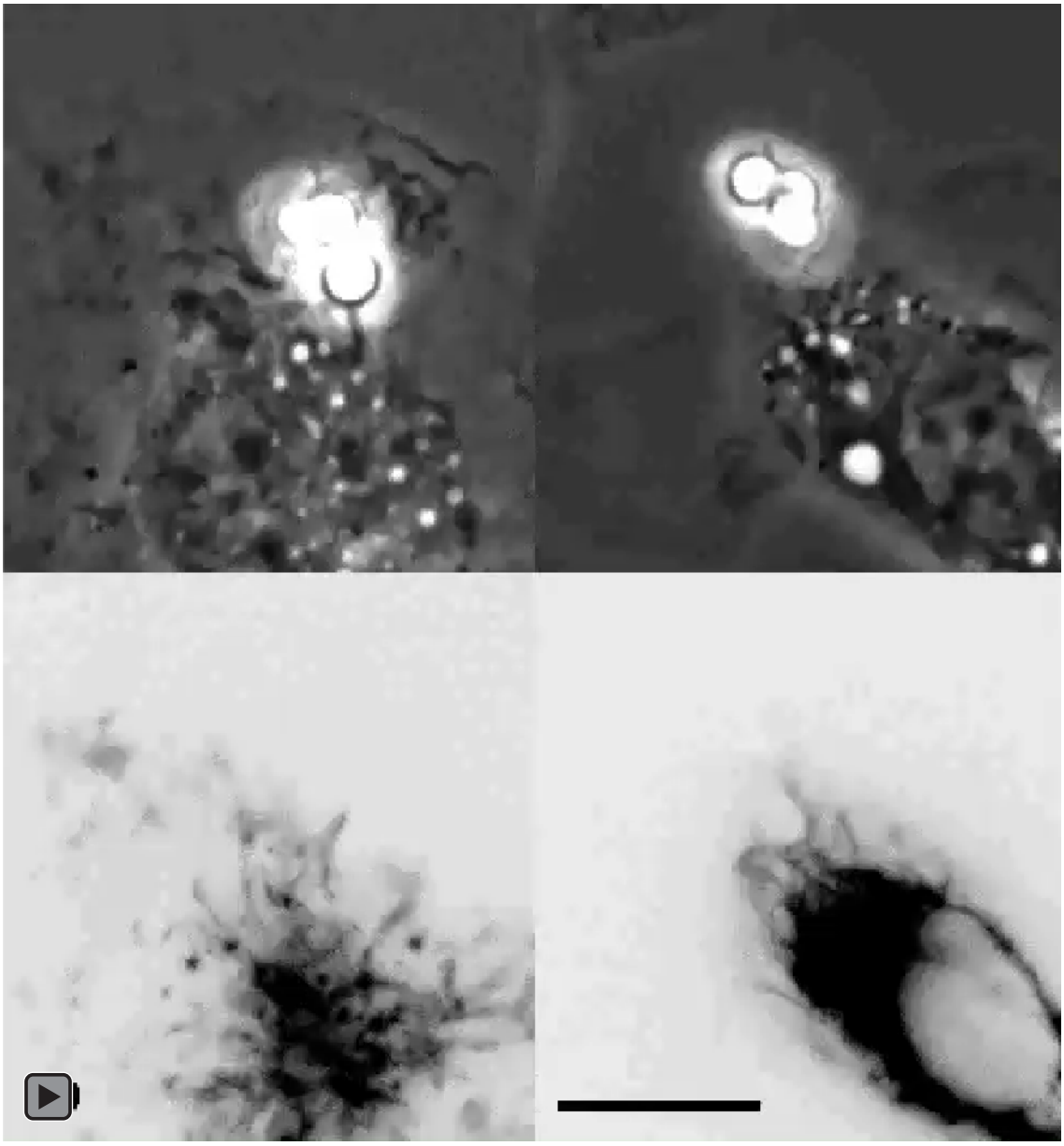

Supplementary Video 5. Vacuoles formed following phagocytosis of BSA-coated beads do not persist.

Time-lapse videos of two representative LPS-treated BMM with LY-labelled lysosomes fed BSA-coated beads at the start of imaging. Phase contrast (top) and LY fluorescence (bottom; inverted contrast) images were taken every 20 seconds for one hour. Dynamic membrane ruffling and macropinocytosis accompanied bead phagocytosis, but vacuoles appearing next to beads quickly shrank and did not persist. Scale bar, 10 μm.

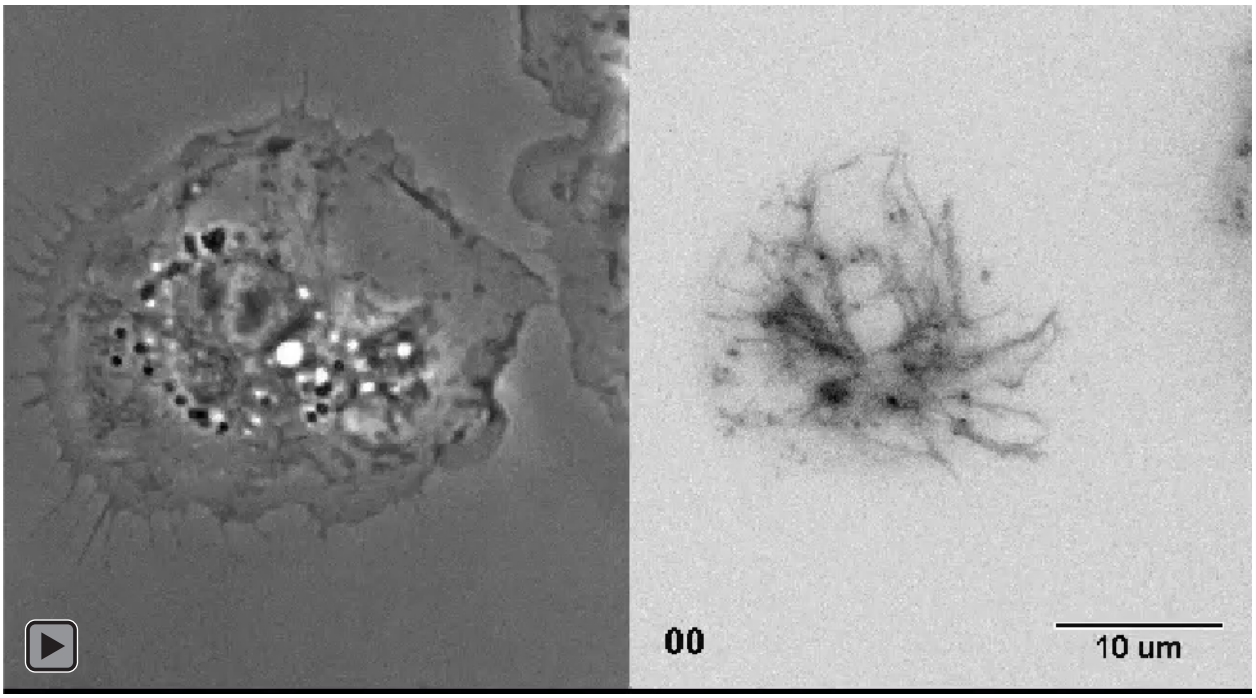

Supplementary Video 6 (Related to Figure 2.5.B). Vacuole formation accompanies the phagocytosis of IgG-opsonized sheep red blood cells in LPS-treated macrophages.

Time-lapse video of an LPS-treated BMM with LY-labelled lysosomes fed IgG-opsonized sheep red blood cells (IgG-sRBCs) at the start of imaging. Phase contrast (top) and LY fluorescence (bottom; inverted contrast) images were taken every 20 seconds for one hour. A vacuole formed coincident with IgG-sRBC uptake 43 min after the start of imaging and persisted through the remaining time points imaged. Scale bar, 10 μm.

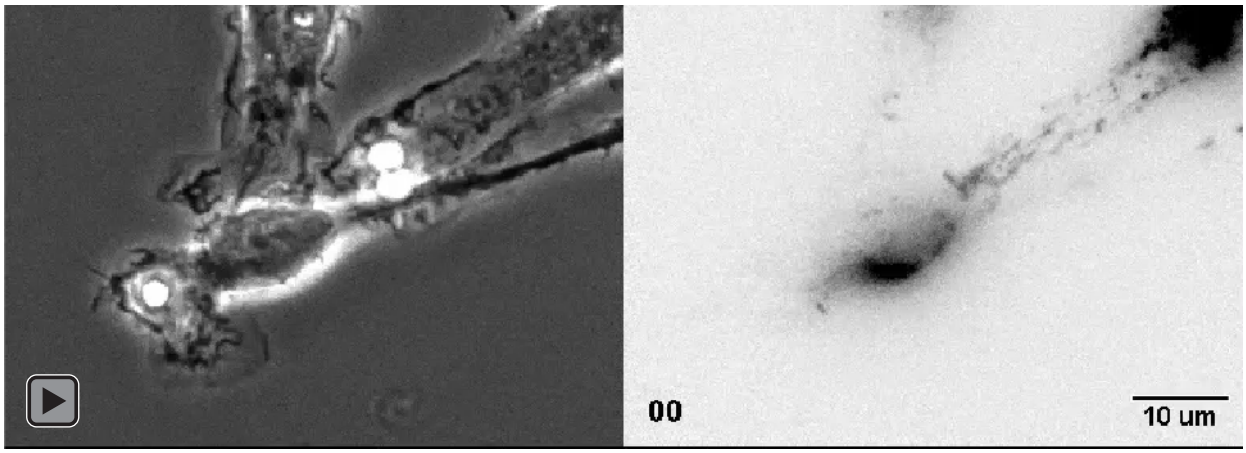

Supplementary Video 7 (Related to Figure 2.5.C). Absence of vacuole formation in resting macrophages following uptake of BSA-coated beads.

Time-lapse video of a resting BMM with LY-labelled lysosomes fed BSA-coated beads at the start of imaging. Phase contrast (top) and LY fluorescence (bottom; inverted contrast) images were taken every 20 seconds for one hour. Membrane ruffling without accompanying macropinocytosis or vacuole formation was observed. Scale bar, 10 μm.

CHAPTER 3

Macrophage Inflammatory State Influences Susceptibility to Lysosomal Damage

This work was performed in collaboration with Matangi Marthi, Michele S. Swanson, and Joel A. Swanson. A.O.W, M.M., and J.A.S. designed the project and performed experiments. M.S.S participated in data analysis. A.O.W. wrote this chapter.

3.1 Abstract

Here we surveyed the range of macrophage populations capable of exhibiting renitence, a property of enhanced resistance to lysosomal damage previously reported for macrophages individually stimulated with LPS, peptidoglycan (PGN), IFN-γ, and TNF-α. In this study, we expanded the macrophage subtypes examined to include the following macrophage populations for which functional roles *in vivo* have been reported and whose inflammatory phenotypes are well-defined: classically activated (CA-Mφ), alternatively activated macrophages (AA-Mφ), and regulatory macrophages (Reg-Mφ). We also characterized the inflammatory state of LPS-activated macrophages, which of all macrophage subtypes examined exhibited the highest capacity for renitence. We determined that renitence is a property of CA-Mφ and Reg-Mφ, but not of AA-Mφ, and that LPS-activated macrophages possess features of both CA-Mφ and Reg-Mφ, based on their profiles of inflammatory and immunosuppressive cytokine secretion. As the generation of these three classes of renitent macrophages required exposure to LPS, a Toll-like receptor (TLR) ligand, we assessed whether TLR stimulation generally induced renitence. Stimulation of TLRs 2/1, 3, and 4 induced renitence, whereas stimulation of TLRs 7/8 and 9

induced modest levels of protection. The formation of renitence vacuoles and macropinosomes, shown in Chapter 2 to contribute to renitence in LPS-activated macrophages, was observed in several renitent and non-renitent activated macrophage populations, and as such not sufficient for renitence. Together, this work expands our understanding of the immunological contexts of renitence, and provides the foundation for future investigations into the functional role of renitence in macrophages.

3.2 Introduction

Macrophages exist in metazoan organisms not as one homogenous population, but instead as cells exhibiting enormous functional heterogeneity and plasticity (Mosser and Edwards, 2008; Wynn *et al.*, 2013). The functional state a macrophage assumes is influenced by the particular tissue in which it resides and the signals it receives within the tissue environment. While this model allows for a very large number of possible activation states, extensive efforts have been made to characterize three major functional classes with distinct roles *in vivo*. These include classically-activated macrophages (CA-Mφ), alternatively-activated macrophages (AA-Mφ), and regulatory macrophages (Reg-Mφ), which have specialized functions in host defense, wound healing, and dampening of immune responses, respectively (Mosser and Edwards, 2008). The signals that induce macrophage differentiation into these subtypes *in vivo* can be used to generate macrophages of the analogous classes *in vitro*: stimulating macrophages with IFN-γ and TNF-α (or Toll-like receptor agonists that induce macrophages to secrete TNF-α) generates CA-Mφ; IL-4 and/or IL-13 stimulation induces the generation of AA-Mφ; Toll-like receptor (TLR) stimulation coupled with a second signal provided by IgG immune complexes, prostaglandin E2 (PGE2), or adenosine (Ado), generates Reg-Mφ (Mosser and Edwards, 2008; Fleming *et al.*, 2015). These secondary signals "reprogram" macrophages so that following TLR activation they

adopt an immunosuppressive rather than inflammatory phenotype (Mosser and Edwards, 2008). These three macrophage subtypes can be distinguished by their relative secretion of the pro-inflammatory cytokine IL-12p40 and the anti-inflammatory cytokine IL-10: CA-Mφ produce high levels of IL-12p40 but low levels of IL-10; Reg-Mφ produce low levels of IL-12p40 but high levels of IL-10; AA-Mφ do not produce abundant levels of either cytokine (Mosser and Zhang, 2008). Elevated expression levels of *Relm-α* (also called *Fizz1*), a gene not expressed in CA-Mφ or Reg-Mφ, is used as a marker of AA-Mφ.

Recent work in our lab uncovered a novel macrophage activity called "inducible renitence," which describes the enhanced ability of macrophages stimulated with LPS, peptidoglycan (PGN), IFN-γ, or TNF-α to resist damage to their phagolysosomes following the phagocytosis of membrane-damaging silica beads (Davis *et al.*, 2012). As phagolysosomal damage represents a common threat inflicted by pathogens, and as the factors found to induce renitence correspond to microbial ligands or host pro-inflammatory cytokines, we reasoned that renitence is a consequence of classical macrophage activation. However, macrophage stimulation with other inflammatory cytokines, including IL-6, IL-1β and IFN-β, did not induce renitence (Davis *et al.*, 2012). Moreover, other types of activated macrophage not yet examined might conceivably have mechanisms for limiting damage to their lysosomes. Here we sought to determine the range of macrophages subtypes capable of inducing renitence. Coupled together with knowledge of the immunological and functional properties of these macrophage differentiation states, this understanding will move us toward our ultimate goal of determining how regulation of lysosomal integrity relates to macrophage function.

Of the macrophage activation states examined in previous work, macrophages stimulated overnight with LPS exhibited the most pronounced and consistent protection against lysosomal

damage (Davis *et al.*, 2012). While LPS-activated macrophages, like CA-Mφ, have been noted for their anti-microbial properties (Kornbluth *et al.*, 1989; Rosenberger *et al.*, 2000), their precise activation state has not been well-defined. That they are generated in the absence of IFN-γ suggests they may not represent canonical CA-Mφ, whose generation occurs under substantially different conditions – namely, several hours of IFN-γ priming followed by overnight stimulation with LPS and IFN-γ (Mosser and Zhang, 2008). Supporting this idea, TLR stimulation of macrophages in the absence of IFN-γ priming induces the differentiation of macrophages that initially resemble CA-Mφ in terms of their pattern of cytokine secretion, but that over several hours transition to an immunosuppressive state (Cohen *et al.*, 2015). The regulatory cascade driving this transition has been proposed to serve as an autoregulatory mechanism used by macrophages to prevent the development of hyperinflammatory responses following TLR activation (Cohen and Mosser, 2013). According to this model, the release of pro-inflammatory cytokines following TLR stimulation is accompanied by the release of low levels of adenosine triphosphate (ATP), which after several processing steps mediated by extracellular enzymes, including ENTPDase1/CD39, is converted into adenosine (Ado), a signal that promotes the generation of immunosuppressive Reg-Mφ (Cohen *et al.*, 2013; Cohen and Mosser, 2013). Ado acts as a ligand for the adenosine 2b receptor (A2bR), whose activation triggers downstream signaling leading to the expression of Reg-Mφ genes (Cohen *et al.*, 2013). Thus, in the absence of IFN-γ priming, TLR-stimulated macrophages assume a transient pro-inflammatory state and possess cell-intrinsic mechanisms for initiating the transition to Reg-Mφ. This transition is avoided in macrophages primed with IFN-γ, as IFN-γ inhibits the expression of A2bR, such that cells become unresponsive to Ado (Cohen *et al.*, 2015). Likewise, pharmacological inhibition or

genetic deficiency of CD39 or A2bR leads to a hyper-inflammatory state recapitulating that of CA-Mφ (Cohen *et al.*, 2013; Cohen *et al.*, 2015).

Based on the above model, we predicted that macrophages observed previously to undergo renitence (namely, LPS-activated macrophages stimulated in the absence of IFN-γ priming) may harbor characteristics of Reg-Mφ. This work thus has two related aims: (1) to identify the immunological contexts in which renitence acts, and (2) to define and compare the inflammatory states of macrophages that do or do not induce renitence.

We report that only a subset of macrophage subtypes induced renitence. These included CA-Mφ, Reg-Mφ, and macrophages treated with ligands of TLRs 2/1, 3, and 4. Macrophages that did not induce or only modestly induced renitence included AA-Mφ and macrophages treated with ligands of TLRs 7/8 and 9. Building upon these observations, we examined connections between the inflammatory state of macrophages and renitence capacity, the dependence of TLR signaling for renitence, and the role for "renitence vacuoles," found in Chapter 2 to contribute to renitence protection in LPS-activated macrophages, in renitence in other macrophage types. Together, this work expands our understanding of the conditions that induce renitence and supports the concept that the polarization state of macrophages affects their susceptibility to lysosomal damage.

3.3 Materials and Methods

3.3.1 Mice and macrophage isolation

C57BL6/J mice were purchased from The Jackson Laboratory (Bar Harbor, ME). *Myd88*$^{-/-}$, *Trif*$^{e/-}$, and *Myd88/Trif*$^{e/-}$ mice were generously provided by Gabriel Nuñez (University of Michigan). All mice were maintained under specific pathogen-free conditions at the University of Michigan. Bone marrow-derived macrophages (BMM) were obtained as

previously described (Davis *et al.*, 2012), with slight modification. Bone marrow cells isolated from the femurs and tibia of mice were differentiated into macrophages through culture for 6-8 days in DMEM containing 10% FCS and 50 ng/ml recombinant M-CSF.

3.3.2 Cell culture and stimulation

CA-Mφ were generated by priming BMM with 150 U/ml IFN-γ (R&D Systems, Minneapolis, MN) for 6 h, and then stimulating cells overnight with 150 U/ml IFN-γ and 100 ng/ml LPS (from *Salmonella typhimurium*; no. 225; List Biological Laboratories, Campbell, CA). AA-Mφ were generated by stimulating macrophages overnight with 20 ng/ml IL-4 (R&D Systems, Minneapolis, MN). Reg-Mφ were generated by stimulating macrophages overnight with 100 ng/ml LPS and either 200 nM PGE2 (Cayman Chemical, Ann Arbor, MI) or 200 μM adenosine (Sigma-Aldrich, St. Louis, MO). Studies of macrophages stimulated overnight with TLR agonists were performed with the following reagents: Pam3CSK4 (100 ng/ml); poly(I:C) (10 ug/ml); ultrapure flagellin from Salmonella typhimurium (FLA-ST; 100 ng/ml); R848 (100 ng/ml), ODN 1826 (1 Um). All TLR agonists were purchased from Invivogen (San Diego, CA) with the exception of poly(I:C), which was purchased from Tocris (Bristol, United Kingdom).

For experiments in which both RNA isolation and cytokine analyses were performed, 6 x 10^6 cells were plated onto 12 mm^2 dishes. For experiments in which cytokine analyses were performed and RNA was not isolated, 1 x 10^5 cells were plated onto 24-well plates. For assays of lysosomal damage, 8 x 10^4 cells were plated onto MatTek dishes.

3.3.3 Gene expression analysis

RNA was isolated using a Qiagen RNeasy Mini Kit (74104; Venlo, Netherlands) and converted into cDNA using MMLV-Reverse Transcriptase from ThermoFisher (28025013; Waltham, MA). Quantitative PCR (qPCR) analysis was performed using an Applied Biosystems

7500 Fast Real-Time PCR system (ThermoFisher) and Brilliant II SYBR Green Master Mix (600830; Agilent, Santa Clara, CA). Primer pairs used for amplification of specific gene products are listed in Table 3.1. Relative expression levels were calculated using the $\Delta\Delta C_T$ method, using *Gapdh* as the reference gene for normalization (Schmittgen and Livak, 2008).

3.3.4 Cytokine measurements

Mouse IL-12p40, mouse TNF-α, and mouse IL-10 cytokine concentrations were determined using ELISA DuoSet kits (R&D Systems, Minneapolis, MN). ELISA assays were performed using the services of the University of Michigan Immune Monitoring Core.

3.3.5 Particle preparation

3 μm silica dioxide microspheres were purchased from Microspheres-Nanospheres, a subsidiary of Corpuscular Inc (Cold Spring, NY). To clean the particles of debris, microspheres were acid-washed (AW) overnight in 1N HCl, then rinsed several times with Milli-Q water.

3.3.6 Measurement of lysosomal damage by ratiometric imaging

Damage to macrophage lysosomes was measured using an assay for ratiometric measurement of pH, as described in Chapter 2. Steps of lysosomal labeling and ratiometric imaging are briefly described here.

To label macrophage lysosomes, BMM were incubated overnight with 150 ug/ml 3 kDa average molecular weight fluorescein dextran (Fdx; ThermoFisher). During this overnight pulse, cells also were treated with the appropriate polarizing cytokines for generating various macrophage subtypes. The next day, cells were rinsed in Ringer's buffer, and returned to unlabeled media for at least 3 hours before the start of imaging. Lysosomal damage was induced by feeding BMM 3 μm AW beads in RPMI lacking serum for 60 min. AW beads were added at a concentration empirically determined to result in uptake of on average 3 to 4 beads per cell by

both resting and LPS-activated BMM. All analyses of damage were performed on cells that had internalized 3 to 7 beads per cell.

To monitor dye release, BMM containing Fdx-labelled lysosomes were imaged by fluorescence microscopy after 60 min incubation in the presence or absence of AW beads. For each field of cells imaged, three images were acquired: one phase-contrast image, which allowed enumeration of bead number per cell, and two fluorescent images, captured using a single emission filter centered at 535 nm and two different excitation filters, centered either at 440 nm or 490 nm, the pH insensitive and pH sensitive wavelengths, respectively, for fluorescein. Taking the ratio of fluorescence intensities captured in the 490 and 440 channels (Fdx ex. 490/Fdx ex. 440) yielded pH information for each pixel in the image. To convert 490 nm/440 nm fluorescence intensities into pH values, a calibration curve was generated by measuring 490 nm/440 nm excitation ratios of Fdx in BMMs exposed to the ionophores nigericin and valinomycin (10 uM) in fixed pH clamping buffers (Davis *et al.*, 2012). Image acquisition and analysis were performed using Metamorph software (Molecular Devices, Sunnyvale, CA).

3.3.7 Analysis of vacuole frequency

Renitence vacuole (RV) frequency was quantified in images of resting and variously activated BMM from which measurements of lysosomal damage were made in Fig 3.1.C. Images were scored for the presence or absence of RVs by the following criteria: (1) appearance on the phase contrast image as a circumscribed phase-dense region adjacent to an internalized bead, and (2) presence of Fdx within the structure. RV frequency was quantified as the percent of cells containing one or more vacuoles within a given condition. All cells containing at least one bead were included in the analysis.

3.3.8 Macropinosome counting assay

BMM plated on 12 mm circular coverslips were stimulated overnight with various TLR agonists or left unstimulated. To label macropinosomes, BMM were pulsed for 10 min with 70 kDa Fdx (0.5 mg/ml), and then washed with HBSS to remove uningested probe. Cells were fixed for 30 min at 37°C with fixation buffer (75 mM lysine-HCl, 37.5 mM Na_2HPO_4, 4.5% sucrose, 2% paraformaldehyde, 10 mM sodium periodate), and imaged by fluorescence microscopy. As a positive control, macropinocytosis was stimulated by inclusion of M-CSF (200 ng/ml) during the time of the Fdx pulse. MetaMorph software was used to merge phase contrast and background-subtracted Fdx images. The number of MPs per cell was determined by scoring the number of Fdx-positive phase bright vesicles in the merged images. At least 25 cells were scored for each experiment.

3.3.9 Statistical methods

Statistical analysis was performed using GraphPad Prism software (GraphPad Software Inc; La Jolla, CA). For gene expression and cytokine secretion analyses, statistical significance relative to unstimulated cells was determined using a two-tailed, unpaired, nonparametric t-test (Mann-Whitney). Lysosomal damage levels between groups were compared using two-way ANOVA with Tukey's multiple comparisons. Frequency of vacuole or MP formation between groups was compared using a two-tailed, unpaired t-test.

3.4 Results

3.4.1 Generation and characterization of variously activated macrophages

CA-Mφ, AA-Mϕ, and Reg-Mφ were generated and assessed for their ability to undergo renitence. To generate macrophages of each subtype, we exposed murine bone marrow-derived macrophages (BMM) in culture to the appropriate polarizing cytokines (see Methods for details). By gene expression and cytokine secretion analysis, we confirmed that these treatments

successfully generated macrophages of the expected subtypes. LPS and IFN-γ treatment of macrophages first primed for 6h with IFN-γ generated CA-Mφ producing high levels of IL-12p40 and TNF-α, and low levels of IL-10 (Fig. 3.1.A and B). Macrophages treated with LPS in combination with either prostaglandin E2 (PGE2) or adenosine (Ado) generated Reg-Mφ producing low levels of IL-12p40 and TNF-α, and high levels of IL-10. Finally, IL-4 stimulation of macrophage yielded AA-Mϕ producing low levels of IL-12p40 and IL-10, but expressing high levels of *Relm-α*. As expected, this gene was not abundantly expressed in either CA-Mφ or Reg-Mφ (Fig. 3.1.A).

While macrophages stimulated overnight with LPS are commonly regarded as CA-Mφ, their activation status has not been precisely defined. We determined that macrophages stimulated overnight with LPS exhibit features of both CA-Mφ and Reg-Mφ. In addition to producing high levels of IL-12p40 and TNF-α, as measured by ELISA, LPS-treated macrophages also produced high levels of IL-10, to an extent similar to that produced by Reg-Mφ (Fig. 3.1.B). Placed on the spectrum of macrophage activation, macrophages stimulated overnight with LPS assume an intermediate phenotype between that of CA-Mφ and Reg-Mφ.

3.4.2 Classically activated and regulatory macrophages exhibit renitence

Having confirmed that the cell stimulations employed yield macrophages of the expected subtypes, we next assessed the ability of macrophages of each functional class to undergo renitence. Renitence we defined previously as the ability of cells to limit damage to their lysosomes against induced injury (Davis *et al.*, 2012), a phenomenon discovered using a live-cell, fluorescence microscopy-based assay for measuring lysosomal damage (Davis and Swanson, 2010). BMM whose lysosomes were pulse-chase labelled with the pH-sensitive dye, fluorescein dextran (Fdx), were then fed acid-washed, 3 μm diameter acid-washed silica beads

(AW beads), which have the potential to damage endolysosomal membranes. After a 60 min incubation with the AW beads, ratiometric fluorescence imaging was performed to determine the proportion of the dye that had leaked into the cytoplasm (see Methods for details). Damage to lysosomes was quantified on a per-cell basis, and reported as the average percent release of Fdx from lysosomes into the cytoplasm for all cells analyzed in a given condition.

As previously demonstrated (Davis *et al.*, 2012), resting macrophages challenged with AW beads experienced considerable damage that was significantly reduced in cells pre-treated with LPS (Fig 3.1.C). Reg-Mφ generated through two different treatments (LPS+PGE2; LPS+Ado) showed a similar degree of protection from AW bead-mediated damage as that seen in LPS-treated macrophages. The protective effect was dependent on the presence of LPS, as single treatment with either PGE2 or Ado did not confer protection. CA-Mφ showed protection against AW bead-mediated damage, but to a lesser degree than that seen in Reg-Mφ or LPS-treated macrophages. AA-Mφ, unlike Reg-Mφ or CA-Mφ, did not exhibit protection from AW bead-mediated damage, experiencing similar levels of damage as that seen in resting macrophages. Together, these results demonstrate that renitence is a property of Reg-Mφ and CA-Mφ, but not of AA-Mφ. The pattern of protected versus unprotected subsets suggests that renitence is an activity characteristic of macrophages specialized in host defense either in their present state (CA-Mφ) or in their recent past (Reg-Mφ). Indeed, CA-Mφ and Reg-Mφ share a common requirement for their generation: exposure to a microbial ligand – namely, LPS. As LPS activates downstream signaling in macrophages through stimulating Toll-like receptor (TLR) 4, we next asked whether stimulation of other TLRs also confers protection against lysosomal damage in macrophages.

3.4.3 TLR stimulation by a subset of agonists induces renitence

We previously observed that stimulating cells with peptidoglycan (PGN), a TLR2 agonist, induced renitence to a similar degree as that induced by LPS (Davis *et al.*, 2012), suggesting that TLR stimulation induces renitence. To address this possibility, we exposed BMM to a panel of TLR agonists, and assessed the ability of each agonist to protect macrophage lysosomes from AW bead-mediated injury. Of the agonists tested, only a subset induced renitence. These included the synthetic triacylated lipopeptide Pam3CSK4, a bacterial ligand that activates TLR2/1; poly(I:C), an analog of dsRNA, which activates TLR3; and LPS, a component of the cell wall of gram-negative bacteria and canonical TLR4 ligand (Fig. 3.2.A). R848 (Resiquimod), an anti-viral compound that activates TLR7/8, and ODN 1826, a synthetic oligonucleotide containing unmethylated CpG motifs, which activates TLR9, induced much more modest protection against lysosomal damage. Flagellin purified from *S. typhimurium* (FLA-ST), an agonist of TLR5, appeared to offer no protection from lysosomal damage. However, based on cytokine secretion analysis of BMM treated with the various TLR agonists, FLA-ST stimulation did not induce secretion of TNF-α, an expected secreted product following TLR stimulation (Fig. 3.2.B). In contrast, all other TLR agonists tested induced robust secretion of TNF-α and variable levels of secretion of other cytokines probed (IL-12p40 and IL-10). FLA-ST thus seems to have failed to activate its cognate receptor, TLR5, in our experiments. The inability of FLA-ST to activate BMM has been noted previously by others and is attributed to low levels of TLR5 expression in mouse BMM (Means *et al.*, 2003; Molofsky *et al.*, 2006)

Our results demonstrate that activation of TLRs 2/1, 3, and 4 induces renitence, whereas activation of TLRs 7/8 and 9 induces a modest level of protection. The TLRs belonging to either group differ in terms of which signaling adaptors (i.e. MyD88 vs TRIF) they recruit, which intracellular compartment (i.e. cell surface vs endosomal) they signal from, and which class of

ligands (i.e. bacterial vs viral) they recognize. As such, the pattern revealed does not immediately suggest a mechanistic basis for renitence that relates to any of these variables. We considered whether the differential ability of TLR agonists to induce renitence might reflect differences in the inflammatory state produced by stimulation with the agonists. That is, does the set of agonists capable of inducing renitence generate macrophages of a different activation state than those agonists that do not induce renitence? By examining cytokine secretion levels in macrophages stimulated with each of the TLR agonists, we determined that all TLR agonists tested (with the exception of FLA-ST) were capable of inducing similar levels of TNF-α secretion regardless of their ability to induce renitence (Fig 3.2.B). The level of IL-10 secretion induced by the panel of agonists was more variable, but likewise did not correlate with either the ability or inability to induce renitence. Levels of IL-12p40 secretion, however, widely differed between the two groups. The agonists with less renitence-inducing potential (R848 and ODN 1826) induced markedly higher production of IL-12 p40 than the set of agonists capable of inducing renitence (Pam3CSK4, Poly(I:C), and LPS) (Fig 3.2.B). These results suggest that IL-12p40 is inversely correlated with, and perhaps antagonizes, renitence. More replicates will need to be performed to establish that these results are reproducible and statistically significant.

3.4.4 Renitence induced by TLR ligands requires intact TLR signaling

To determine whether the induction of renitence by TLR ligands depends on the canonical pathways of TLR signaling, we measured lysosomal damage following 60 min AW bead incubation in C57/BL6 (WT) and *Myd88* and *Trif*-deficient (*Myd88/Trif*$^{-/-}$) BMM stimulated with the same panel of TLR agonists used in Figure 3.2.A, excluding FLA-ST. As MyD88 (Myeloid differentiation primary response 88) and TRIF (TIR-domain-containing adapter-inducing interferon-β) are the major signaling adaptors responsible for propagating

signaling downstream of TLR activation, macrophages deficient in these two adaptors lack functional TLR signaling. In WT BMM, stimulation with the panel of TLR agonists induced the same pattern of protection as seen in Figure 3.2.A (Fig. 3.3.A). Impairment of TLR signaling in *Myd88/Trif*$^{-/-}$ BMM eliminated renitence by all agonists tested except for ODN 1826. As ODN 1826 stimulation failed to confer much, if any, protection from damage in WT BMM (Fig. 3.2.A), the finding of no exacerbation of damage in *Myd88/Trif*$^{-/-}$ BMM is not surprising. Together, these results suggest that renitence stimulated by TLR agonists requires functional TLR signaling.

3.4.5 TLR signaling adaptor requirements for renitence differ from those for NF-κB activation

To dissect which signaling adaptor(s) (i.e. MyD88 and/or TRIF) contribute to renitence induced by each TLR, we measured lysosomal damage in BMM with single gene deficiencies in either *Myd88* or *Trif* (*Myd88*$^{-/-}$ *or Trif*$^{-/-}$ BMM respectively). We predicted that the pattern of adaptor usage downstream of TLR signaling for renitence would parallel the established patterns of involvement of MyD88 vs TRIF in TLR signaling leading to NF-κB activation: namely, that TLRs 2/1, 7/8, and 9 signal through MyD88 only, TLR3 signals through TRIF only, and TLR4 signals through both MyD88 and TRIF (Akira *et al.*, 2006). Comparing the effect of each individual knockout on renitence induced by each TLR agonist revealed the following adaptor usage requirements for renitence. TLR2/1 stimulation by Pam3CSK4 induced renitence through signaling that requires MyD88 but not TRIF, as renitence was eliminated in *Myd88*$^{-/-}$ BMM (Fig 3.3.B) but unaffected in *Trif*$^{-/-}$ BMM (Fig 3.3.C). In contrast, renitence induced by LPS stimulation of TLR4, whose activation at the cell surface recruits MyD88 as a signaling adaptor and whose activation within endosomes recruits TRIF, depended only on signaling through TRIF

but not MyD88. This result suggests that endosomal but not cell-surface TLR4 signaling is necessary for LPS-induced renitence. Although renitence induced through TLR4 requires TRIF, TRIF deficiency led only to a partial abrogation of protection, suggesting that other pathways downstream of TLR4 signaling contribute to renitence.

While the results described so far are consistent with the known adaptor usage patterns for TLR signaling leading to NF-κB activation, those we obtained for the other TLR agonists tested did not segregate according to these established patterns. Specifically, renitence induced by stimulation of TLRs 3 and 7/8 (receptors for poly(I:C) and R848 respectively) required both MyD88 and TRIF even though canonically TLR3 signals only through TRIF and TLR7/8 signals only through MyD88 (Fig 3.3.B and C). Moreover, deficiency of either MyD88 or TRIF completely abrogated TLR7/8-induced renitence by R848, but only partially abrogated TLR3-induced renitence by poly(I:C). The results obtained for TLR3-induced renitence were therefore unexpected in two ways – first for its requirement for MyD88, which is not involved in canonical TLR3 signaling, and second for the residual renitence observed in BMM deficient in TRIF, whose deficiency based on canonical TLR signaling would be expected to completely abrogate downstream effector functions, including renitence. Similarly, how TRIF deficiency leads to the complete abrogation of renitence induced by TLR7/8 activation when canonical signaling downstream of the receptor does not require TRIF is unclear. Finally, TLR9 activation by ODN 1826, noted in Fig 3.2.A and Fig 3.3.A for its inability to induce renitence, was unaffected by knockout of either MyD88 or TRIF. Together, these studies find that the requirement for MyD88 or TRIF for renitence varies depending on the TLR stimulated, and that the pattern of receptor usage necessary for renitence deviates for some TLRs (namely TLRs 3 and 7/8) from the pattern expected for NF-κB activation.

3.4.6 Renitence vacuole and macropinosome formation are not sufficient for renitence

In Chapter 2 we showed that AW bead uptake by LPS-treated BMM induced the formation of "renitence vacuoles" (RVs), periphagosomal structures derived from macropinosomes (MPs) that assist in the protection against bead-mediated lysosomal damage. With expanded knowledge of the conditions that do and do not induce renitence, here we asked whether renitence vacuole formation might serve as a general protective mechanism against phagolysosomal damage in other types of renitent macrophages. If so, we would expect RV formation to occur at higher frequency in activation states that confer renitence. To determine whether such a correlation exists, we quantified vacuole frequency in variously activated BMM in micrographs from which lysosomal damage was measured (Fig 3.1.C and Fig 3.2.A). As in Chapter 2, vacuoles were scored as phase-dense vacuolar structures that (1) appeared adjacent to an internalized bead and (2) had received Fdx from pre-labelled lysosomes (indicating mixing of the compartment with lysosomes). Of the major functional macrophage classes examined, RV formation after 60 min AW bead challenge was observed at highest frequency in CA-Mφ (LPS+ IFN-γ) and Reg-Mφ generated by stimulation with LPS and PGE2 (Fig 3.4.A). In fact, both groups formed RVs at even greater frequency than that detected in LPS-treated BMM. Reg-Mφ generated by stimulation with LPS and Ado formed RVs at lower frequency than Reg-Mφ (LPS+PGE2), but still at higher frequency than that seen in resting macrophages. Notably, AA-Mφ (IL-4) formed RVs with similar frequency as Reg-Mφ (LPS+Ado), even though AA-Mφ in Fig 3.1.C did not exhibit renitence. Thus, while RVs were generally seen at higher frequency in renitent macrophages (CA-Mφ, Reg-Mφ (LPS+PGE2), LPS-treated BMM) and at lower frequency in non-renitent macrophages (AA-Mφ), not all renitent macrophages formed RVs at high levels (Reg-Mφ (LPS+Ado)), and activated macrophages that were non-renitent could still

induce RV formation above the level seen in resting macrophages (AA-Mφ). We conclude that the extent of vacuole formation does not correlate directly with renitence capacity, with the caveat that the differences observed here did not reach statistical significance. More analyses will be needed to gain the power necessary to make a determination of significance. The results, however, suggest a correlation between macrophage activation and RV formation, as all activated macrophages observed, regardless of their ability to induce renitence, were able to form RVs at higher levels than those observed in resting macrophages.

Analysis of vacuole frequency in TLR-stimulated macrophages supports the same conclusion. All TLR agonists tested induced RV formation to a similar degree, including those that do (Pam3CSK4, Poly(I:C), LPS) and do not (FLA-ST, R848, ODN 1826) induce renitence (Fig 3.4.B). Why stimulation with FLA-ST induces RV formation despite its inability to activate macrophages is unclear. Together, the results from Fig 3.4.A and B show that macrophage activation induces RV formation. As RV formation can be induced in the absence of renitence, RVs are not sufficient to induce renitence.

In a related observation in Chapter 2, we determined that renitence in LPS-treated BMM requires macropinocytosis, an endocytic mechanism for internalizing extracellular fluid into vesicles called "macropinosomes" (MPs) (Fig 2.6.D). Moreover, LPS stimulation of macrophages robustly induced MP formation (Fig 2.6.A). As performed for RVs, we assessed whether the ability of variously activated macrophages to induce renitence might correlate with their ability to perform macropinocytosis. After stimulating macrophages overnight with inducers that either do (LPS, poly (I:C)) or do not (R848, IL-4) induce renitence, we quantified the extent of macropinocytosis in each condition as the average number of MPs per cell. Acute stimulation of cells with M-CSF served as a positive control for macropinocytosis.

We found that stimulation by all three TLR agonists tested induced macropinocytosis to comparable levels as that as induced by M-CSF (Fig 3.4.C). Thus, TLR stimulation generally induces both macropinocytosis (Fig 3.4.C) and RV formation (Fig 3.4.B). However, despite its ability to induce RV formation, IL-4 treatment did not stimulate macropinocytosis (Fig 3.4.C), suggesting that not all forms of activated macrophages induce macropinocytosis. Additionally, as R848 could induce macropinocytosis while only modestly inducing renitence, the presence of macropinocytosis does not necessarily predict renitence. We thus conclude that macropinocytosis, like RV formation, while perhaps necessary for renitence, is not sufficient to induce renitence.

3.5 Discussion

Here we report differential susceptibility to silica bead-mediated lysosomal injury in macrophages of various polarization states. Exhibiting the greatest capacity for renitence were macrophages activated overnight with LPS. Other macrophages capable of inducing renitence were closely related in their activation state. These included macrophages singly stimulated with Pam3CSK4 or poly(I:C) (agonists of TLRs 2/1 and 3 respectively) as well as Reg-Mφ and CA-Mφ. Other subtypes examined displayed a much lower capacity to protect their lysosomes from damage. Modest protection was observed in macrophages stimulated with R848 or ODN 1826 (agonists of TLRs 7/8 and 9 respectively). Of all activated macrophages analyzed, AA-Mφ were the least renitent, experiencing damage levels comparable to those seen in resting macrophages.

These results are summarized in Figure 3.5, which depicts the degree of renitence capacity exhibited by macrophages arranged in order of their ability to secrete pro-inflammatory cytokines. Viewing macrophages as existing along a spectrum of macrophage activation, we conclude that renitence is a property of macrophages occupying positions on the spectrum

between Reg-Mφ and CA-Mφ, with peak renitence noted in LPS-activated macrophages. Based on their ability to secrete high levels of both pro-inflammatory (IL-12p40, TNF-α) and anti-inflammatory (IL-10) cytokines, LPS-activated macrophages assume an intermediate activation state between those of Reg-Mφ and CA-Mφ (Fig 3.5.A). Consistent with this finding, Mosser and colleagues report that prolonged TLR stimulation of macrophages leads to the reprogramming of macrophages such that they convert from a CA-Mφ-like state into one characteristic of Reg-Mφ (Cohen *et al.*, 2015).

Our observation that LPS-activated macrophages and Reg-Mφ induce renitence to a similar degree, and to a greater extent than CA-Mφ, raises the question of whether LPS-activated macrophages might more closely resemble Reg-Mφ than CA-Mφ. More specifically, are the Reg-Mφ properties of LPS-activated macrophages more essential for renitence than their CA-Mφ-like properties? The detailed characterization of the steps involved in Reg-Mφ conversion by Mosser and colleagues has led to the development of tools that can be used to address this question. For example, genetic or pharmacological inhibition of CD39, the ectoenzyme responsible for converting extracellular ATP into the Reg-Mφ reprogramming signal adenosine (Ado), prevents Reg-Mφ conversion following TLR stimulation, sustaining a CA-Mφ-like state (Cohen *et al.*, 2013). Conversely, overexpression of A2bR, the receptor that recognizes Ado and induces downstream signaling leading to Reg-Mφ gene expression, permits the development of Reg-Mφ even in the presence of IFN-γ, which normally antagonizes A2bR activity (Cohen *et al.*, 2015). Using these tools, we can ask the following questions: (1) does inhibiting Reg-Mφ conversion also inhibit renitence in LPS-activated macrophages and Reg-Mφ, and (2) does skewing CA-Mφ toward a Reg-Mφ phenotype by A2bR overexpression enhance renitence? If indeed renitence is a particular property of Reg-Mφ that is reduced in a regulated manner in CA-

Mφ (for example, as a consequence of IFN-γ priming), then we would expect both predictions to be true.

The above findings suggest a link between the inflammatory state of a macrophage and its capacity to induce renitence. Further supporting this connection, macrophages singly stimulated with individual TLR agonists varied in their susceptibility to lysosomal damage according to their inflammatory state. That is, the TLR agonists capable of inducing renitence (Pam3CSK4, poly (I:C), and LPS) also induced the generation of macrophages exhibiting similar activation states. Likewise, those agonists that induced a modest level of renitence (R848, ODN 1826) produced macrophages of a common activation state that was distinct from the activation state held by the set of renitent macrophages. Specifically, the production of high levels of IL-12p40 distinguished the latter group of macrophages from the former. Notably, CA-Mφ, which on the spectrum of renitence capacity fall between that of the renitent and non-renitent groups of TLR-stimulated macrophages, also produce high levels of IL-12p40. Thus, in several examples, IL-12p40 inversely correlates with renitence. Whether IL-12p40 in fact antagonizes renitence is not known, and will be tested in future studies. If production of the cytokine indeed antagonizes renitence, we would expect that antibody neutralization of IL-12 would enhance renitence in R848 or ODN 1826-treated macrophages as well as in CA-Mφ. While the IL-12 secreted by macrophages acts primarily on NK cells and T cells (which in turn respond by producing the IFN-γ necessary for classical macrophage activation), an autocrine function for IL-12 in macrophages has been reported (Munder *et al.*, 1998). Thus, it is possible that IL-12p40 negatively regulates renitence in an autocrine manner.

Beyond the noted differences in inflammatory state, the set of renitent vs non-renitent TLR-stimulated macrophages did not group according to any known parameters associated with

TLR signaling. TLRs 2/1, 3, and 4, all of which induce renitence, differ in the signaling adaptors they recruit (TLR2/1 signals through MyD88, TLR3 through TRIF, and TLR4 through either MyD88 or TRIF), in their subcellular localizations (TLR2/1 becomes activated at the cell surface, TLR3 within endosomes, and TLR4 at either location), and in the class of ligands they recognize (TLR2/1 recognizes various ligands found in gram-negative and gram-positive bacteria, mycobacteria and yeast; TLR3 recognizes viral dsRNA; TLR4 recognizes lipopolysaccharide, a cell wall component of gram-negative bacteria) (Akira 2006). Neither do the TLRs whose activation did not profoundly induce renitence share obvious commonalities. TLRs 7/8 and 9 are both endosomally located, but recognize compounds of different classes: TLR 7/8 recognize viral ssRNA as a natural ligand, whereas TLR9 recognizes DNA containing unmethylated CpG motifs, found more abundantly in bacterial than mammalian DNA (Akira *et al.*, 2006). The induction of renitence by certain TLR agonists but not others suggests renitence is not a mechanism broadly upregulated by TLR activation. Dissection of the pathways upregulated or downregulated by activation of TLRs 2/1, 3, and 4, but not by activation of TLRs 7/8 and 9 could in future work provide a starting point for identifying the cellular and molecular activities that underlie renitence.

The pattern of signaling adaptor requirements revealed here for TLR-induced renitence deviates from the well-established adaptor requirements for TLR signaling leading to NF-κB activation. The main points of deviation lay with the endosomal TLRs 3 and 7/8: the dependence on MyD88 for poly(I:C)-induced renitence, and the requirement for TRIF for R848-induced renitence. These results suggest that cross-talk between MyD88 and TRIF may be necessary for renitence induced downstream of these TLRs. A role for MyD88 in negatively regulating the inflammatory response associated with poly(I:C)-induced TLR3 signaling has

been reported in a model of corneal inflammation (Johnson *et al.*, 2008) as well as in immortalized BMM (Kenny *et al.*, 2009). However, this negative regulation of TRIF signaling by MyD88 was absent in primary mouse BMM (Johnson *et al.*, 2008). Likewise, the dependency of R848-induced TLR7/8 signaling on TRIF has to our knowledge never been described. The deviation we observe could thus possibly be explained by a novel pathway of cross-talk between MyD88 and TRIF.

This study finds that multiple macrophage subtypes other than LPS-activated macrophages can induce renitence. Whether a common mechanism for renitence exists in each of these subtypes is not known. If such a mechanism does exist, it likely does not depend on the formation of renitence vacuoles (RVs) or macropinosomes (MPs), determined in Chapter 2 to be essential for LPS-induced renitence, but which were found here to form in several types of activated macrophages regardless of their ability to induce renitence. That is, while RVs do represent damage-resistant structures within individual cells, their presence was not sufficient to confer renitence at the population level. Methods for eliminating RV formation are needed to formally test the necessity of RVs for renitence. Based on the available evidence, we conclude that while RVs may be necessary for renitence in some macrophage subtypes, it likely represents one of several mechanisms that contribute to lysosomal damage protection by renitence. Other possible vacuole-independent mechanisms for protection are considered in Chapter 4.

By systematically evaluating the inflammatory state and renitence capacity of a large range of activated macrophages, here we refined our understanding of the immunological contexts of renitence. As renitence is a property of CA-Mφ and Reg-Mφ, as well as a subset of TLR-stimulated macrophages, it likely contributes to cellular functions important for host defense and/or immune regulation. A proposed model for the functional role of renitence in the

immune response and possible approaches for testing this model will be explored in the Discussion of this thesis.

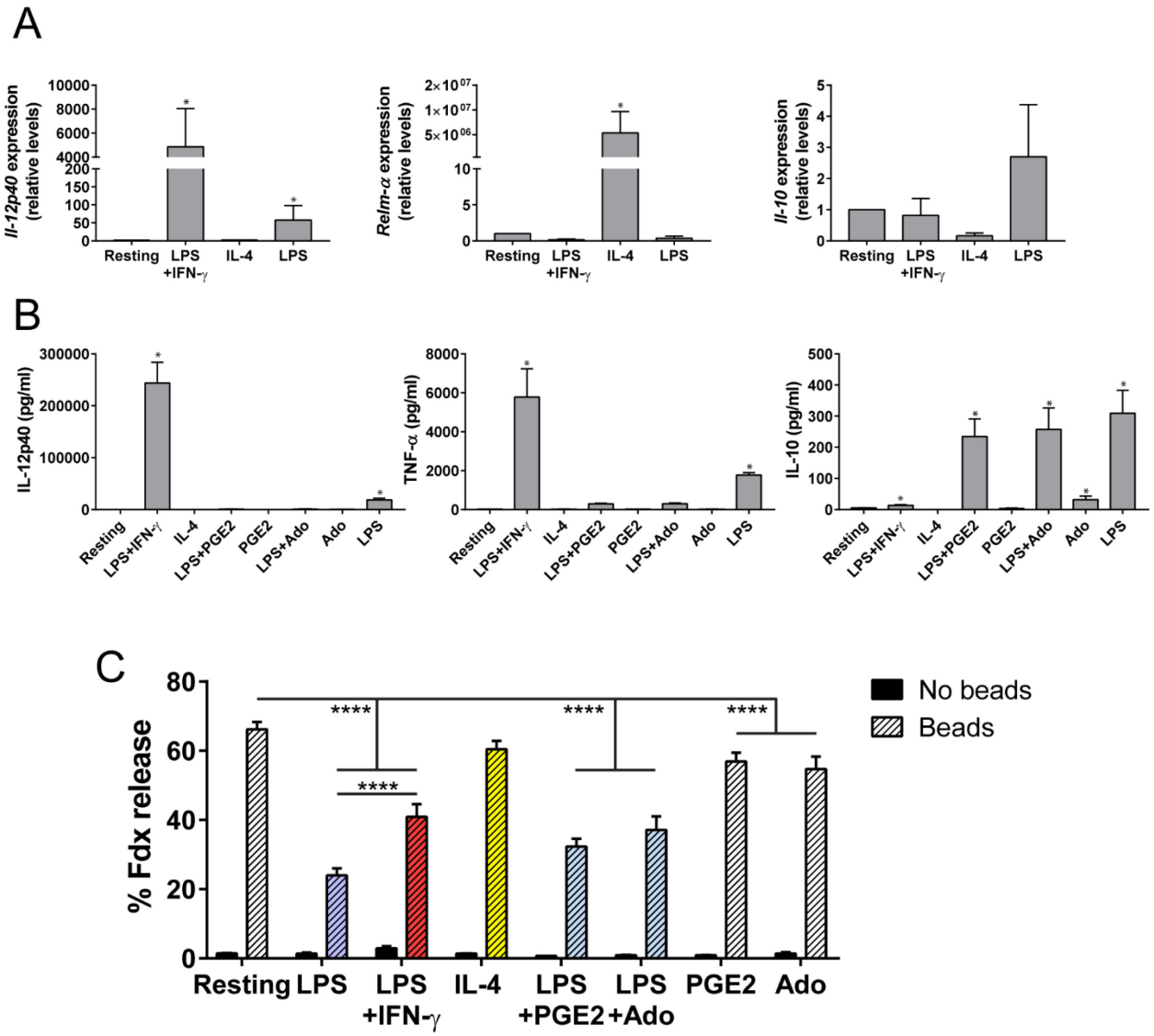

Figure 3.1. Renitence is a property of classically activated and regulatory macrophages, but not of alternatively activated macrophages.

(A) BMM treated overnight with LPS and IFN-γ (after initial 6 h IFN-γ priming), IL-4, or LPS alone, or left unstimulated (Resting). For each condition, mRNA expression of *Il-12p40*, *Relm-α*, and *Il-10* relative to levels expressed in resting BMM was determined by qPCR. Bars represent mean ± SEM calculated from at least two (*Il-10*) or three (*IL-12p40*, *Relm-α*) independent experiments. Statistical significance relative to expression levels in resting BMM is indicated. *$p \leq 0.05$.

(B) BMM were subjected to the following treatments for generating classically activated (CA-Mφ), alternatively activated (AA-Mφ), or regulatory macrophages (Reg-Mφ): 6 h IFN-γ priming followed by overnight stimulation with LPS and IFN-γ to generate CA-Mφ; overnight

stimulation with IL-4 to generate AA-Mφ; overnight stimulation with LPS in combination with prostaglandin E2 (PGE2) or adenosine (Ado) to generate Reg-Mφ. As controls, macrophages were left unstimulated (Resting) or treated overnight with LPS, PGE2, or Ado alone. Levels of IL-12p40, TNF-α, and IL-10 in cell supernatants from each condition were measured by ELISA. Each bar represents mean ± SEM of at least three independent experiments. Statistical significance relative to levels of cytokine secretion in resting BMM is shown. $*p \leq 0.05$.

(C) BMM were pulsed overnight with fluorescein dextran (Fdx) while subjected to the indicated treatments for generating CA-Mφ (red), AA-Mφ (yellow), Reg-Mφ (blue), or control macrophages, which included resting macrophages and BMM singly treated with LPS (purple), PGE2, or Ado. The next day, cells were chased for 3 h to move Fdx into lysosomes, fed acid-washed (AW) beads for 60 min to initiate membrane damage, and imaged to measure lysosomal damage. Damage measurements are reported as the average percent of Fdx release ± SEM per condition in cells that have internalized 3 to 7 beads. Data for each condition was obtained from at least two or three independent experiments (n > 100 cells). $****p \leq 0.0001$.

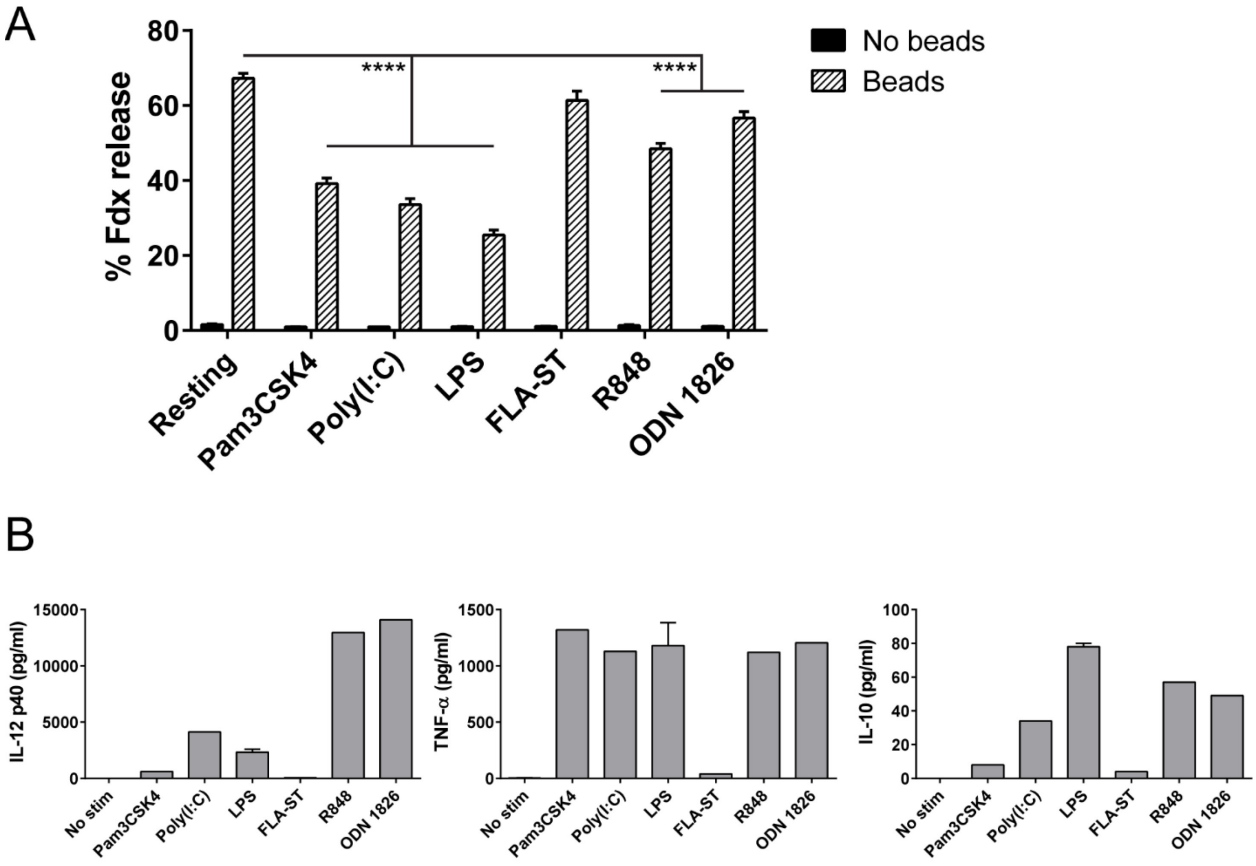

Figure 3.2. A subset of TLR agonists induces renitence.

(A) BMM were pulsed overnight with Fdx while undergoing stimulation with the indicated TLR agonists or left untreated. The next day, cells were chased for 3 h, fed AW beads for 60 min, and imaged to detect Fdx release. Bars represent average percent Fdx release ± SEM for cells taking up 3-7 beads per cell. Data shown are from ≥3 experiments, with > 180 cells analyzed. ****$p \leq$ 0.0001.

(B) BMM were stimulated overnight with the indicated TLR agonists or left untreated. Levels of IL-12p40, TNF-α, and IL-10 in cell supernatants were measured by ELISA. Data shown is from one experiment. (Not enough replicates to perform t-test. As such, test of significance was not performed.)

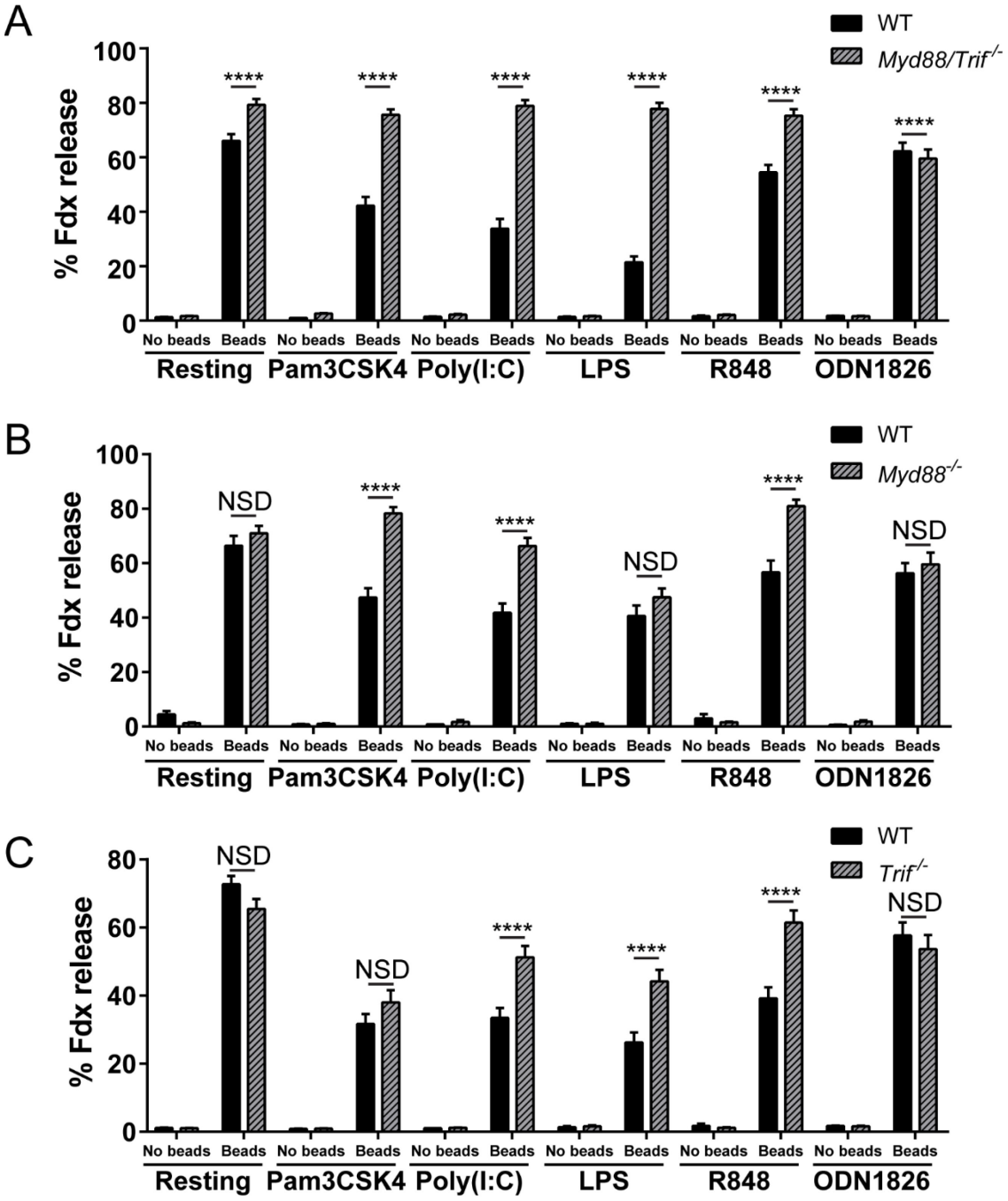

Figure 3.3. Renitence requires intact TLR signaling, with differential requirement for MyD88 or TRIF for each agonist.

(A) BMM were isolated from C57/B6 (WT) mice and mice deficient in *Myd88* and *Trif* (*Myd88/Trif*$^{-/-}$). Both groups of BMM were treated overnight with the indicated TLR agonists concurrent with pulse-chase labeling of lysosomes with Fdx. Bars represent the average percent Fdx release ± SEM after 60 min AW bead incubation in cells receiving 3-7 beads per cell. Data shown are from 2 independent experiments (n > 100 cells for each group). ****$p \leq 0.0001$.

(B) WT and *Myd88*$^{-/-}$ BMM were subjected to pulse-chase labeling of lysosomes with Fdx and concurrently stimulated with the indicated TLR agonists. BMM were then fed AW beads for 60 min and assayed for lysosomal damage. Bars represent the average percent Fdx release ± SEM cells receiving 3-7 beads per cell. Data shown are from 2 independent experiments (n > 60 cells for each group). ****$p \leq 0.0001$. NSD: no significant difference.

(C) WT and *Trif*$^{-/-}$ BMM were subjected to pulse-chase labeling of lysosomes with Fdx and concurrently stimulated with the indicated TLR agonists. BMM were then fed AW beads for 60 min and assayed for lysosomal damage. Bars represent the average percent Fdx release ± SEM cells receiving 3-7 beads per cell. Data shown are from 2 independent experiments (n > 85 cells for each group). ****$p \leq 0.0001$. NSD: no significant difference.

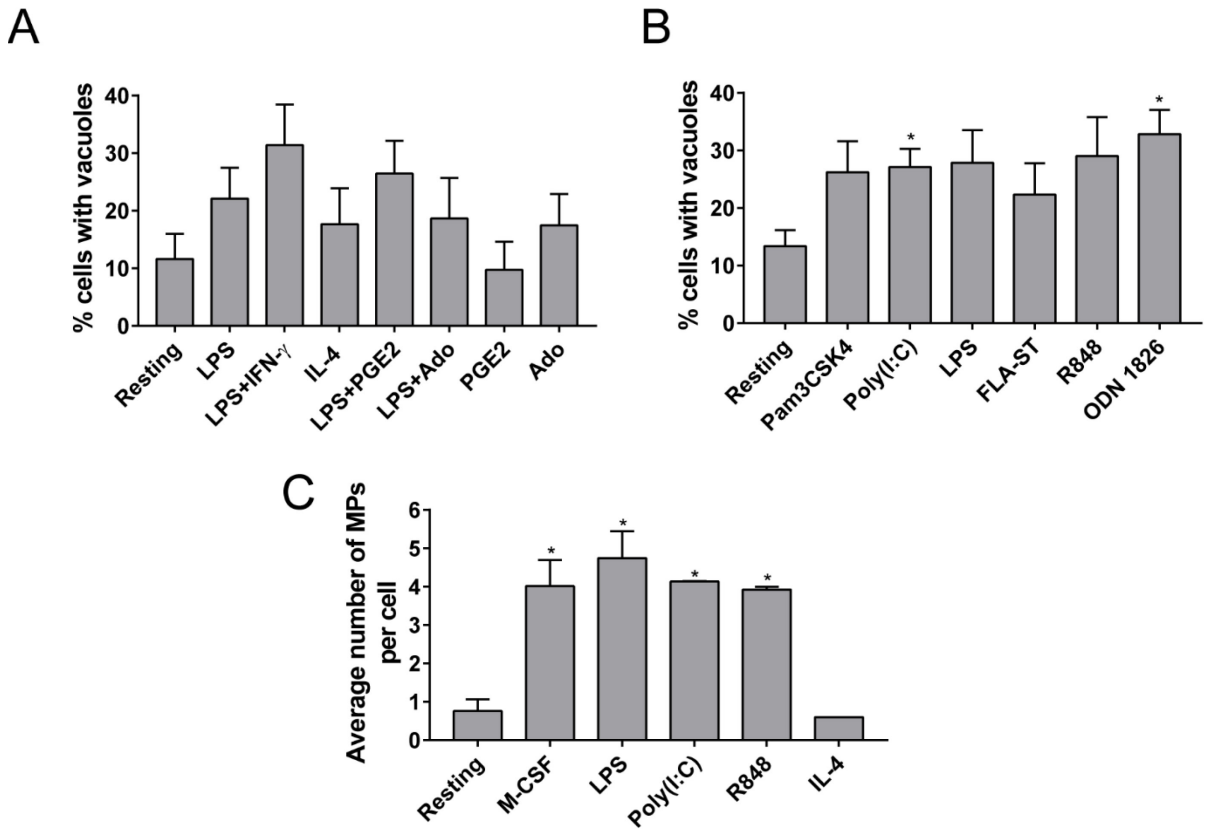

Figure 3.4. Renitence vacuole and macropinosome formation is not sufficient to induce renitence.

(A) Frequency of renitence vacuole (RV) formation in variously activated macrophages. Micrographs of BMM subjected to 60 min AW bead incubation in Fig 3.1.C were analyzed for vacuole frequency. For each condition, the percent of cells harboring one or more vacuoles was quantified. Bars represent the average ± SEM vacuole frequency from 2 (LPS+Ado, Ado), 3 (LPS+IFN-γ, IL-4, PGE2), or 4 (Resting, LPS, LPS+PGE2) independent experiments (n > 100 cells per condition). Applying an unpaired, two-tailed t-test, none of the differences observed were found to reach statistical significance.

(B) Frequency of RV formation in TLR-stimulated macrophages. Micrographs of BMM subjected to 60 min AW bead incubation in Fig 3.2.A were analyzed for vacuole frequency. Bars represent the average percent of cells ± SEM within each condition harboring one or more vacuoles. Data shown are from 2 (ODN 1826) or 3 (all others) independent experiments. Statistical significance relative to vacuole frequency in resting macrophages is indicated. $*p \leq 0.05$.

(C) Extent of macropinocytosis in variously activated macrophages. BMM stimulated overnight with the indicated stimuli were pulsed for 10 min with 70 kDa Fdx, which upon endocytic uptake labels macropinosomes. Cells were then washed to remove extracellular probe, fixed, and imaged by fluorescence microscopy. Macropinosomes were scored as phase bright structures within cells that co-localized with 70 kDa Fdx. As a positive control, the extent of

macropinocytosis was measured in BMM stimulated with macrophage colony stimulating factor (M-CSF) during the 10 min Fdx pulse. Data shown is from one experiment (with 2 technical replicates and ≥ 25 cells analyzed per replicate). Statistical significance relative to extent of MP formation in resting macrophages is indicated. *$p \leq 0.05$.

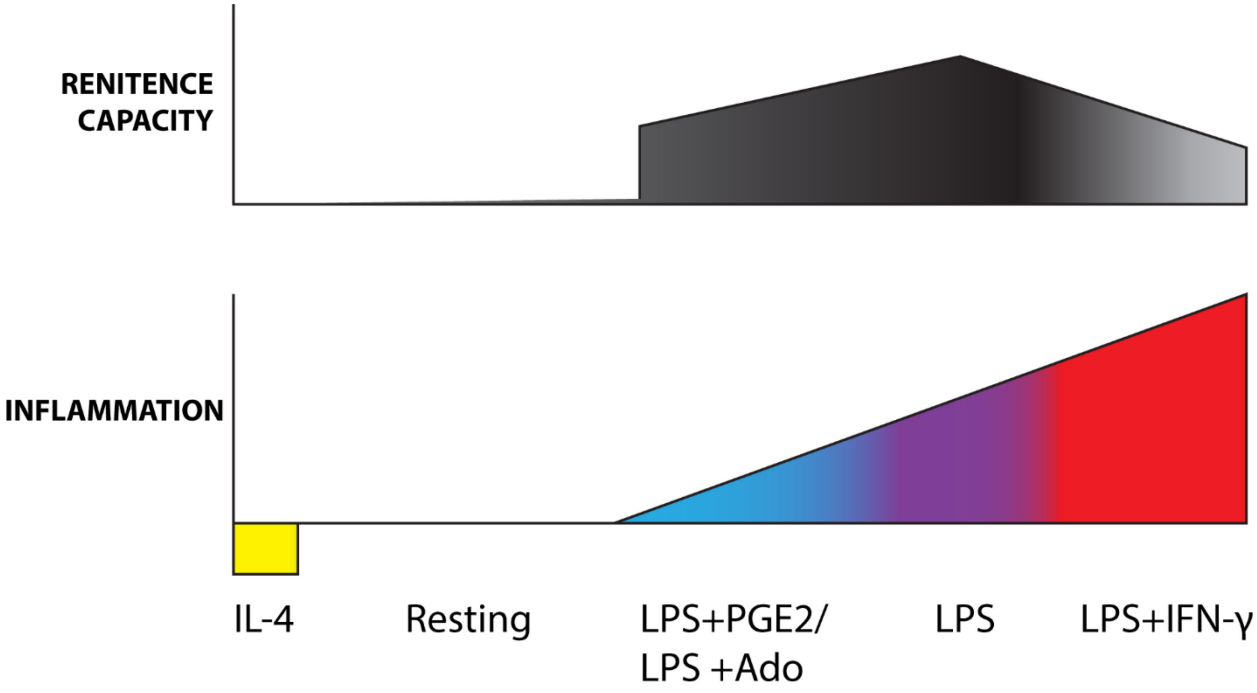

	IL-4	Resting	LPS+PGE2/ LPS +Ado	LPS	LPS+IFN-γ
IL-12p40	-	-	-	++	+++
TNF-α	-	-	+	++	+++
IL-10	-	-	++	++	-
RELM-α	+++	-	-	-	-

Figure 3.5. Renitence capacity in variously activated macrophages.

Schematic depicting the extent of renitence exhibited by variously activated macrophages arranged in order of their ability to secrete pro-inflammatory cytokines. This graphic adopts the analogy proposed by Mosser and colleagues, in which various classes of activated macrophages are represented by different shades of colors on a color wheel (Mosser and Edwards, 2008). The three primary colors, red, yellow, and blue, respectively represent the three major functional classes studied: CA-Mφ, AA-Mφ, and Reg-Mφ. Here we add two more macrophage classes – resting and LPS-activated macrophages - to the model, and, for simplicity, depict these activation states on a linear scale.

On the far left are IL-4-treated AA-Mφ, which do not secrete substantial levels of any of the pro-inflammatory (IL-12p40, TNF-α) or anti-inflammatory (IL-10) cytokines surveyed, but do robustly express the AA-Mφ marker *Relm-α* - as summarized in the table below the schematic. The other activated macrophages analyzed all produce varying levels of the three cytokines, and are arranged in order of lowest to highest pro-inflammatory cytokine secretion. Graphically, this is represented as a gradient that increases in height from left to right. As the cytokine secretion

profile of AA-Mφ differs drastically from that of the other activated macrophage classes, their inflammatory status is represented on the opposite side of the axis.

The spectrum of macrophages exhibiting the capacity for renitence is indicated in the top-most panel, in which the height and intensity of the monochromatic gradient correlates with a higher capacity for renitence. As indicated, renitence is a property of Reg-Mφ, LPS-activated macrophages, and CA-Mφ. When viewed together with the Inflammation gradient in the middle panel, we see that these renitent macrophages are closely related in activation state, especially when compared with their resting and AA-Mφ counterparts. Thus, renitence appears to be a property of macrophages involved in host defense (CA-Mφ) and immune suppression (Reg-Mφ). Of unknown significance, peak renitence is consistently exhibited by LPS-activated macrophages, whose special propensity for renitence is the focus of the present work.

Primer name	Sequence (5'→ 3')
Il-12p40 F	AAGACGTTTATGTTGTAGAGGTGGAC
Il-12p40 R	ACTGGCCAGGATCTAGAAACTCTTT
Il-10 F	GACTTTAAGGGTTACTTGGGTTGC
Il-10 R	TCTTATTTTCACAGGGGAGAAATCG
Relm-α F	AATCCAGCTAACTATCCCTCCA
Relm-α R	CAGTAGCAGTCATCCCAGCA
Gapdh F	AAGGTCGGTGTGAACGGATTT
Gapdh R	AATTTGCCGTGAGTGGAGTCATAC

Table 3.1. Primers for measuring the expression of target genes in variously activated macrophages by qPCR.

CHAPTER 4

Investigating Molecular Mechanisms of Renitence

This work was performed in collaboration with Matangi Marthi, Sei Yoshida, Brian Gregorka, Chan Chung, Andrew P. Lieberman, Michele S. Swanson, and Joel A. Swanson. A.O.W, M.M., and J.A.S. designed the project and performed experiments. S.Y. performed Western blots. B.G and M.S.S participated in data analysis. C.C. and A.P.L contributed reagents and technical expertise. A.O.W. wrote this chapter.

4.1 Abstract

This chapter describes a candidate approach taken for uncovering the molecular mechanisms underlying renitence. From a theoretical standpoint, a mechanism for reinforcing lysosomal integrity would likely involve either an increase in the intrinsic resistance of lysosomal membranes against damage or the activation of a rapid response for repairing membrane damage. Several mechanisms falling under either category were considered for their contribution to renitence. These candidate mechanisms included the following: increased membrane resistance through the structural fortification of lysosomal membranes by cholesterol, and induction of membrane repair facilitated by synaptotagmin-7 or autophagy. Using genetic and pharmacological tools for manipulating lysosomal cholesterol content, we determined that cholesterol accumulation within lysosomes enhanced protection from damage, and depletion of cholesterol from cholesterol-loaded states abrogated the protective effect. Thus, cholesterol

within lysosomes acts as a protective species against membrane damage. However, as LPS treatment of macrophages does not increase cellular (and likely lysosomal) cholesterol levels above those seen in resting macrophages, renitence occurs independently of cholesterol accumulation. Despite its established role in mediating plasma membrane repair, the calcium sensor synaptotagmin-7 promotes membrane damage to macrophage lysosomes. Autophagy, well-established to clear damaged organelles within cells, only modestly contributed to renitence. Finally, activation of the signaling kinase Akt is likely necessary for the formation of the renitence vacuoles first described in Chapter 2, as inhibition of Akt with the pharmacological inhibitor MK-2206 eliminated renitence vacuole formation in LPS-activated macrophages. This last finding connects the molecular efforts undertaken here and the cell biological characterization of renitence made in Chapter 2.

4.2 Introduction

Renitence we have defined as an activity that enhances the protection of macrophage lysosomes against damaging insults, such as those incurred by pathogens or, in the case of our model system, silica beads. In Chapter 2 we determined that renitence is a mechanism that acts quickly (within 15 to 30 min after silica bead uptake) and limits the release of small but not large molecular-weight molecules from lysosomes. Here we sought to determine the molecular mechanisms underlying this cellular activity. Several candidate mechanisms were considered on the basis of their involvement in other forms of membrane protection as well as for their noted ability to interact with lysosomes. These mechanisms – cholesterol accumulation, synaptotamin-7, autophagy, and Akt activation – will be considered in turn.

Guiding this candidate approach is the thinking that renitence likely operates through mechanisms that enhance the resistance of lysosomes against damage or enable the rapid repair

of damaged membranes. The former would likely serve as a mechanism to prevent damage, for example through structural fortification of membranes. As cholesterol affects the fluidity of membranes, we reasoned that its abundance within lysosomal membranes might affect the susceptibility of lysosomes to damage. Supporting this point, early, cell-free experiments by de Duve found that cholesterol stabilizes lysosomes against damage (De Duve *et al.*, 1962). More recent studies have determined that the depletion of cholesterol from lysosomes following methyl-cyclodextrin treatment of HepG2 cells destabilizes lysosomal membranes (Jadot *et al.*, 2001). Additionally, as LPS treatment of RAW 264.7 macrophages was found to induce the generation of cholesterol-laden foam cells (Funk *et al.*, 1993), we investigated whether LPS treatment might induce renitence through increasing the cholesterol content of lysosomes.

Niemann-Pick C (NPC) disease is a lysosomal storage disease that manifests with severe symptoms of neurodegeneration and is characterized at the cellular level by cholesterol accumulation within lysosomes (Vanier, 2013). The disease is caused by mutations in the genes encoding Npc1 or Npc2, lysosomal proteins involved in the transport of cholesterol from lysosomes to other cellular compartments (Kwon *et al.*, 2009). Cells deficient in either Npc1 or Npc2 accumulate cholesterol within their lysosomes. In this study, macrophages from mice deficient in Npc1 will be used to model a state of lysosomal cholesterol accumulation.

Synaptotagmin-7 (Syt7), like Npc1, is a lysosomal membrane protein, but one that serves a very different role, and is considered here for its possible involvement in the repair of damaged lysosomes. Syt7 is a Ca^{2+} sensor that mediates the fusion of lysosomes with other cellular membranes, including the plasma membrane during repair after mechanical injury (Chakrabarti *et al.*, 2003). That is, wounding of the plasma membrane triggers an influx of Ca^{2+} into the cell, which is recognized by Syt7. Upon Ca^{2+} sensing, Syt7 facilitates the exocytosis of lysosomes,

and lysosomes delivered to the site of plasma membrane injury serve as a source of membrane for repair (Andrews *et al.*, 2014). We considered here whether Syt7 might facilitate the repair of damaged lysosomes in an analogous process to plasma membrane repair.

Autophagy, an intracellular pathway for delivering cytoplasmic components to the lysosome for degradation, shares several similarities with renitence. In sequestering and clearing damaged organelles, including mitochondria, lysosomes, and phagolysosomes damaged by intracellular pathogens, autophagy, like renitence, serves as a response to membrane damage (Randow and Youle, 2014). In addition, many of the factors that induce renitence (eg. LPS, IFN-γ) also upregulate autophagy (Gutierrez *et al.*, 2004; Xu *et al.*, 2007). While autophagy's role in clearing damaged organelles has been well-established, recent evidence suggests an additional role in the direct repair of damaged bacteria-containing vacuoles (Kreibich *et al.*, 2015). Here we considered the hypothesis that autophagy may contribute to renitence by providing a source a membrane for the repair of damaged lysosomes.

In the final section of this chapter, we sought to continue work begun in Chapter 2 by identifying molecular factors contributing to renitence vacuole (RV) formation. As the TLR4-PI3K-Akt-mTOR signaling axis induced by LPS is involved in macropinosome (MP) formation in macrophages (Wall *et al.*, 2017), we investigated whether perturbing this pathway might affect the frequency of formation of RVs, which are derived from MPs.

Together, this chapter brings together the findings of several efforts aimed at uncovering the molecular mechanism underlying renitence.

4.3 Materials and Methods

4.3.1 Mice and macrophage isolation

C57BL6/J mice were purchased from The Jackson Laboratory (Bar Harbor, ME). *Npc1*$^{-/-}$ mice and *Npc1*$^{+/+}$ littermate controls were generously provided by Andrew Lieberman. *Atg7*$^{fl/fl}$-Lyz-*Cre* and Atg7$^{fl/fl}$-WT mice were obtained from Herbert Virgin (Washington University in St. Louis). *Syt7*$^{-/-}$ mice were obtained from Norma Andrews (University of Maryland). As the *Syt7*$^{-/-}$ mice were generated on a C57BL6/J background (Chakrabarti *et al.*, 2003), BMM isolated from C57BL6/J mice were used as WT controls in experiments in which lysosomal damage in *Syt7*$^{-/-}$ BMM was examined. All mice were maintained under specific pathogen-free conditions at the University of Michigan. Bone marrow-derived macrophages (BMM) from mice of each genotype were obtained as described in Chapters 2 and 3. Briefly, bone marrow cells isolated from the femurs and tibia of mice were differentiated into macrophages through culture for 6-8 days in DMEM containing 10% FCS and 50 ng/ml recombinant M-CSF.

4.3.2 Cell treatments for manipulating lysosomal cholesterol content

Cholesterol accumulation within WT BMM was induced by overnight treatment with 1 μg/ml U18666A (Enzo Life Sciences, Farmingdale, NY). U18666A and LPS (100 ng/ml) were added to cells at the same time for cells undergoing LPS activation. To extract cholesterol from WT and *Npc1*$^{-/-}$ BMM, cells were treated for 48 h with 300 μM hydroxypropyl beta-cyclodextrin (HP-βCD; Sphingo Biotechnology, Inc., Alachua, FL) in the presence or absence of simultaneous treatment with 100 ng/ml LPS (List Biological Laboratories; Campbell, CA).

4.3.3 Filipin staining

WT or *Npc1*$^{-/-}$ BMM plated on 12 mm coverslips were left untreated or stimulated overnight with U18666A or for 48 h with HP-βCD. Cells were fixed for 20 min at 37°C in fixation buffer (75 mM lysine-HCl, 37.5 mM Na_2HPO_4, 4.5% sucrose, 2% paraformaldehyde, 10 mM sodium periodate), and washed with DPBS. Samples were then stained with 0.05 mg/ml

filipin (Sigma-Aldrich, St. Louis, MO) in DPBS containing 10% FCS for 2 h at room temperature. After several rinses, samples were mounted on microscope slides using Prolong Gold (ThermoFisher, Waltham, MA). Samples were imaged on an inverted fluorescence microscope using a 402-455 filter set combination to visualize fluorescence emitted by filipin. The average fluorescence intensity of filipin per cell, normalized for cell area, was determined using MetaMorph software (Molecular Devices, Sunnyvale, CA).

4.3.4 Measurement of lysosomal damage by ratiometric imaging

Labeling of macrophage lysosomes with fluorescein dextran (Fdx), acid-washed silica bead preparation, and lysosomal damage measurements were performed as described in Chapters 2 and 3.

4.3.5 Photooxidative damage of lysosomes

BMM were plated onto glass-bottom microwell dishes (MatTek Corporation, Ashland, MA) in RPMI 1640 containing 10% FCS. Lysosomes within BMM were pulse-chase labelled with 150 μg/ml Fdx (ThermoFisher, Waltham, MA) and 75 μg/ml Texas Red dextran (TRDx; average molecular weight 10 kDa; ThermoFisher, Waltham, MA). Fdx is used as a reporter of pH, and TRDx serves as a photosensitizer. BMM were washed with Ringer's buffer and mounted for imaging. Cells were then exposed to 580 nm light, which excites TRDx, every 90 seconds for 1 second intervals, to induce photodamage. Fdx images (ex. 440-em. 525 and ex. 485-em. 525) were collected between each exposure. The average percent Fdx release for cells of a given condition was determined for each time point. MetaMorph software was used for image processing.

4.3.6 Cell treatments for inhibiting Akt and mTOR

For studies involving the inhibition of Akt or mTOR activation, BMM were pre-treated with either MK-2206 (2 μM; APExBIO, Houston, TX) or Torin 1 (500 nM; Cell Signaling, Danvers, MA) for 30 min before the start of bead incubation. The inhibitors were also included in the media for the duration of bead incubation.

4.3.7 Analysis of vacuole frequency

Renitence vacuole (RV) frequency was quantified in images of resting and LPS-treated BMM from which measurements of lysosomal damage were made in Fig 4.6.A and Fig 4.6.E. Images were scored for the presence or absence of RVs by the following criteria: (1) appearance on the phase contrast image as a circumscribed phase-dense region adjacent to an internalized bead, and (2) presence of Fdx within the structure. RV frequency was quantified as the percent of cells containing one or more vacuoles within a given condition. All cells containing at least one bead were included in the analysis.

4.3.8 Macropinosome counting assay

To measure macropinocytosis, resting or LPS-treated BMM plated on 12 mm circular coverslips were pulsed for 10 min with 70 kDa Fdx (0.5 mg/ml) after receiving pre-treatments with MK-2206 or Torin 1. In control conditions, macropinocytosis was stimulated by inclusion of M-CSF (200 ng/ml) during the time of the Fdx pulse. Cells were gently washed with HBSS to remove uningested probe, fixed for 30 min at 37°C with fixation buffer (see 4.3.3 above), and imaged by fluorescence microscopy. MetaMorph software was used to merge phase contrast and background-subtracted Fdx images. The number of MPs per cell was determined by scoring the number of Fdx-positive phase bright vesicles in the merged images.

4.3.9 Western blotting

Resting or LPS-treated BMM receiving the MK-2206 or Torin 1 pre-treatments described above were lysed for 10 min in ice-cold lysis buffer (40 mM HEPES, pH 7.5, 120 mM NaCl, 1 mM EDTA, 10 mM pyrophosphate, 10 mM glycerophosphate, 50 mM NaF, 1.5 mM Na_3VO_4, 0.3% CHAPS, and a mixture of protease inhibitors; Roche), as previously described (Yoshida *et al.*, 2011). Lysates were cleared by centrifugation at 13,000 × *g* for 15 min at 4°C. Supernatants were mixed with 4× SDS sample buffer and boiled for 5 min. The samples were run on SDS-PAGE and subjected to Western blot analysis using the following antibodies: anti–S6K (2708), anti–phospho-S6K (Thr389; 9234), anti–Akt (9272), anti–phospho-Akt (Thr308; 4056), anti–Erk1/2 (4695), anti–phospho-Erk1/2 (Thr202/Tyr204; 4376). All of these antibodies were purchased from Cell Signaling (Danvers, MA); catalog numbers are noted above in parentheses.

For confirming the absence or presence of Atg7 protein in *Atg7*$^{fl/fl}$-Lyz-*Cre* and Atg7$^{fl/fl}$-WT BMM respectively, cell lysates were prepared as described above. Western blots were probed with antibodies against Atg7 (Abcam; Cambridge, United Kingdom) and β-actin (Sigma; St. Louis, MO).

4.3.10 Statistical Methods

Statistical analysis was performed using GraphPad Prism software (GraphPad Software Inc; La Jolla, CA). Differences in lysosomal damage and average filipin staining intensity between groups were compared using two-way ANOVA with Tukey's multiple comparisons. Frequency of vacuole or MP formation between groups was compared using a two-tailed, unpaired t-test.

4.4 Results

4.4.1 Macrophages deficient in Npc1 resist lysosomal damage induced by chemical or photooxidative stress

To investigate whether inducing cholesterol accumulation within macrophage lysosomes confers protection from lysosomal damage, we measured AW bead-mediated lysosomal damage in resting and LPS-treated BMM isolated from WT and *Npc1*$^{-/-}$ mice. Compared to WT BMM, macrophages deficient in Npc1 displayed significantly lower levels of lysosomal damage following 60 min AW bead incubation (Fig 4.1.A). This enhanced protection conferred by Npc1 deficiency was observed for both resting and LPS-treated macrophages.

Macrophages deficient in Npc1 have reported defects in phagosome maturation (Huynh *et al.*, 2008). Thus, the results obtained above could be due to the impaired delivery of membrane-damaging beads to lysosomes in *Npc1*$^{-/-}$ but not WT BMM. To rule out this possibility, we used an alternative method of inducing lysosomal damage that is independent of phagosome trafficking. In this method, cells whose lysosomes are pre-loaded with two different fluorescent probes – Fdx, as used in our bead-damage assay, and Texas Red dextran (TRDx) – are alternatively exposed to bright light that excites TRDx and causes photooxidative damage to lysosomes, and to low intensity light that excites Fdx without causing photodamage and permits pH measurements for determining the extent of Fdx release. Through successively exposing a given field of cells to photodamage and capturing Fdx images at regular intervals over time, a plot of Fdx release values across increasing time of photoexposure can be obtained. Steeper curves on these plots represent damage that is incurred more rapidly. After about seven cycles of such photoexposure, lysosomes within resting WT BMM released nearly all of their dye (Fig 4.1.B). Complete dye release from lysosomes within LPS-treated BMM did not occur until much later cycles, confirming the enhanced ability of LPS-activated macrophages to resist

lysosomal damage. Strikingly, lysosomes within resting and LPS-treated *Npc1*$^{-/-}$ BMM did not completely release their dye even by the final round of photoexposure. Thus, the capacity of cholesterol-loaded lysosomes to resist lysosomal damage is profound, and even greater than that observed in LPS-treated BMM.

4.4.2 Depletion of cholesterol from Npc1-deficient macrophages partially abrogates lysosomal damage protection

To confirm that the protective effect observed in *Npc1*$^{-/-}$ BMM is specifically due to their accumulation of lysosomal cholesterol, we tested whether depleting lysosomal cholesterol in these cells would reverse protection. We treated resting and LPS-treated *Npc1*$^{-/-}$ BMM with hydroxypropyl-β-cyclodextrin, (HP-βCD) a molecule that extracts cholesterol from the lysosomes of cells, although non-specifically (Atger *et al.*, 1997; Rosenbaum *et al.*, 2010). To confirm the effect of the drug on cholesterol levels, we imaged fixed cells stained with filipin, a dye that binds unesterified cholesterol (Gimpl and Gehrig-Burger, 2007). As classically described in other cell types (Sokol *et al.*, 1988), *Npc1*$^{-/-}$ macrophages harbored numerous cholesterol-laden granules (Fig 4.2.A). Quantification of the average filipin staining intensity in micrographs of cells treated with or without HP-βCD indicated that the drug reduced but did not completely eliminate cholesterol accumulation within *Npc1*$^{-/-}$ BMM (Fig 4.2.B).

In the filipin staining experiments described here and later in the chapter, the extent of total cellular rather than lysosomal cholesterol was quantified. While simultaneous labeling of lysosomes within these cells was performed (data not shown), determining the threshold for lysosomal as opposed to background, non-lysosomal signal proved technically challenging in WT resting BMM, in which the lysosomal staining was bright and diffusely localized throughout the cell. However, as most of the cholesterol within *Npc1*$^{-/-}$ cells accumulates within lysosomes

(Mukherjee and Maxfield, 2004), we would not expect that the quantification of lysosomal as opposed to cellular cholesterol would give a different result to the questions posed.

We next tested the effect of HP-βCD on lysosomal damage in WT and *Npc1*$^{-/-}$ BMM. As seen previously, in the absence of drug treatment, macrophages deficient in Npc1 displayed reduced lysosomal damage compared to their WT resting and LPS-treated counterparts. 48 h pre-treatment of cells with HP-βCD partially abrogated protection in resting *Npc1*$^{-/-}$ BMM but had no effect on LPS-treated *Npc1*$^{-/-}$ BMM (Fig 4.2.C), even though the drug was more effective at extracting cholesterol from the latter group of cells (Fig 4.2.B). Thus, cholesterol accumulation specifically protects against lysosomal damage in resting but not LPS-treated macrophages.

4.4.3 LPS treatment of macrophages does not induce cellular cholesterol accumulation

As LPS treatment and Npc1 deficiency both enhance lysosomal damage protection in macrophages, we wondered whether LPS treatment induces renitence through increasing cholesterol levels within macrophage lysosomes. To address this question, we treated cells with U18666A, a drug that mimics the effect of Npc1 deficiency by blocking the exit of cholesterol from lysosomes (Liscum, 1990). As confirmed by quantification of filipin staining intensity, overnight treatment of resting and LPS-treated BMM with U18666A induced cholesterol accumulation within cells (Fig 4.4.C). Recapitulating the phenotype of *Npc1*$^{-/-}$ BMM, U18666A treatment led to a reduction in AW bead-mediated damage in both resting and LPS-treated BMM (Fig 4.3.A). However, comparison of the extent of cholesterol accumulation within resting and LPS-treated BMM in the absence of drug treatment revealed that LPS-treated BMM harbor no more intracellular cholesterol than resting macrophages, suggesting that LPS treatment does not induce lysosomal cholesterol accumulation in macrophages (Fig 4.3.C). Thus, the enhanced

protection from lysosomal damage observed in LPS-treated and cholesterol-loaded macrophages likely occurs through independent mechanisms.

4.4.4 Synaptotagmin 7 promotes lysosomal membrane damage in macrophages

A second candidate whose contribution to renitence was evaluated was synaptotagmin-7 (Syt7), a lysosomal membrane protein implicated in the repair of plasma membrane damage through facilitating the exocytosis of lysosomes. We hypothesized that Syt7 might also promote the repair of damaged lysosomes through facilitating the fusion of intact with damaged lysosomes. To test this model, we measured lysosomal damage in WT and *Syt7*$^{-/-}$ BMM, with the expectation that deficiency of Syt7 would exacerbate damage. Contrary to our expectations, we observed that Syt7 deficiency significantly reduced damage in resting macrophages, and had no effect on the ability of LPS-treated macrophages to resist damage (Fig 4.4.A). A similar result was obtained in phototoxicity assays. Both resting and LPS-treated *Syt7*$^{-/-}$ BMM were able to hold off complete rupture of lysosomes for a longer duration than did their WT counterparts, although in these experiments LPS treatment of WT BMM did not substantially enhance cells' ability to resist damage following photo-injury (Fig 4.4.B). These findings suggest that Syt7 promotes rather than protects lysosomal damage in macrophages.

4.4.5 Autophagy partially contributes to renitence

Given its well-established roles in facilitating the clearance of damaged organelles, including damaged lysosomes, we considered whether autophagy might contribute to renitence. Our studies were performed using macrophages from mice harboring a myeloid cell-specific deficiency in Atg7, an essential autophagy protein. These mice (*Atg7*$^{fl/fl}$-Lyz-*Cre)* express Cre recombinase under the control of the LyzM promoter, which restricts the deficiency to cells of the myeloid lineage (DeSelm *et al.*, 2011). Mice harboring floxed alleles of Atg7, but that do not

express Cre recombinase (*Atg7$^{fl/fl}$*-WT*)* were used as controls. The deficiency of Atg7 protein in *Atg7$^{fl/fl}$*-Lyz-*Cre* BMM (and its presence in control BMM) was confirmed by Western blot (Fig 4.5.B). As expected, LPS treatment of BMM from control mice significantly protected against lysosomal damage following 60 min AW bead incubation (Fig 4.5.A). In BMM deficient in Atg7, however, LPS treatment led to a less pronounced reduction in damage, suggesting that Atg7 partially contributes to the protective effect of renitence (Fig 4.5.A).

4.4.6 Inhibition of Akt activation reduces renitence vacuole formation and eliminates renitence

In Chapter 2, we identified a key role for macropinosomes (MPs) and renitence vacuoles (RVs) in renitence in LPS-activated macrophages. As the molecular events associated with LPS-induced macropinocytosis in macrophages involves activation of the PI3K-Akt pathway (Wall *et al.*, 2017), we tested whether inhibition of this pathway might affect RV formation and, in turn, renitence. Strikingly, treatment of LPS-activated macrophages with the Akt inhibitor MK-2206 eliminated both RV formation (Fig 4.6.B) and renitence (Fig 4.6.A) following 60 min AW bead incubation. We confirmed that 30 min pre-treatment of BMM with MK-2206 before 60 min AW bead incubation indeed blocked Akt activation induced by overnight LPS stimulation, as judged by Western blot analysis of pAKT(308) levels (Fig 4.6.D). The inhibition was specific to the Akt pathway, as MK-2206 pre-treatment did not inhibit ERK activity. Thus, RV formation is necessary for renitence, and both processes depend on Akt activation. Interestingly, Akt inhibition had no effect on MP formation induced either by M-CSF (as reported in Yoshida *et al.* 2015b) or LPS (Figure 4.6.C). These results suggest that Akt activation is not necessary for MP formation, yet contributes to RV formation. We thus postulate that MP formation occurs independently of Akt, but Akt promotes the persistence of vacuoles, a critical feature of RVs.

We next investigated whether activation of mTOR, a major downstream target of Akt, contributes to renitence. Treatment of resting and LPS-activated BMM with Torin 1, an inhibitor of mTOR, had no effect on renitence (Fig 4.6.E) or RV formation (Fig 4.6.F), despite its complete inhibition of mTOR-dependent S6K phosphorylation (Fig 4.6.H). However, Torin 1 treatment of macrophages also prevents the activation of Akt, based on its inhibition of pAKT(308) (Fig 4.6.H). This finding complicates our interpretation of the effects of MK-2206 noted above. That is, both MK-2206 and Torin 1 appear to block Akt activation, but only MK-2206 treatment has a noticeable effect on renitence and RV formation. These results suggest that the effects induced by MK-2206 occur through a different target than Akt.

4.5 Discussion

Here we considered multiple molecular candidates for their contribution to renitence. Of the candidates surveyed, Npc1 and Syt7 stood out as factors whose genetic deficiencies rendered macrophages better able to resist multiple forms of lysosomal damage. The mechanism that likely accounts for enhanced protection in *Npc1*$^{-/-}$ BMM is the accumulation of lysosomal cholesterol. Interestingly, a recent study reported a role for Syt7 in mediating the transport of cholesterol from lysosomes to peroxisomes, such that deficiency of Syt7 also leads to a phenotype of cholesterol buildup within lysosomes (Chu *et al.*, 2015). However, in examining filipin-stained *Syt7*$^{-/-}$ BMM, we were not able to detect accumulated lysosomal cholesterol (data not shown), suggesting the phenotype reported might be cell-type specific.

The finding here that Npc1 deficiency protects against lysosomal damage conflicts with others' findings that lysosomes within *Npc1*$^{-/-}$ cells or cells from other models of lysosomal storage disorders are more rather than less susceptible to damage (Amritraj *et al.*, 2009; Gabande-Rodriguez *et al.*, 2014; Chung *et al.*, 2016). This discrepancy could be explained by

several differences between the conditions used in our study and in those previously reported. These include differences in (1) the method used to detect lysosomal damage, (2) the context in which lysosomal damage was studied (i.e. baseline leakage vs responses to induced insults), and (3) the cell types examined. In the studies cited, the presence of lysosomal proteases called cathepsins in the cytosol of cells, as detected by immunofluorescence microscopy or Western blotting of different subcellular fractions, was used as a marker for lysosomal damage. However, cathepsins are quickly degraded once they enter the cytosol, complicating the interpretation of these results (Turk and Turk, 2009). Furthermore, cell types might differ in their expression levels of cathepsins, making the direct comparison of results between multiple studies difficult.

While our study examined the ability of *Npc1*$^{-/-}$ macrophages to resist lysosomal injury induced by silica beads or photo-oxidative damage, most previous reports examined cytosolic levels of cathepins in the absence of induced injury. However, no baseline leakage of 3 kDa Fdx was detected in *Npc1*$^{-/-}$ BMM examined in our studies. How proteases leak from lysosomes at baseline when a small molecular weight dye does not is difficult to envision without invoking the possibility of an active mechanism for cathepsin translocation into the cytoplasm. Suggestive of a difference in the susceptibility of *Npc1*$^{-/-}$ cells to induced insults versus baseline injury, in a case in which the ability of U18666A-treated and *Npc1*$^{-/-}$ cells to resist damage by several lysosomotropic detergents was examined, lysosomal cholesterol accumulation was found to prevent lysosomal membrane permeablization induced by these agents (Appelqvist *et al.*, 2011).

Finally, these discrepancies could be explained by differences in baseline lysosomal leakage in different cell types. As Niemann Pick C disease most prominently affects cells of the central nervous system, most of the aforementioned studies examined lysosomal damage in

neurons from *Npc1*$^{-/-}$ animals. As the cellular functions of neurons and macrophages differ, it is possible that their baseline susceptibility to lysosomal leakage reflects these differences.

Using macrophages deficient in Atg7, we determined that Atg7, and presumably autophagy, partially contributes to renitence. In preliminary studies, we found that BMM deficient in another essential autophagy gene, Atg5, showed no impairment in LPS-induced renitence (data not shown). The modest role for autophagy in renitence suggested by this work is somewhat surprising, considering the preponderance of evidence suggesting that autophagy is directly involved in the clearance of damaged lysosomes following injury by various lysosomotropic or pathogenic agents (Maejima *et al.*, 2013; Kreibich *et al.*, 2015). However, it is possible that while autophagy participates in the clearance of damaged organelles, it does not serve as a mechanism for preventing or repairing small membrane breaches, such as those formed upon the uptake of silica beads. Additionally, the timing with which autophagy adaptors and proteins are recruited to damaged membranes (in one study, occurring around 30 to 50 min after photo-oxidative damage) (Hung *et al.*, 2013) is likely too slow to account for renitence, which is induced within the first 15 to 30 min of silica bead-induced damage, as determined in Chapter 2. Consistent with this idea are preliminary findings that the autophagic marker LC3 is recruited to silica bead-containing phagosomes at similar frequency in resting and LPS-treated macrophages, and that the peak level of LC3 recruitment occurs after the limited time window in which renitence acts (Zachary Mendel, data not shown).

Here, in continuation of work begun in Chapter 2, we attempted to manipulate renitence vacuole (RV) formation using inhibitors that target molecules known to be involved in LPS-induced macropinocytosis. We determined that treatment of macrophages with MK-2206, a commercially available inhibitor of Akt activation, inhibited RV formation and renitence. We

thus initially concluded that RV formation and renitence depend on Akt activation. However, the finding that Torin 1 treatment also inhibits Akt activation without affecting RV formation or renitence suggests the original effects observed following MK-2206 treatment could be due to its inhibition of a target other than Akt. While this is the most straightforward interpretation of the data, MK-2206 has been shown to be a highly selective inhibitor of Akt (Yap *et al.*, 2011). Genetic approaches utilizing BMM from *Akt1*$^{-/-}$ and *Akt2*$^{-/-}$ mice could help to determine whether Akt indeed contributes to RV formation and renitence, and if so, which specific isoforms contribute.

Our attempts to identify the molecular determinants of renitence have yielded many insights on the factors that impact lysosomal integrity in macrophages. This understanding will assist our continued efforts to arrive at a unifying explanation for renitence. Approaches toward this goal that build on the findings presented in this thesis will be considered in the Discussion.

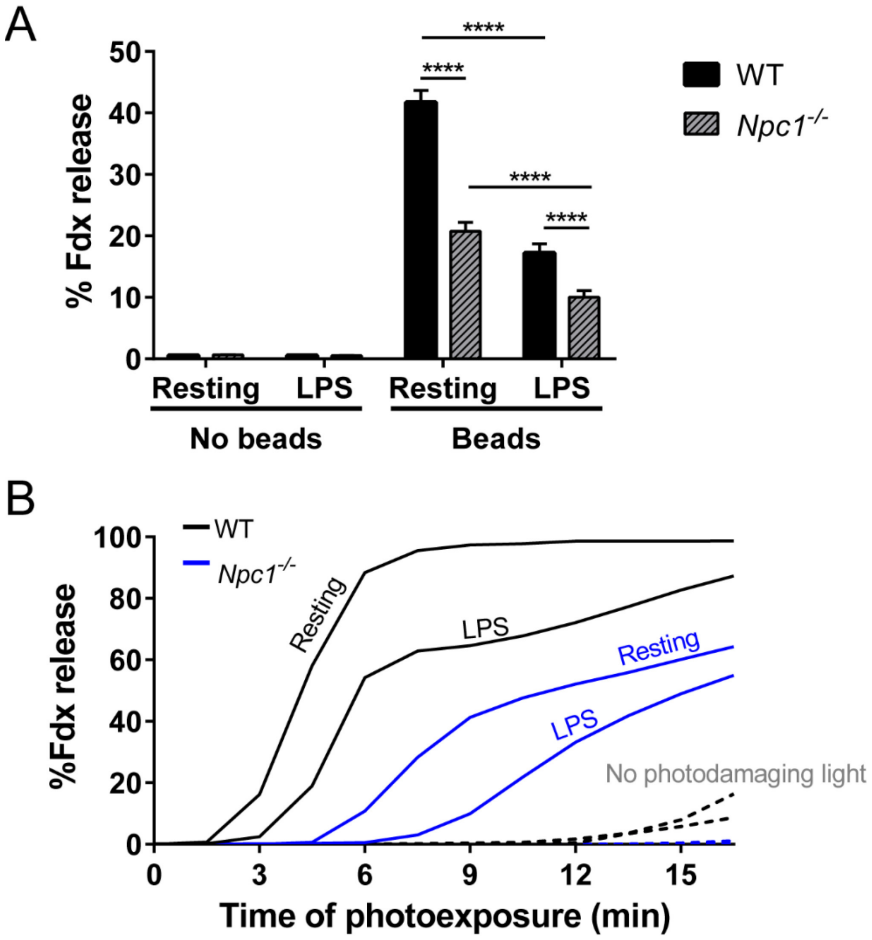

Figure 4.1. Npc1 deficiency in macrophages enhances protection from lysosomal damage.

(A) Average percent Fdx release ± SEM from pre-labelled lysosomes 60 min after AW bead incubation in WT and *Npc1*$^{-/-}$ BMM pre-treated overnight with LPS or not. As a negative control, lysosomal damage was measured in cells not administered beads. Data are from 4 independent experiments, in which cells containing 3-7 beads were analyzed. ****$p \leq 0.0001$.

(B) Lysosomal damage with increasing time of photoexposure in resting and LPS-activated WT and *Npc1*$^{-/-}$ BMM. After pre-labelling of BMM lysosomes with Fdx and TRDx, cells were exposed to a one second pulse of 580 nm light every 90 seconds to incite photodamage. Fdx pH images were acquired between each pulse. To determine the baseline level of leakage caused by excitation of Fdx, Fdx release values were determined for cells loaded with both Fdx and TRDx but subjected only to excitation of Fdx but not of TRDx (n>32 cells per genotype).

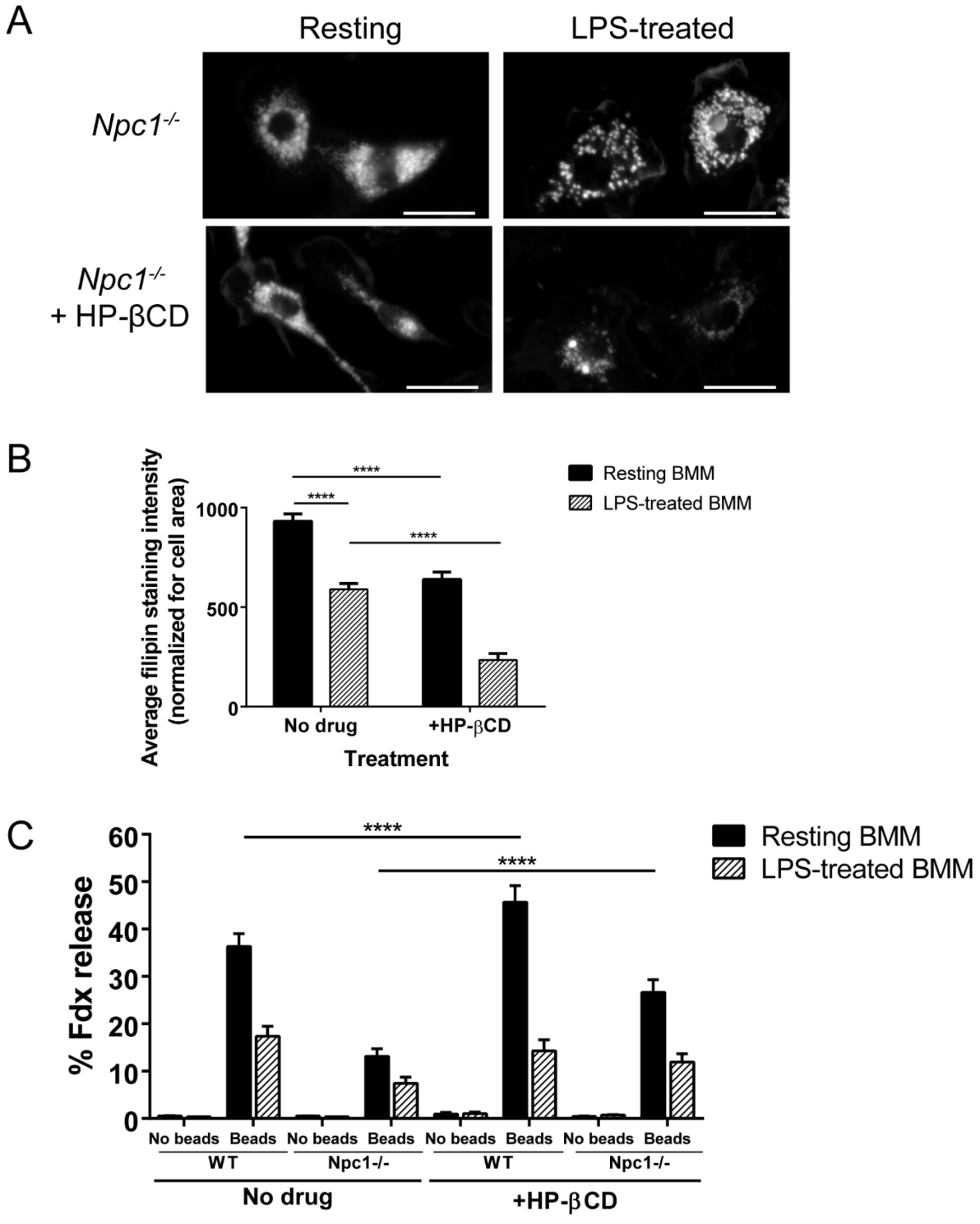
A
Resting
LPS-treated
Npc1-/-
Npc1-/-
+ HP-βCD
B
Average filipin staining intensity
(normalized for cell area)
1000
500
0
****
****
****
Resting BMM
LPS-treated BMM
No drug
+HP-βCD
Treatment
C
% Fdx release
60
50
40
30
20
10
0
****
****
Resting BMM
LPS-treated BMM
No beads
Beads
No beads
Beads
No beads
Beads
No beads
Beads
WT
Npc1-/-
WT
Npc1-/-
No drug
+HP-βCD

Figure 4.2. Depletion of cholesterol from cholesterol-loaded macrophages partially abrogates lysosomal damage protection.

(A) Unesterified cholesterol within resting or LPS-treated *Npc1*$^{-/-}$ BMM treated with hydroxypropyl beta-cyclodextran (HP-βCD) for extracting lysosomal cholesterol was visualized by filipin staining. Untreated BMM and BMM treated for 48 h with 300 μM HP-βCD were fixed and stained with 0.05 mg/ml filipin for 2 h at room temperature. Specimens were imaged on an inverted fluorescence microscope using a 402-455 filter set combination to visualize fluorescence emitted by filipin. Scale bar: 20 μm.

(B) Quantification of average filipin staining intensity per cell (±- SEM) in indicated conditions in (A), normalized for cell area. Over 100 cells per condition were analyzed between two experiments. ****$p \leq 0.0001$.

(C) Lysosomal damage after 60 min AW bead incubation in resting and LPS-treated WT and *Npc1*$^{-/-}$ BMM treated or not for 48 h with HP-βCD. ****$p \leq 0.0001$.

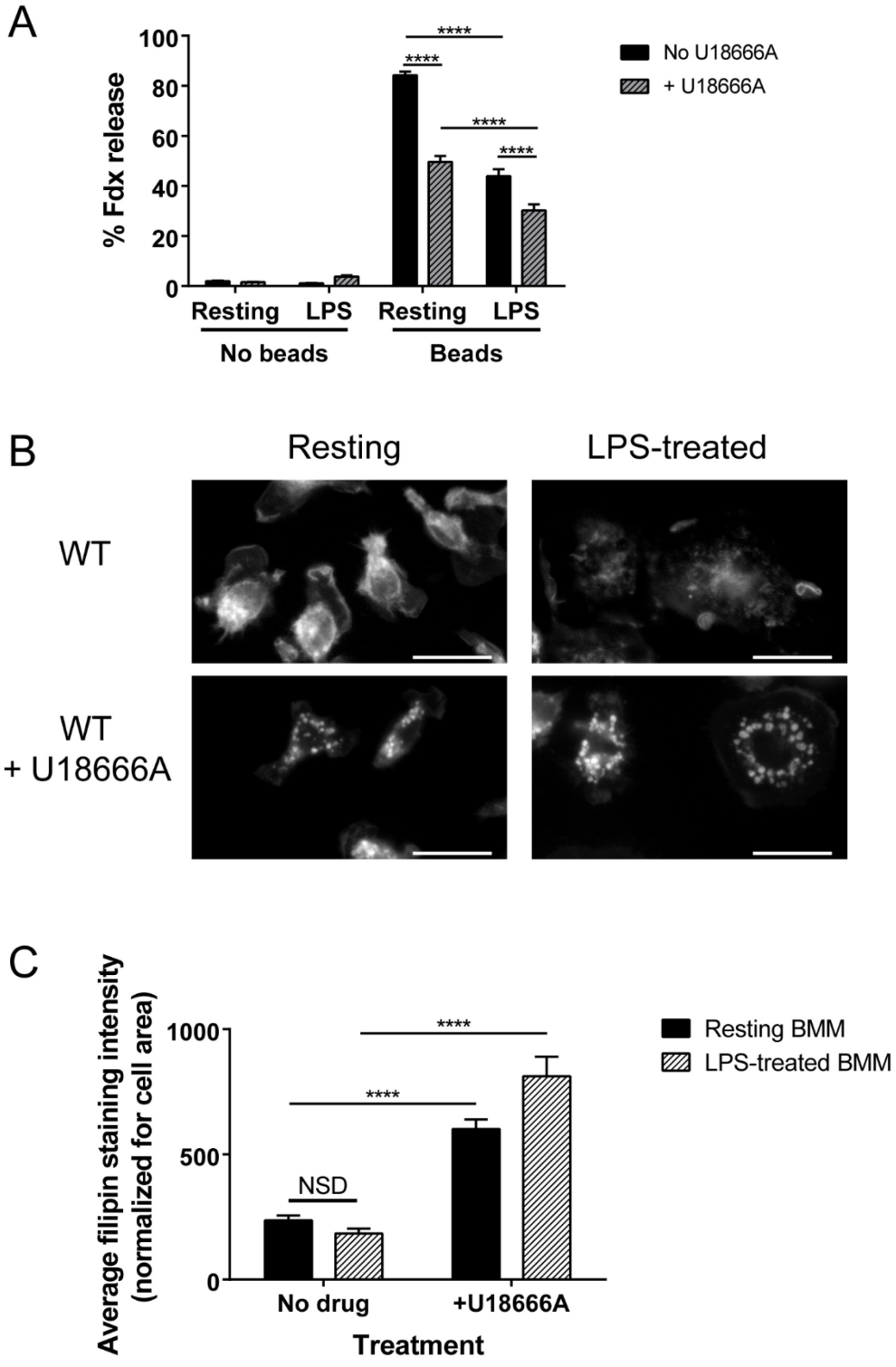
A
100
80
60
40
20
0
% Fdx release
****
****
****
****
No U18666A
+ U18666A
Resting
LPS
Resting
LPS
No beads
Beads
B
Resting
LPS-treated
WT
WT
+ U18666A
C
Average filipin staining intensity
(normalized for cell area)
1000
500
0
****
****
NSD
Resting BMM
LPS-treated BMM
No drug
+U18666A
Treatment

Figure 4.3. LPS stimulation and cholesterol accumulation protect macrophage lysosomes from damage through independent mechanisms.

(A) Lysosomal damage in resting and LPS-treated WT BMM following overnight incubation or not with 1 μg/ml U18666A to induce cholesterol accumulation. Average percent Fdx release ± SEM in each condition was measured following 60 min AW bead incubation. Data are from 4 independent experiments, in which cells containing 3-7 beads were analyzed. ****$p \leq 0.0001$.

(B) Filipin staining of unesterified cholesterol within resting or LPS-treated WT BMM treated overnight or not with U18666A. Scale bar: 20 μm.

(C) Quantification of average filipin staining intensity per cell (+/- SEM) in indicated conditions in (A), normalized for cell area. Data are from one experiment in which at least 25 cells per condition were analyzed. ****$p \leq 0.0001$. NSD: no significant difference.

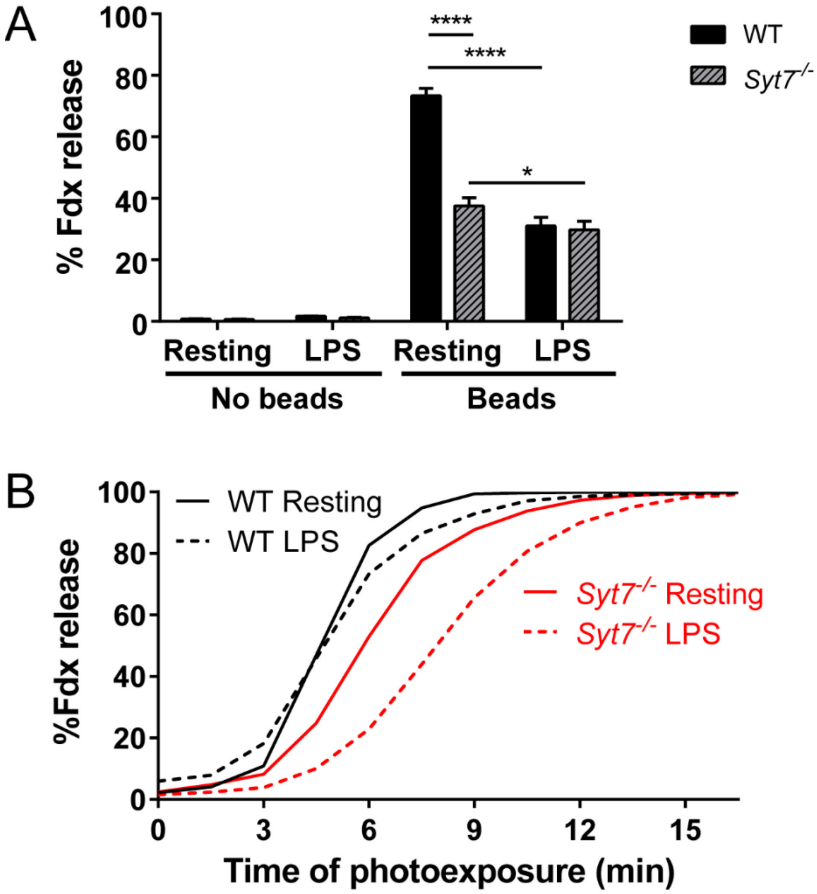

Figure 4.4. Synaptotagmin-7 promotes lysosomal membrane damage in macrophages.

(A) Average percent Fdx release ± SEM from pre-labelled lysosomes 60 min after AW bead incubation in WT and *Syt7*$^{-/-}$ BMM pre-treated overnight with LPS or not. Data are from 3 independent experiments, in which cells containing 3-7 beads were analyzed. *$p \leq 0.05$, ****$p \leq 0.0001$.

(B) Lysosomal damage with increasing time of photoexposure in resting and LPS-activated WT and *Syt7*$^{-/-}$ BMM. Averaged data from 4 independent experiments are shown. (n>150 cells per genotype).

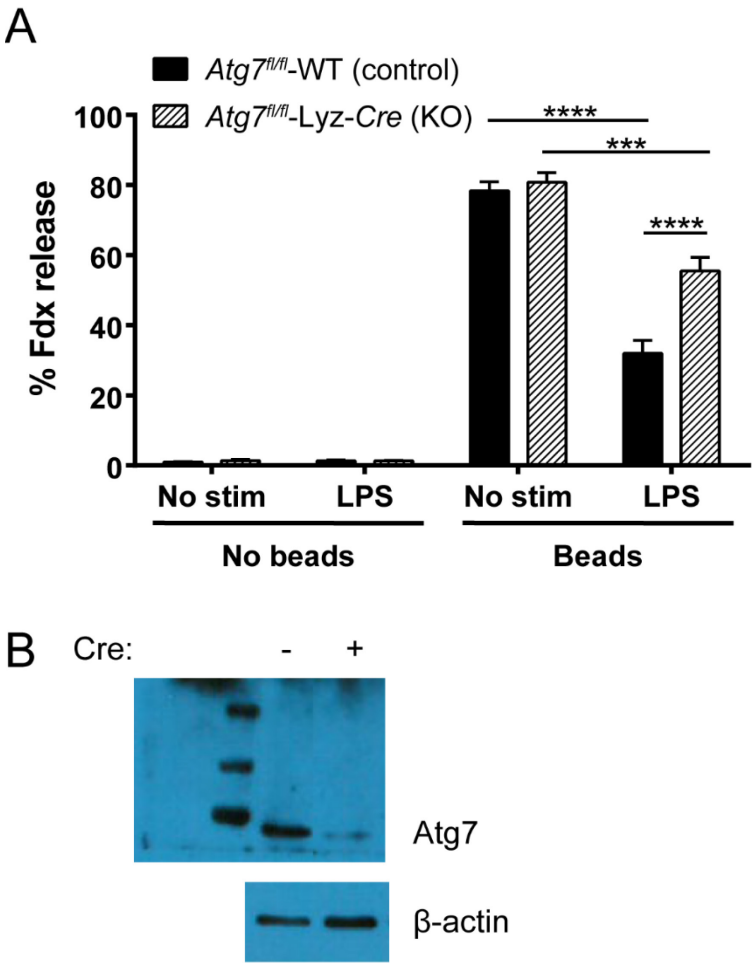

Figure 4.5. Atg7 partially contributes to renitence.

(A) Average percent Fdx release ± SEM from pre-labelled lysosomes 60 min after AW bead incubation in Atg7-deficient (*Atg7*$^{fl/fl}$-Lyz-*Cre*) and control (*Atg7*$^{fl/fl}$-WT) BMM pre-treated overnight with LPS or not. Data are from 3 independent experiments, in which cells containing 3-7 beads were analyzed. ***$p \leq 0.001$, ****$p \leq 0.0001$.

(B) Western blot confirming deficiency of Atg7 protein in Cre-positive (*Atg7*$^{fl/fl}$-Lyz-*Cre*) BMM and presence of the protein in control, Cre-negative (Atg7$^{fl/fl}$-WT) BMM.

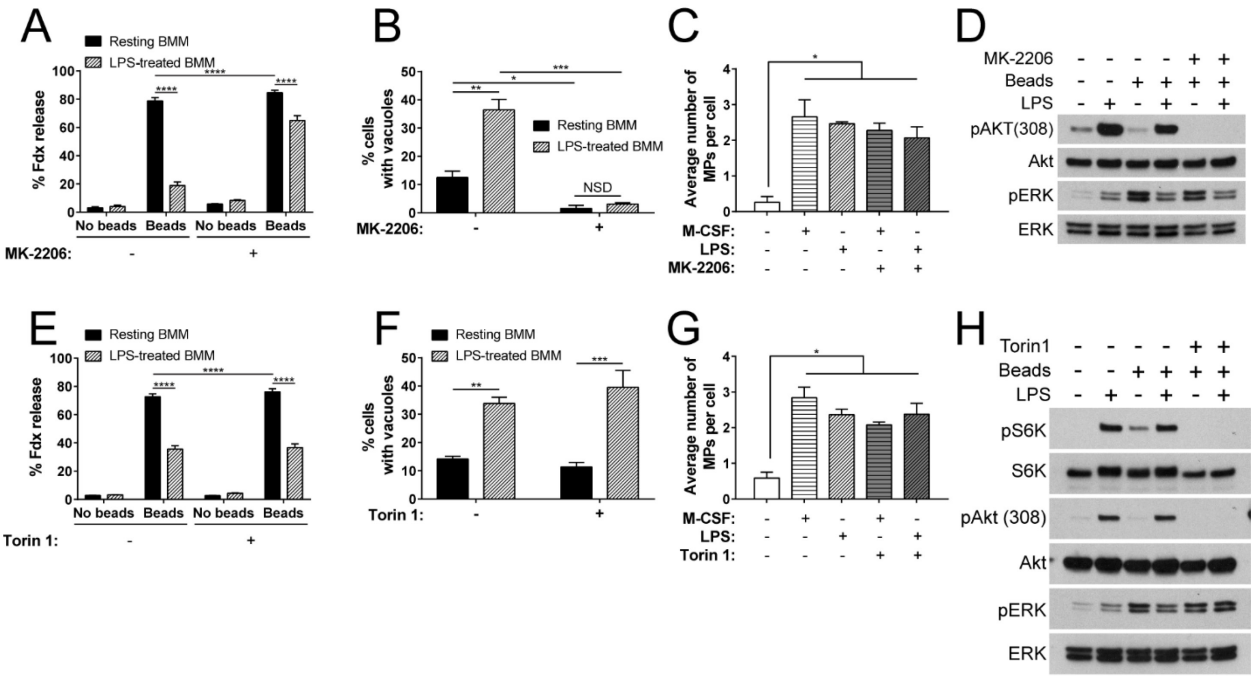

Figure 4.6. MK-2206, an inhibitor of Akt activation, reduces renitence vacuole formation and eliminates renitence.

(A-D) Effect of Akt inhibiton on renitence, RV formation, and macropinocytosis.

(A and B) Resting and LPS-treated BMM containing Fdx-labelled lysosomes were pre-treated with the MK-2206 (2 μM), an inhibitor of Akt activation, for 30 min or left unstimulated. After 60 min challenge with AW beads, average percent Fdx release ± SEM (A) and vacuole frequency (B) in each condition were measured. Data shown are from three independent experiments. (C) Resting and LPS-treated BMM were pre-treated or not for 30 min with MK-2206 before undergoing a 10 min pulse with 70 kDa Fdx in the presence or absence of M-CSF (200 ng/ml). Cells were washed, fixed, imaged, and scored for MP number. Bars represent the average number of MP per cell ± SEM. Data shown are from 2 independent experiments. (D) Western blot confirmation of MK-2206 inhibition of Akt activation.

(E-H) Effect of mTOR inhibition on renitence, vacuole formation, and macropinocytosis.

(E and F) Fdx-loaded resting and LPS-treated BMM were pre-treated or not with Torin 1 (500 nM), an inhibitor of mTOR activation, for 30 min then fed AW beads for 60 min. Average percent Fdx release ± SEM (E) and vacuole frequency (F) were measured from cells of each condition. (G) Resting and LPS-treated BMM were pre-treated or not for 30 min with Torin 1, then pulsed for 10 min with 70 kDa Fdx in the presence or absence of M-CSF. Cells were then rinsed, fixed, and imaged for MP number. Bars represent the average number of MP per cell ± SEM from 2 independent experiment. (H) Western blot confirmation of Torin 1 inhibition of mTORC1 activation and determination of effect of Torin 1 inhibition on Akt activation. *$p \leq 0.05$, **$p \leq 0.01$, ***$p \leq 0.001$, ****$p \leq 0.0001$.

CHAPTER 5

Discussion

Macrophages are professional phagocytes with diverse roles in immunobiology. These range from the clearance of apoptotic bodies to the elimination of pathogenic microbes. While the former task may not seem to qualify as an immune function, the macrophage's ability to internalize cells derived from one's own tissues without initiating inappropriate immune signaling requires careful regulation. In the hands (or phagosome) of the wrong macrophage, uptake of apoptotic bodies can in fact lead to the presentation of self-antigen and development of autoimmune pathologies (Uderhardt *et al.*, 2012). Likewise, not all forms of macrophages are equally equipped to effect destruction of intracellular pathogens following their phagocytic uptake. Macrophages specialized to participate in the wound healing response, for example, are more rather than less susceptible to many infections (Kreider *et al.*, 2007; Raes *et al.*, 2007). These examples illustrate the concept that while the unifying function of macrophages is their ability to perform phagocytosis, the immunological context in which phagocytosis takes place strongly influences the fate of the phagocytic target intracellularly and the cellular consequences for the host. Thus, the cellular function of a macrophage is closely tied to its inflammatory state.

The work described in this thesis establishes the same principle for another cellular property of macrophages – namely, their susceptibility to lysosomal damage. In the Introduction, we speculated that renitence, or a cell's capacity to reinforce lysosomal integrity against membrane damage, is likely important for host defense, given the large number of pathogens capable of perforating phagolysosomes. Thus, we expected that macrophages

exposed to microbial stimuli or undergoing classical activation would display a high capacity for renitence. While results supporting this hypothesis were obtained, we also discovered another class of macrophages that was equally if not better equipped to induce renitence: the regulatory macrophage (Reg-Mφ).

Several decades of work from David Mosser's laboratory have established Reg-Mφ to be immunoregulatory macrophages with key roles in suppressing the immune response following clearance of an infection. Their generation is not thought to occur *de novo* at the onset of immune resolution, but instead to involve the reprogramming of inflammatory macrophages previously exposed to TLR stimuli into immunosuppresive macrophages upon recognition of a second signal that stimulates this differentiation. Considered in this way, CA-Mφ and Reg-Mφ should not be viewed as separate macrophage entities formed under disparate contexts, but as different states that can be assumed by the same macrophage at different stages of the immune response. If this model is correct, these two macrophage subtypes, examined here *in vitro*, could represent predominant cell types at different stages of the immune response *in vivo*. That is, whereas Reg-Mφ likely represent macrophages present at the resolution of an immune response, CA-Mφ likely represent macrophages present at the peak of the immune response, formed after the recruitment of NK cells and Th1 cells, the major sources of IFN-γ *in vivo*, to the site of infection. To complete the model, we propose that macrophages present in the early stages of infection might be represented by macrophages stimulated briefly (eg. for one to two hours) with LPS. Macrophages receiving such short-term treatments with LPS were previously noted for their inability to induce renitence (Davis *et al.*, 2012). Thus, they represent a different activation state than that embodied by either CA-Mφ or Reg-Mφ, both of which are equipped to induce renitence.

By mapping our knowledge of the susceptibility to lysosomal damage in each of these three macrophages subtypes - 1 to 2 h LPS-stimulated macrophages, CA-Mφ, and Reg-Mφ - to a framework in which these subtypes represent macrophages involved in early, intermediate, and late stages of infection respectively, we can track how renitence capacity within macrophages may vary throughout the course of infection. This temporal framework serves as the foundation of a model we propose for the functional relevance of renitence at different stages of the immune response. This model is summarized in Fig 5.1.

Within this temporal framework, renitence is absent in early stages of infection, first observed in macrophages following IFN-γ exposure, and highest in Reg-Mφ involved in the resolution of inflammation. Phrased another way, susceptibility to lysosomal damage is highest in early stages of infection, and decreases as the infection progresses and resolves. This pattern of lysosomal damage susceptibility, we propose, is consistent with the functional role assumed by macrophages at each stage of infection.

Early during an infection, the main functions of macrophages are the detection of infection and coordination of a proportionate response. A lysosomal network that is more rather than less susceptible to damage may facilitate both of these goals. For example, the release of microbial products from endolysosomes allows for their detection by inflammasomes in the cytosol, thereby alerting cells of a potential infection by an intracellular pathogen. Although excessive lysosomal damage is deleterious for the cell, trace amounts of leakage that allow for the detection of infection likely promote host defense. Likewise, the increased permeability of lysosomes at this stage could provide a means for the leakage of endosomally-derived antigens for loading onto major histocompatibility complex I (MHC I) molecules in a process termed antigen cross-presentation (Cruz *et al.*, 2017).

During later stages of infection, the emphasis shifts from detection of infection to mechanisms for promoting pathogen killing. At this stage, permissiveness to lysosomal leakage would seem to offer little functional benefit, whereas increased resistance against damage conceivably could. Exposure to IFN-γ, a necessary signal for CA-Mφ generation, is also necessary for macrophages to successfully restrict infection by several intracellular pathogens. For example, IFN-γ treatment of macrophages infected with *Listeria monocytogenes* prevents escape of the pathogen from phagolysosomes, a strategy utilized by *L.m.* to reach its replicative niche in the cytosol (Portnoy *et al.*, 1989). Likewise, IFN-γ treatment releases the block on phagosome-lysosome fusion imposed by *Mycobacterium tuberculosis*, which upon infection of macrophages induces such a block to prevent its delivery to the degradative lysosome (Schaible *et al.*, 1998; Via *et al.*, 1998). In both situations, the increased load of pathogen delivery to lysosomes (due to fewer pathogens being lost by escape or stalled in phagosomes) would reasonably be accompanied by an increased capacity by the macrophage to avoid lysosomal membrane perforation by the pathogens or virulence factors being received.

Following pathogen clearance, the goal of the immune system is to limit rather than to sustain inflammation. Reg-Mφ are key contributors to this process of immune resolution. By actively suppressing inflammation, they help to prevent the development of chronic inflammatory states, many of which are associated with an inability of macrophages to reverse classical activation (Flavell, 2002; Gordon *et al.*, 2012). A mechanism for preventing the leakage of lysosomal contents into the cytoplasm (such as renitence) would likely facilitate the goal of immune resolution.

The model presented here relies on the assumption that the *in vitro* macrophage subtypes noted indeed represent physiologically-relevant cell types that predominate in a given state of

infection. To directly test this model, *ex vivo* analysis of macrophages isolated from *in vivo* mouse models of sepsis or infection could be performed. For example, using an infection model for which the kinetics of infection and immune clearance are well-established, macrophages isolated from mice after various time points of infection could be subjected to cytokine secretion analysis and assays for measuring susceptibility to lysosomal damage. By performing this analysis on mice infected with pathogens of various classes (eg. extracellular vs intracellular bacteria or viruses vs bacteria), we could gain an understanding of not only how susceptibility to lysosomal damage in macrophages varies throughout the immune response, but also whether this pattern is a generalized one or varies depending on the pathogen encountered.

Future work could extend these studies to tissue-specific macrophages as well as to human macrophages. Beyond the chronic inflammatory conditions known to be caused by environmental exposure to particles that cause lysosomal damage (eg. silicosis, asbestosis), it would be interesting to determine whether humans with various diseases might possess macrophages with defects in responding to lysosomal damage under infectious or other settings. For example, whether lysosomal damage might contribute to the pathology of and could serve as therapeutic targets for other chronic inflammatory diseases, lysosomal storage diseases, immunodeficiencies, neurodegenerative diseases, aging, or cancer is a subject only starting to be explored (Boya and Kroemer, 2008; Gomez-Sintes *et al.*, 2016).

A second aim of this thesis was to determine the mechanism underlying renitence. In characterizing the nature of lysosomal damage induced by silica bead uptake, we determined that the size of the membrane breach formed by the beads permitted small but not large molecular-weight dyes to leak. The extent of leakage permitted resembled that induced by *L. monocytogenes* at early stages of infection (Shaughnessy *et al.*, 2006), suggesting the extent of

damage induced by the beads represents that encountered in physiologically-relevant situations. This finding allowed us to more precisely define our research question. That is, any mechanism underlying renitence likely enables the cell to resist or repair small rather than large membrane breaches.

The formation of renitence vacuoles (RVs) and their pathogen-induced counterpart, spacious phagosomes (SPs), likely are induced following small membrane breaches to phagolysosomes. However, while morphologically similar, RVs and SPs are not structurally analogous, as the topological relationship between RVs and SPs to the phagosome differ significantly. Whereas RVs seem to represent a distinct compartment from the bead-containing phagosome, SPs, as their name implies, represent phagolysosomal compartments that enlarge following pathogen uptake. To further dissect the functional role of RVs and their contribution to renitence, studies clarifying the topological relationships between RVs, phagosomes, and lysosomes should be performed. While the challenge of sample preparation of cells containing glass beads for electron microscopy might preclude its use as a method, we can begin to get at this question by determining the membrane markers (eg. Rab5, Rab7, LAMP1) that RVs carry at different stages after the phagocytosis of silica beads. These studies would allow us to identify the cellular compartments of the endocytic pathway with which RVs interact and exchange membrane. Preliminary studies in which cells expressing fluorescent chimeras of these membrane markers are examined for their co-localization with RVs are underway.

While the ability of RVs to maintain their acidity despite their localization next to a damaged phagosome suggests they represent damage-resistant structures within individual cells, their absolute requirement for renitence has not been definitively shown. In fact, in our analyses of RV frequency in cells after 60 min AW bead incubation, we found that cells that contain

vacuoles on average are no more protected from lysosomal damage than cells that do not contain vacuoles (data not shown). Consistent with this observation, RVs appeared in all types of activated macrophages analyzed regardless of their ability to induce renitence. Thus, RV formation is not sufficient to induce renitence and seems to be actively induced in response to phagolysosomal injury in multiple classes of activated macrophages. Interestingly, pharmacological inhibition of Akt, a protein activated in both CA-Mφ and AA-Mφ (Covarrubias *et al.*, 2015), renitent and non-renitent macrophages respectively, eliminated RV formation in LPS-activated macrophages. Future studies could determine whether Akt inhibition eliminates RV formation in other macrophage subtypes. In investigating the potential contribution of Akt activation to RV formation, the possible off-target effects of MK-2206, a commercially available inhibitor of Akt activation, brought out by studies in Chapter 4, will need to be addressed. Still, it is tempting to speculate that RV formation following phagolysosomal damage may depend on the activity of this key signaling kinase.

At the conclusion of this thesis, several questions about renitence, particularly pertaining to its mechanism, remain. Given the importance of maintaining lysosomal integrity for cellular homeostasis and the many trafficking pathways that converge on the lysosome (eg. phagocytosis, receptor-mediated endocytosis, macropinocytosis, multiple forms of autophagy), it might be expected that several cellular processes and pathways contribute to the mechanism of renitence and would be difficult to dissect. A way forward might be achieved through combining the approaches of the two parts of this thesis. Now that we have defined several stimulation conditions that do or do not induce renitence, it should be possible to begin to pursue unbiased approaches for identifying genes, proteins, and pathways upregulated in renitent but not in non-renitent cells. Advances in methods for genetically modifying primary macrophages, such as

CRISPR-Cas 9 screening libraries (Parnas *et al.*, 2015), when combined with a high-throughput method for measuring lysosomal damage and sorting away damaged vs non-damaged cells (Davis *et al.*, 2015), could also aid in this effort.

With a burgeoning interest in harnessing macrophages of various polarization states for their therapeutic potential, and the realization of the central role of lysosomes in not only degradation but also nutrient sensing and cell signaling, it is an exciting time to be studying macrophages and lysosomes. These two fields have a rich and connected history and their future promises many fruitful new discoveries to appreciate and fascinating questions to pursue.

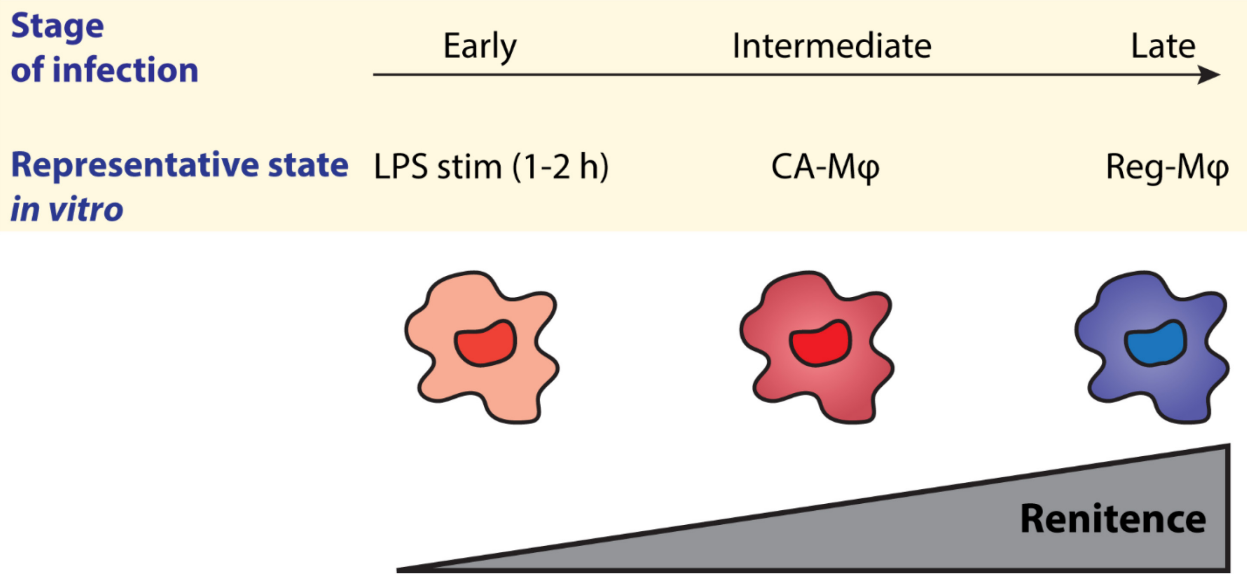

Figure 5.1. Renitence capacity in macrophages at different stages of infection.

This model proposes that three populations of macrophages studied here and in previous studies *in vitro* – macrophages stimulated for 1 to 2 h with LPS, CA-Mφ, and Reg-Mφ – represent the predominant form of macrophages formed at early, intermediate, and late stages of infection *in vivo*. In the above schematic, these macrophages are arranged in their temporal order of generation in the immune response. Overlaying the renitence capacity for each macrophage subtype on top of this temporal framework allows us to visualize changes in renitence capacity through the course of the immune response. According to this model, renitence is absent early in infection, is upregulated at intermediate stages of infection, and is highest at the stage of immune resolution. Possible explanations for the functional relevance of lysosomal leakiness versus resistance at each stage of the immune response are provided in the text.

REFERENCES

Adams DO, Hamilton TA (1984). The cell biology of macrophage activation. Annu Rev Immunol 2, 283-318.

Akira S, Uematsu S, Takeuchi O (2006). Pathogen recognition and innate immunity. Cell 124, 783-801.

Alpuche-Aranda CM, Racoosin EL, Swanson JA, Miller SI (1994). Salmonella stimulate macrophage macropinocytosis and persist within spacious phagosomes. J Exp Med 179, 601-608.

Amritraj A, Peake K, Kodam A, Salio C, Merighi A, Vance JE, Kar S (2009). Increased activity and altered subcellular distribution of lysosomal enzymes determine neuronal vulnerability in niemann-pick type c1-deficient mice. Am J Pathol 175, 2540-2556.

Andrews NW, Almeida PE, Corrotte M (2014). Damage control: Cellular mechanisms of plasma membrane repair. Trends Cell Biol 24, 734-742.

Appelqvist H, Nilsson C, Garner B, Brown AJ, Kagedal K, Ollinger K (2011). Attenuation of the lysosomal death pathway by lysosomal cholesterol accumulation. Am J Pathol 178, 629-639.

Atger VM, de la Llera Moya M, Stoudt GW, Rodrigueza WV, Phillips MC, Rothblat GH (1997). Cyclodextrins as catalysts for the removal of cholesterol from macrophage foam cells. J Clin Invest 99, 773-780.

Bergsbaken T, Fink SL, Cookson BT (2009). Pyroptosis: Host cell death and inflammation. Nat Rev Microbiol 7, 99-109.

Berwick DC, Dell GC, Welsh GI, Heesom KJ, Hers I, Fletcher LM, Cooke FT, Tavare JM (2004). Protein kinase b phosphorylation of pikfyve regulates the trafficking of glut4 vesicles. J Cell Sci 117, 5985-5993.

Bhavsar AP, Guttman JA, Finlay BB (2007). Manipulation of host-cell pathways by bacterial pathogens. Nature 449, 827-834.

Birmingham CL, Smith AC, Bakowski MA, Yoshimori T, Brumell JH (2006). Autophagy controls salmonella infection in response to damage to the salmonella-containing vacuole. J Biol Chem 281, 11374-11383.

Blum JS, Wearsch PA, Cresswell P (2013). Pathways of antigen processing. Annu Rev Immunol 31, 443-473.

Boya P, Kroemer G (2008). Lysosomal membrane permeabilization in cell death. Oncogene 27, 6434-6451.

Broz P, Dixit VM (2016). Inflammasomes: Mechanism of assembly, regulation and signalling. Nat Rev Immunol 16, 407-420.

Case ED, Smith JA, Ficht TA, Samuel JE, de Figueiredo P (2016). Space: A final frontier for vacuolar pathogens. Traffic 17, 461-474.

Chakrabarti S, Kobayashi KS, Flavell RA, Marks CB, Miyake K, Liston DR, Fowler KT, Gorelick FS, Andrews NW (2003). Impaired membrane resealing and autoimmune myositis in synaptotagmin vii-deficient mice. J Cell Biol 162, 543-549.

Chu BB, Liao YC, Qi W, Xie C, Du X, Wang J, Yang H, Miao HH, Li BL, Song BL (2015). Cholesterol transport through lysosome-peroxisome membrane contacts. Cell 161, 291-306.

Chung C, Puthanveetil P, Ory DS, Lieberman AP (2016). Genetic and pharmacological evidence implicates cathepsins in niemann-pick c cerebellar degeneration. Hum Mol Genet 25, 1434-1446.

Cohen HB, Briggs KT, Marino JP, Ravid K, Robson SC, Mosser DM (2013). Tlr stimulation initiates a cd39-based autoregulatory mechanism that limits macrophage inflammatory responses. Blood 122, 1935-1945.

Cohen HB, Mosser DM (2013). Extrinsic and intrinsic control of macrophage inflammatory responses. J Leukoc Biol 94, 913-919.

Cohen HB, Ward A, Hamidzadeh K, Ravid K, Mosser DM (2015). Ifn-gamma prevents adenosine receptor (a2br) upregulation to sustain the macrophage activation response. J Immunol 195, 3828-3837.

Covarrubias AJ, Aksoylar HI, Horng T (2015). Control of macrophage metabolism and activation by mtor and akt signaling. Semin Immunol 27, 286-296.

Craven RR, Gao X, Allen IC, Gris D, Bubeck Wardenburg J, McElvania-Tekippe E, Ting JP, Duncan JA (2009). Staphylococcus aureus alpha-hemolysin activates the nlrp3-inflammasome in human and mouse monocytic cells. PLoS One 4, e7446.

Cruz FM, Colbert JD, Merino E, Kriegsman BA, Rock KL (2017). The biology and underlying mechanisms of cross-presentation of exogenous antigens on mhc-i molecules. Annu Rev Immunol 35, 149-176.

Davis MJ, Eastman AJ, Qiu Y, Gregorka B, Kozel TR, Osterholzer JJ, Curtis JL, Swanson JA, Olszewski MA (2015). Cryptococcus neoformans-induced macrophage lysosome damage crucially contributes to fungal virulence. J Immunol 194, 2219-2231.

Davis MJ, Gregorka B, Gestwicki JE, Swanson JA (2012). Inducible renitence limits listeria monocytogenes escape from vacuoles in macrophages. J Immunol 189, 4488-4495.

Davis MJ, Swanson JA (2010). Technical advance: Caspase-1 activation and il-1beta release correlate with the degree of lysosome damage, as illustrated by a novel imaging method to quantify phagolysosome damage. J Leukoc Biol 88, 813-822.

de Chastellier C, Forquet F, Gordon A, Thilo L (2009). Mycobacterium requires an all-around closely apposing phagosome membrane to maintain the maturation block and this apposition is re-established when it rescues itself from phagolysosomes. Cell Microbiol 11, 1190-1207.

De Duve C, Wattiaux R, Wibo M (1962). Effects of fat-soluble compounds on lysosomes in vitro. Biochem Pharmacol 9, 97-116.

Deng W, Marshall NC, Rowland JL, McCoy JM, Worrall LJ, Santos AS, Strynadka NCJ, Finlay BB (2017). Assembly, structure, function and regulation of type iii secretion systems. Nat Rev Micro 15, 323-337.

DeSelm CJ, Miller BC, Zou W, Beatty WL, van Meel E, Takahata Y, Klumperman J, Tooze SA, Teitelbaum SL, Virgin HW (2011). Autophagy proteins regulate the secretory component of osteoclastic bone resorption. Dev Cell 21, 966-974.

Dostert C, Guarda G, Romero JF, Menu P, Gross O, Tardivel A, Suva ML, Stehle JC, Kopf M, Stamenkovic I*, et al.* (2009). Malarial hemozoin is a nalp3 inflammasome activating danger signal. PLoS One 4, e6510.

Edwards JP, Zhang X, Frauwirth KA, Mosser DM (2006). Biochemical and functional characterization of three activated macrophage populations. J Leukoc Biol 80, 1298-1307.

Er EE, Mendoza MC, Mackey AM, Rameh LE, Blenis J (2013). Akt facilitates egfr trafficking and degradation by phosphorylating and activating pikfyve. Sci Signal 6, ra45.

Finlay BB, Falkow S (1997). Common themes in microbial pathogenicity revisited. Microbiol Mol Biol Rev 61, 136-169.

Flavell RA (2002). The relationship of inflammation and initiation of autoimmune disease: Role of tnf super family members. Curr Top Microbiol Immunol 266, 1-9.

Fleming BD, Chandrasekaran P, Dillon LA, Dalby E, Suresh R, Sarkar A, El-Sayed NM, Mosser DM (2015). The generation of macrophages with anti-inflammatory activity in the absence of stat6 signaling. J Leukoc Biol 98, 395-407.

Fredlund J, Enninga J (2014). Cytoplasmic access by intracellular bacterial pathogens. Trends Microbiol 22, 128-137.

Funk JL, Feingold KR, Moser AH, Grunfeld C (1993). Lipopolysaccharide stimulation of raw 264.7 macrophages induces lipid accumulation and foam cell formation. Atherosclerosis 98, 67-82.

Gabande-Rodriguez E, Boya P, Labrador V, Dotti CG, Ledesma MD (2014). High sphingomyelin levels induce lysosomal damage and autophagy dysfunction in niemann pick disease type a. Cell Death Differ 21, 864-875.

Geissmann F, Manz MG, Jung S, Sieweke MH, Merad M, Ley K (2010). Development of monocytes, macrophages, and dendritic cells. Science 327, 656-661.

Gerber JS, Mosser DM (2001). Reversing lipopolysaccharide toxicity by ligating the macrophage fc gamma receptors. J Immunol 166, 6861-6868.

Gimpl G, Gehrig-Burger K (2007). Cholesterol reporter molecules. Biosci Rep 27, 335-358.

Ginhoux F, Greter M, Leboeuf M, Nandi S, See P, Gokhan S, Mehler MF, Conway SJ, Ng LG, Stanley ER*, et al.* (2010). Fate mapping analysis reveals that adult microglia derive from primitive macrophages. Science 330, 841-845.

Gomez-Sintes R, Ledesma MD, Boya P (2016). Lysosomal cell death mechanisms in aging. Ageing Res Rev 32, 150-168.

Gordon RA, Grigoriev G, Lee A, Kalliolias GD, Ivashkiv LB (2012). The interferon signature and stat1 expression in rheumatoid arthritis synovial fluid macrophages are induced by tumor necrosis factor alpha and counter-regulated by the synovial fluid microenvironment. Arthritis Rheum 64, 3119-3128.

Gordon S, Taylor PR (2005). Monocyte and macrophage heterogeneity. Nat Rev Immunol 5, 953-964.

Gutierrez MG, Master SS, Singh SB, Taylor GA, Colombo MI, Deretic V (2004). Autophagy is a defense mechanism inhibiting bcg and mycobacterium tuberculosis survival in infected macrophages. Cell 119, 753-766.

Halle A, Hornung V, Petzold GC, Stewart CR, Monks BG, Reinheckel T, Fitzgerald KA, Latz E, Moore KJ, Golenbock DT (2008). The nalp3 inflammasome is involved in the innate immune response to amyloid-beta. Nat Immunol 9, 857-865.

Hamidzadeh K, Christensen SM, Dalby E, Chandrasekaran P, Mosser DM (2017). Macrophages and the recovery from acute and chronic inflammation. Annu Rev Physiol 79, 567-592.

Hemmi H, Takeuchi O, Sato S, Yamamoto M, Kaisho T, Sanjo H, Kawai T, Hoshino K, Takeda K, Akira S (2004). The roles of two ικb kinase-related kinases in lipopolysaccharide and double stranded rna signaling and viral infection. The Journal of Experimental Medicine 199, 1641-1650.

Hoeffel G, Wang Y, Greter M, See P, Teo P, Malleret B, Leboeuf M, Low D, Oller G, Almeida F*, et al.* (2012). Adult langerhans cells derive predominantly from embryonic fetal liver monocytes with a minor contribution of yolk sac-derived macrophages. J Exp Med 209, 1167-1181.

Hornung V, Bauernfeind F, Halle A, Samstad EO, Kono H, Rock KL, Fitzgerald KA, Latz E (2008). Silica crystals and aluminum salts activate the nalp3 inflammasome through phagosomal destabilization. Nat Immunol 9, 847-856.

Huang J, Canadien V, Lam GY, Steinberg BE, Dinauer MC, Magalhaes MA, Glogauer M, Grinstein S, Brumell JH (2009). Activation of antibacterial autophagy by nadph oxidases. Proc Natl Acad Sci U S A 106, 6226-6231.

Hung Y-H, Chen LM-W, Yang J-Y, Yuan Yang W (2013). Spatiotemporally controlled induction of autophagy-mediated lysosome turnover 4, 2111.

Huynh KK, Gershenzon E, Grinstein S (2008). Cholesterol accumulation by macrophages impairs phagosome maturation. J Biol Chem 283, 35745-35755.

Jadot M, Andrianaivo F, Dubois F, Wattiaux R (2001). Effects of methylcyclodextrin on lysosomes. Eur J Biochem 268, 1392-1399.

Janeway CA, Jr. (1989). Approaching the asymptote? Evolution and revolution in immunology. Cold Spring Harb Symp Quant Biol 54 Pt 1, 1-13.

Johnson AC, Li X, Pearlman E (2008). Myd88 functions as a negative regulator of tlr3/trif-induced corneal inflammation by inhibiting activation of c-jun n-terminal kinase. J Biol Chem 283, 3988-3996.

Jorgensen I, Miao EA (2015). Pyroptotic cell death defends against intracellular pathogens. Immunol Rev 265, 130-142.

Joshi GN, Goetjen AM, Knecht DA (2015). Silica particles cause nadph oxidase-independent ros generation and transient phagolysosomal leakage. Mol Biol Cell 26, 3150-3164.

Joung SM, Park Z-Y, Rani S, Takeuchi O, Akira S, Lee JY (2011). Akt contributes to activation of the trif-dependent signaling pathways of tlrs by interacting with tank-binding kinase 1. The Journal of Immunology 186, 499-507.

Kawai T, Akira S (2010). The role of pattern-recognition receptors in innate immunity: Update on toll-like receptors. Nat Immunol 11, 373-384.

Kenny EF, Talbot S, Gong M, Golenbock DT, Bryant CE, O'Neill LA (2009). Myd88 adaptor-like is not essential for tlr2 signaling and inhibits signaling by tlr3. J Immunol 183, 3642-3651.

Kono H, Rock KL (2008). How dying cells alert the immune system to danger. Nat Rev Immunol 8, 279-289.

Kornbluth RS, Oh PS, Munis JR, Cleveland PH, Richman DD (1989). Interferons and bacterial lipopolysaccharide protect macrophages from productive infection by human immunodeficiency virus in vitro. J Exp Med 169, 1137-1151.

Kreibich S, Emmenlauer M, Fredlund J, Ramo P, Munz C, Dehio C, Enninga J, Hardt WD (2015). Autophagy proteins promote repair of endosomal membranes damaged by the salmonella type three secretion system 1. Cell Host Microbe 18, 527-537.

Kreider T, Anthony RM, Urban JF, Jr., Gause WC (2007). Alternatively activated macrophages in helminth infections. Curr Opin Immunol 19, 448-453.

Krishna S, Palm W, Lee Y, Yang W, Bandyopadhyay U, Xu H, Florey O, Thompson CB, Overholtzer M (2016). Pikfyve regulates vacuole maturation and nutrient recovery following engulfment. Dev Cell 38, 536-547.

Kwon HJ, Abi-Mosleh L, Wang ML, Deisenhofer J, Goldstein JL, Brown MS, Infante RE (2009). Structure of n-terminal domain of npc1 reveals distinct subdomains for binding and transfer of cholesterol. Cell 137, 1213-1224.

Lamkanfi M, Dixit VM (2009). Inflammasomes: Guardians of cytosolic sanctity. Immunol Rev 227, 95-105.

Latz E, Xiao TS, Stutz A (2013). Activation and regulation of the inflammasomes. Nat Rev Immunol 13, 397-411.

Levine B, Mizushima N, Virgin HW (2011). Autophagy in immunity and inflammation. Nature 469, 323-335.

Liscum L (1990). Pharmacological inhibition of the intracellular transport of low-density lipoprotein-derived cholesterol in chinese hamster ovary cells. Biochim Biophys Acta 1045, 40-48.

Loke P, Gallagher I, Nair MG, Zang X, Brombacher F, Mohrs M, Allison JP, Allen JE (2007). Alternative activation is an innate response to injury that requires cd4+ t cells to be sustained during chronic infection. J Immunol 179, 3926-3936.

Mackaness GB (1962). Cellular resistance to infection. J Exp Med 116, 381-406.

Mackaness GB (1970). The monocyte in cellular immunity. Semin Hematol 7, 172-184.

MacMicking J, Xie QW, Nathan C (1997). Nitric oxide and macrophage function. Annu Rev Immunol 15, 323-350.

Maejima I, Takahashi A, Omori H, Kimura T, Takabatake Y, Saitoh T, Yamamoto A, Hamasaki M, Noda T, Isaka Y*, et al.* (2013). Autophagy sequesters damaged lysosomes to control lysosomal biogenesis and kidney injury. EMBO J 32, 2336-2347.

Mariathasan S, Weiss DS, Newton K, McBride J, O'Rourke K, Roose-Girma M, Lee WP, Weinrauch Y, Monack DM, Dixit VM (2006). Cryopyrin activates the inflammasome in response to toxins and atp. Nature 440, 228-232.

Martinez J, Almendinger J, Oberst A, Ness R, Dillon CP, Fitzgerald P, Hengartner MO, Green DR (2011). Microtubule-associated protein 1 light chain 3 alpha (lc3)-associated phagocytosis is required for the efficient clearance of dead cells. Proc Natl Acad Sci U S A 108, 17396-17401.

Matsuura M (2013). Structural modifications of bacterial lipopolysaccharide that facilitate gram-negative bacteria evasion of host innate immunity. Front Immunol 4.

Means TK, Hayashi F, Smith KD, Aderem A, Luster AD (2003). The toll-like receptor 5 stimulus bacterial flagellin induces maturation and chemokine production in human dendritic cells. J Immunol 170, 5165-5175.

Medzhitov R (2009). Approaching the asymptote: 20 years later. Immunity 30, 766-775.

Mizushima N, Yoshimori T, Levine B (2010). Methods in mammalian autophagy research. Cell 140, 313-326.

Mizushima N, Yoshimori T, Ohsumi Y (2011). The role of atg proteins in autophagosome formation. Annu Rev Cell Dev Biol 27, 107-132.

Molofsky AB, Byrne BG, Whitfield NN, Madigan CA, Fuse ET, Tateda K, Swanson MS (2006). Cytosolic recognition of flagellin by mouse macrophages restricts legionella pneumophila infection. J Exp Med 203, 1093-1104.

Mosser DM (2003). The many faces of macrophage activation. J Leukoc Biol 73, 209-212.

Mosser DM, Edwards JP (2008). Exploring the full spectrum of macrophage activation. Nat Rev Immunol 8, 958-969.

Mosser DM, Zhang X (2008). Activation of murine macrophages. Curr Protoc Immunol Chapter 14, Unit 14.12.

Mukherjee S, Maxfield FR (2004). Lipid and cholesterol trafficking in npc. Biochim Biophys Acta 1685, 28-37.

Munder M, Mallo M, Eichmann K, Modolell M (1998). Murine macrophages secrete interferon gamma upon combined stimulation with interleukin (il)-12 and il-18: A novel pathway of autocrine macrophage activation. J Exp Med 187, 2103-2108.

Murphy K. (2011). Janeway's immunobiology. Taylor & Francis Group.

Nathan C, Ding A (2010). Nonresolving inflammation. Cell 140, 871-882.

Nauseef WM (2008). Biological roles for the nox family nadph oxidases. J Biol Chem 283, 16961-16965.

Parnas O, Jovanovic M, Eisenhaure TM, Herbst RH, Dixit A, Ye CJ, Przybylski D, Platt RJ, Tirosh I, Sanjana NE*, et al.* (2015). A genome-wide crispr screen in primary immune cells to dissect regulatory networks. Cell 162, 675-686.

Paz I, Sachse M, Dupont N, Mounier J, Cederfur C, Enninga J, Leffler H, Poirier F, Prevost MC, Lafont F*, et al.* (2010). Galectin-3, a marker for vacuole lysis by invasive pathogens. Cell Microbiol 12, 530-544.

Perrin AJ, Jiang X, Birmingham CL, So NS, Brumell JH (2004). Recognition of bacteria in the cytosol of mammalian cells by the ubiquitin system. Curr Biol 14, 806-811.

Portnoy DA, Schreiber RD, Connelly P, Tilney LG (1989). Gamma interferon limits access of listeria monocytogenes to the macrophage cytoplasm. J Exp Med 170, 2141-2146.

Racoosin EL, Swanson JA (1989). Macrophage colony-stimulating factor (rm-csf) stimulates pinocytosis in bone marrow-derived macrophages. J Exp Med 170, 1635-1648.

Racoosin EL, Swanson JA (1993). Macropinosome maturation and fusion with tubular lysosomes in macrophages. J Cell Biol 121, 1011-1020.

Radtke AL, Anderson KL, Davis MJ, DiMagno MJ, Swanson JA, O'Riordan MX (2011). Listeria monocytogenes exploits cystic fibrosis transmembrane conductance regulator (cftr) to escape the phagosome. Proc Natl Acad Sci U S A 108, 1633-1638.

Radtke AL, Delbridge LM, Balachandran S, Barber GN, O'Riordan MX (2007). Tbk1 protects vacuolar integrity during intracellular bacterial infection. PLoS Pathog 3, e29.

Radtke AL, O'Riordan MX (2008). Homeostatic maintenance of pathogen-containing vacuoles requires tbk1-dependent regulation of aquaporin-1. Cell Microbiol 10, 2197-2207.

Raes G, Beschin A, Ghassabeh GH, De Baetselier P (2007). Alternatively activated macrophages in protozoan infections. Curr Opin Immunol 19, 454-459.

Randow F, Youle Richard J (2014). Self and nonself: How autophagy targets mitochondria and bacteria. Cell Host & Microbe 15, 403-411.

Reddick LE, Alto Neal M (2014). Bacteria fighting back: How pathogens target and subvert the host innate immune system. Mol Cell 54, 321-328.

Reese TA, Liang HE, Tager AM, Luster AD, Van Rooijen N, Voehringer D, Locksley RM (2007). Chitin induces accumulation in tissue of innate immune cells associated with allergy. Nature 447, 92-96.

Rosenbaum AI, Zhang G, Warren JD, Maxfield FR (2010). Endocytosis of beta-cyclodextrins is responsible for cholesterol reduction in niemann-pick type c mutant cells. Proc Natl Acad Sci U S A 107, 5477-5482.

Rosenberger CM, Scott MG, Gold MR, Hancock RE, Finlay BB (2000). Salmonella typhimurium infection and lipopolysaccharide stimulation induce similar changes in macrophage gene expression. J Immunol 164, 5894-5904.

Sanjuan MA, Dillon CP, Tait SW, Moshiach S, Dorsey F, Connell S, Komatsu M, Tanaka K, Cleveland JL, Withoff S*, et al.* (2007). Toll-like receptor signalling in macrophages links the autophagy pathway to phagocytosis. Nature 450, 1253-1257.

Schaible UE, Sturgill-Koszycki S, Schlesinger PH, Russell DG (1998). Cytokine activation leads to acidification and increases maturation of mycobacterium avium-containing phagosomes in murine macrophages. J Immunol 160, 1290-1296.

Schmittgen TD, Livak KJ (2008). Analyzing real-time pcr data by the comparative c(t) method. Nat Protoc 3, 1101-1108.

Schnettger L, Rodgers A, Repnik U, Lai RP, Pei G, Verdoes M, Wilkinson RJ, Young DB, Gutierrez MG (2017). A rab20-dependent membrane trafficking pathway controls m. Tuberculosis replication by regulating phagosome spaciousness and integrity. Cell Host Microbe 21, 619-628.e615.

Schroder K, Tschopp J (2010). The inflammasomes. Cell 140, 821-832.

Schulz C, Gomez Perdiguero E, Chorro L, Szabo-Rogers H, Cagnard N, Kierdorf K, Prinz M, Wu B, Jacobsen SE, Pollard JW*, et al.* (2012). A lineage of myeloid cells independent of myb and hematopoietic stem cells. Science 336, 86-90.

Scott CC, Botelho RJ, Grinstein S (2003). Phagosome maturation: A few bugs in the system. J Membr Biol 193, 137-152.

Serhan CN, Savill J (2005). Resolution of inflammation: The beginning programs the end. Nat Immunol 6, 1191-1197.

Settembre C, Fraldi A, Medina DL, Ballabio A (2013). Signals from the lysosome: A control centre for cellular clearance and energy metabolism. Nat Rev Mol Cell Biol 14, 283-296.

Shaughnessy LM, Hoppe AD, Christensen KA, Swanson JA (2006). Membrane perforations inhibit lysosome fusion by altering ph and calcium in listeria monocytogenes vacuoles. Cell Microbiol 8, 781-792.

Shisheva A (2008). Pikfyve: Partners, significance, debates and paradoxes. Cell Biol Int 32, 591-604.

Simeone R, Bobard A, Lippmann J, Bitter W, Majlessi L, Brosch R, Enninga J (2012). Phagosomal rupture by mycobacterium tuberculosis results in toxicity and host cell death. PLoS Pathog 8, e1002507.

Simeone R, Majlessi L, Enninga J, Brosch R (2016). Perspectives on mycobacterial vacuole-to-cytosol translocation: The importance of cytosolic access. Cell Microbiol 18, 1070-1077.

Sokol J, Blanchette-Mackie J, Kruth HS, Dwyer NK, Amende LM, Butler JD, Robinson E, Patel S, Brady RO, Comly ME*, et al.* (1988). Type c niemann-pick disease. Lysosomal accumulation

and defective intracellular mobilization of low density lipoprotein cholesterol. J Biol Chem 263, 3411-3417.

Sutterwala FS, Noel GJ, Clynes R, Mosser DM (1997). Selective suppression of interleukin-12 induction after macrophage receptor ligation. J Exp Med 185, 1977-1985.

Sutterwala FS, Noel GJ, Salgame P, Mosser DM (1998). Reversal of proinflammatory responses by ligating the macrophage fcgamma receptor type i. J Exp Med 188, 217-222.

Swanson JA, Watts C (1995). Macropinocytosis. Trends Cell Biol 5, 424-428.

Thibodeau MS, Giardina C, Knecht DA, Helble J, Hubbard AK (2004). Silica-induced apoptosis in mouse alveolar macrophages is initiated by lysosomal enzyme activity. Toxicol Sci 80, 34-48.

Thiele DL, Lipsky PE (1990). Mechanism of l-leucyl-l-leucine methyl ester-mediated killing of cytotoxic lymphocytes: Dependence on a lysosomal thiol protease, dipeptidyl peptidase i, that is enriched in these cells. Proc Natl Acad Sci U S A 87, 83-87.

Thurston TL, Ryzhakov G, Bloor S, von Muhlinen N, Randow F (2009). The tbk1 adaptor and autophagy receptor ndp52 restricts the proliferation of ubiquitin-coated bacteria. Nat Immunol 10, 1215-1221.

Thurston TL, Wandel MP, von Muhlinen N, Foeglein A, Randow F (2012). Galectin 8 targets damaged vesicles for autophagy to defend cells against bacterial invasion. Nature 482, 414-418.

Turk B, Turk V (2009). Lysosomes as "suicide bags" in cell death: Myth or reality? J Biol Chem 284, 21783-21787.

Uchimoto T, Nohara H, Kamehara R, Iwamura M, Watanabe N, Kobayashi Y (1999). Mechanism of apoptosis induced by a lysosomotropic agent, l-leucyl-l-leucine methyl ester. Apoptosis 4, 357-362.

Uderhardt S, Herrmann M, Oskolkova OV, Aschermann S, Bicker W, Ipseiz N, Sarter K, Frey B, Rothe T, Voll R*, et al.* (2012). 12/15-lipoxygenase orchestrates the clearance of apoptotic cells and maintains immunologic tolerance. Immunity 36, 834-846.

van der Wel N, Hava D, Houben D, Fluitsma D, van Zon M, Pierson J, Brenner M, Peters PJ (2007). M. Tuberculosis and m. Leprae translocate from the phagolysosome to the cytosol in myeloid cells. Cell 129, 1287-1298.

Vance RE, Isberg RR, Portnoy DA (2009). Patterns of pathogenesis: Discrimination of pathogenic and nonpathogenic microbes by the innate immune system. Cell Host Microbe 6, 10-21.

Vanier MT (2013). Niemann-pick diseases. Handb Clin Neurol 113, 1717-1721.

Via LE, Fratti RA, McFalone M, Pagan-Ramos E, Deretic D, Deretic V (1998). Effects of cytokines on mycobacterial phagosome maturation. J Cell Sci 111 (Pt 7), 897-905.

Wall AA, Luo L, Hung Y, Tong SJ, Condon ND, Blumenthal A, Sweet MJ, Stow JL (2017). Small gtpase rab8a-recruited phosphatidylinositol 3-kinase gamma regulates signaling and cytokine outputs from endosomal toll-like receptors. J Biol Chem 292, 4411-4422.

Watarai M, Derre I, Kirby J, Growney JD, Dietrich WF, Isberg RR (2001). Legionella pneumophila is internalized by a macropinocytotic uptake pathway controlled by the dot/icm system and the mouse lgn1 locus. J Exp Med 194, 1081-1096.

Weiner A, Mellouk N, Lopez-Montero N, Chang YY, Souque C, Schmitt C, Enninga J (2016). Macropinosomes are key players in early shigella invasion and vacuolar escape in epithelial cells. PLoS Pathog 12, e1005602.

Wild P, Farhan H, McEwan DG, Wagner S, Rogov VV, Brady NR, Richter B, Korac J, Waidmann O, Choudhary C*, et al.* (2011). Phosphorylation of the autophagy receptor optineurin restricts salmonella growth. Science 333, 228-233.

Wynn TA, Chawla A, Pollard JW (2013). Macrophage biology in development, homeostasis and disease. Nature 496, 445-455.

Xu Y, Jagannath C, Liu XD, Sharafkhaneh A, Kolodziejska KE, Eissa NT (2007). Toll-like receptor 4 is a sensor for autophagy associated with innate immunity. Immunity 27, 135-144.

Yamasaki K, Muto J, Taylor KR, Cogen AL, Audish D, Bertin J, Grant EP, Coyle AJ, Misaghi A, Hoffman HM*, et al.* (2009). Nlrp3/cryopyrin is necessary for interleukin-1beta (il-1beta) release in response to hyaluronan, an endogenous trigger of inflammation in response to injury. J Biol Chem 284, 12762-12771.

Yap TA, Yan L, Patnaik A, Fearen I, Olmos D, Papadopoulos K, Baird RD, Delgado L, Taylor A, Lupinacci L*, et al.* (2011). First-in-man clinical trial of the oral pan-akt inhibitor mk-2206 in patients with advanced solid tumors. J Clin Oncol 29, 4688-4695.

Yoshida S, Hong S, Suzuki T, Nada S, Mannan AM, Wang J, Okada M, Guan KL, Inoki K (2011). Redox regulates mammalian target of rapamycin complex 1 (mtorc1) activity by modulating the tsc1/tsc2-rheb gtpase pathway. J Biol Chem 286, 32651-32660.

Youle RJ, Narendra DP (2011). Mechanisms of mitophagy. Nat Rev Mol Cell Biol 12, 9-14.

Zheng YT, Shahnazari S, Brech A, Lamark T, Johansen T, Brumell JH (2009). The adaptor protein p62/sqstm1 targets invading bacteria to the autophagy pathway. J Immunol 183, 5909-5916.